DISS. ETH NO. 21839

DESIGN OF ADAPTIVE STRUCTURES WITH PIEZOELECTRIC MATERIALS

A thesis submitted to attain the degree of

DOCTOR OF SCIENCES OF ETH ZURICH

(Dr. sc. ETH Zurich)

presented by

TOMMASO DELPERO

Laurea Specialistica in Aeronautical Engineering, Politecnico di Milano

born July 28, 1984
citizen of Italy

accepted on the recommendation of

Prof. Dr. Paolo Ermanni, examiner
Prof. Dr. Massimo Ruzzene, co-examiner
Dr. Andrea Bergamini, co-examiner

2014

ABSTRACT

This doctoral thesis investigates the application of shunted piezoelectric transducers in the design of adaptive structures. The implications of including adaptive materials in the design are considered beyond their immediate intended purpose: while shunted piezoelectric transducers are already known to be an effective technology for reducing structural vibrations, in this work they are considered as additional degrees of freedom to extend the design space and to obtain a qualitative improvement in the dynamic response of the system.

The focus is initially set on controlling structural vibrations by means of piezoelectric shunt damping. A non-conventional design approach, based on finding a compromise between structural stiffness and damping, is proposed in order to extend the design space to lighter, less stiff and more easily damped structures. Achieving this goal requires a high degree of robustness of the shunt damping techniques and of the modeling of their damping performance, which are therefore important intermediate goals. The acquired knowledge is applied to the realistic case study of a scaled model of a rotating blade.

In the second part of this work, the transducers are integrated in the design of structures even at a deeper level, i.e. the metamaterial level. A periodic array of shunted piezoelectric elements exhibits a collective behavior that suggests the application of a metamaterial approach for the investigation of the dynamic properties of the adaptive system. The wave propagation properties of the resulting electromechanical metamaterial are defined by the effective stiffness of the shunted piezoelectric transducers that can be therefore exploited to obtain adaptive bandgaps. Bandgaps are particularly significant because they represent forbidden energy states that, for instance, in a mechanical structure would lead to frequency ranges free from vibrations. Two examples of metamaterials are proposed where resonant shunted piezoelectric discs are arranged in a periodic

configuration to create, cancel or shift acoustic bandgaps. The presented results demonstrate how, thanks to the periodicity of the system, the multi-field coupling of piezoelectric materials allows obtaining remarkable effects in the mechanical response of the system by manipulating energy in the electrical domain, which can be easily done with simple analog circuits.

ZUSAMMENFASSUNG

Diese Dissertation untersucht die Anwendung geschalteter piezoelektrischer Wandler im Designprozess adaptiver Strukturen. Die Auswirkungen der adaptiven Materialien werden über ihre unmittelbare Verwendung hinaus betrachtet: Obwohl geschaltete piezoelektrische Wandler bereits als wirksame Technik zur Dämpfung von Strukturschwingungen bekannt sind, werden sie in dieser Arbeit als zusätzliche Freiheitsgrade betrachtet, um den Design-Raum zu erweitern und eine Verbesserung der dynamischen Antwort des Systems zu erhalten.

Der Augenmerk des ersten Teils dieser Arbeit liegt auf der Dämpfung von Strukturschwingungen. Ein unkonventioneller Designansatz, der auf der Suche nach einem Kompromiss zwischen Struktursteifigkeit und Dämpfung basiert, wird vorgeschlagen, um den Design-Raum mit leichteren, weniger steifen und leicht gedämpften Strukturen zu erweitern. Um dieses Ziel zu erreichen, ist die Robustheit der Dämpfungstechniken und der Modellierung derer Leistungsfähigkeit notwendig, und stellt daher ein wichtiges Zwischenziel dar. Das erworbene Wissen wird an der realistischen Fallstudie des skalierten Modells eines Propellerblatts angewandt.

Im zweiten Teil dieser Arbeit werden die piezoelektrischen Wandler auch in eine tiefere Ebene des Strukturdesigns integriert, d. h. die Metamaterial-Ebene. Eine periodische Anordnung geschalteter Wandler zeigt ein kollektives Verhalten, das es nahelegt, einen Metamaterial-Ansatz zur Untersuchung des periodischen Systems zu verwenden. Die effektive Steifigkeit der geschalteter Wandler kann benutzt werden, um die Wellenausbreitungseigenschaften des elektromechanischen Metamaterials, mit Schwerpunkt auf adaptiven Bandlücken, zu ändern. Bandlücken repräsentieren verbotene Energiezustände, die z. B. in einer mechanischen Struktur zu schwingungsfreien Frequenzbereichen führen würden. Zwei Beispiele von Metamaterialien werden vorgeschlagen, in welchen resonante Wandler in peri-

odischen Konfigurationen angeordnet werden, um akustische Bandlücken zu erzeugen, auszulöschen oder zu verschieben. Die dargestellten Ergebnisse zeigen, wie die elektromechanische Kopplung piezoelektrischer Materialien ermöglicht, die Energie im elektrischen Bereich mit einfachen analogen Schaltungen zu beeinflussen, und durch die Periodizität bemerkenswerte Effekte in der mechanischen Antwort des Systems zu erhalten.

"The myth of collective behavior following from the law is,
as a practical matter, exactly backward.
Law instead follows from collective behavior,
as do things that flow from it, such as logic and mathematics.
The reason our minds can anticipate and master
what the physical world does is not because we are geniuses
but because nature facilitates understanding
by organizing itself and generating law."

— Robert B. Laughlin, 2006

ACKNOWLEDGMENTS

The dynamic properties of adaptive structures, like the acoustic bandgpas investigated in this work, as well as the fundamental properties of materials, such as the stiffness of a steel plate or the hardness of diamond, emerge as collective behaviors from the organizations of large number of 'atoms'. In a similar way, this manuscript is the conclusion of an intense work that could not be accomplished without the valuable contribution of many people, which I am happy to acknowledge in the following lines.

The present thesis collects the results of an exciting and instructive work as research assistant at the Laboratory of Composite Materials and Adaptive Structures (formerly Center of Structure Technologies) at ETH Zurich. Everything began in January 2010 when Prof. Paolo Ermanni offered me the possibility to start a PhD in his group. I owe him my gratitude for the opportunity he gave me to broaden my knowledge in a prestigious and stimulating environment such as the ETH Zurich. I specially thank him for the strong support and interest he demonstrated in this work and for having granted the appropriate conditions to freely conduct my research project.

I wish to thank Prof. Massimo Ruzzene for his always accurate advices and precise feedback, for the beneficial collaboration with the Vibration and Wave Propagation Lab at Georgia Tech and, in particularly, for having expanded my horizons to the fascinating field of periodic structures.

I want to express my most sincere gratitude to Dr. Andrea Bergamini for the numerous discussions and the inspiring suggestions, for having shared his broad scientific knowledge with me, for his creative thinking, for the extreme kindness and the high ethic standards that reflect on his daily work. I am not the only one thinking he is the best supervisor anyone can imagine to have.

I want to thank all the—numerous—colleagues at the Center of Structure Technologies, and in particular Alberto, Andres, Bryan, Claudio, Davi, Florian, Gregoire, Joanna, Mario, Nikolaos, Simon and Wolfram, for their help, the lively discussions, the coffee breaks and the good time spent together. Special thanks to Francesco, Giulio and Luigi, because I have never felt alone during this challenging four years. My sincere thanks also to Filippo Casadei for the valuable collaboration during my stay in Atlanta.

I also want to thank the students that contributed with their work to the results presented in this thesis: Sebastian Krödel, Matthias Heymanns, Luca De Simoni and Mirko Meier.

Finally, I want to express my deepest gratitude to my family who supported me, endlessly: My parents, who granted me the freedom to pursue my goals; my sister with her family, whose happiness is contagious; my brother, who has given me the bravery to follow my dreams; and Serena, for her love, patience and generous support.

CONTENTS

Part I

INTRODUCTION

1

A BRIEF OVERVIEW

1.1 BACKGROUND

Adaptive materials transduce energy between different domains

Adaptive materials have been intensively researched for the past few decades. Their promise is to introduce decisive elements of novelty in the design of mechanical systems through their ability to transduce energy from the mechanical domain to and from various others, such as the electrical, magnetic and thermal domains. From the very intense activity in this field emerged Lead Zirconate Titanate (PZT), Nickel Titanium shape memory alloys (Nitinol) and magneto-rheological fluids to name a few of the most prominent results. These materials have been studied to develop sensors, actuators and—more in general—elements with variable mechanical properties, where the transducive function takes place at the material level. They therefore offer clear advantages in terms of scalability and integration into the host structures compared to classical geometrical-based transducers, which always involve some kinematics of their components.

While on one side the materials research community has developed and improved new adaptive materials, on the other side engineers have focused on exploiting them for the application, optimization and integration in adaptive structures. Adaptive structures take advantage of the adaptive materials in order to alter their mechanical properties in a pre-designed and reproducible way as response to changes in environmental conditions. This can be achieved by introducing actuators that exert additional forces on the structure (for example, in the active control of the surface of a telescope to compensate for distortions), or by modification of its mechanical properties (for instance, magneto-rheological fluids are used in adaptive dampers to control vibrations on bridges or in car shock absorbers).

The development of adaptive structures has been studied in a wide range of industrial applications, but it is particularly advanced in the aerospace and space technology sector with morphing wings, deployable space structures, structural health monitoring, position control and vibration reduction. Besides the number of potential applications, the strong fascination with them in the research community comes from the highly multidisciplinary approach required for their analysis and design, which generally include elements of structures, materials, dynamics and control.

Among the numerous investigated adaptive materials, this thesis focuses on shunted piezoelectric materials and their applications for altering the dynamic behavior of the host structure. The high blocking stress and bandwidth of piezoelectric ceramics, like PZT, make them suitable candidate for controlling structural vibrations that typically occur in the Hz or kHz frequency range. The piezoelectric effect allows exchanging energy between the mechanical and the electrical domain, so that, when a piezoelectric element is shunted through an electrical circuit, it behaves as a time-dependent stiffness element that can be used to dissipate energy or, more in general, to alter the mechanical dynamic behavior of the host structure.

Adaptive materials represent additional degrees of freedom in the structural design

A key point in the design of adaptive structures is the consideration that adaptive materials add degrees of freedom to the design of the host structure. In order to take the greatest advantage of them, the resulting system should not be designed according to conventional purely mechanical approaches, but rather as a more complex multi-field system. An example may be the design of a load carrying structures, where the dynamic behavior is a main design criterion since large amplitude vibrations often interfere with the effective operation and can even lead to failures. When the requirements in terms of dynamic behavior conflict with functional or static ones, the consideration of additional degrees of freedom during the design process may extend the design space to solutions that would otherwise be rejected because they do not fulfill the dynamic requirements. Additionally, given the practicality of manipulating electrical quantities respect to mechanical ones, one can think to use the

additional electrical degrees of freedom in fancy and elaborate ways, and to obtain dynamic responses of the system that differ qualitatively, and not only quantitatively, from the ones of the plain mechanical system.

1.2 STATE OF THE ART

Overview of the research on piezoelectric shunt damping

Shunted piezoelectric elements have been investigated for several years as a promising method to reduce the vibration amplitude of dynamically loaded structures. The general method of shunt damping takes advantage of the relatively strong electromechanical coupling exhibited by piezoelectric ceramics. As the piezoelectric element—bonded on or embedded in the structures—strains, a portion of the mechanical vibration energy is converted into electrical energy, which can be treated in a network of electrical elements connected to the piezoelectric patch. The technique was first introduced by Forward (1979) to damp mechanical vibrations in optical systems, while Hagood and von Flotow (1991) provided the first analytical formulation for the passive shunts. Compared to a classical active control, piezoelectric shunt damping requires neither additional sensor, nor external power source (at least in its purely passive implementation), since the only external element is the electrical network connected to the electrodes of the piezoelectric device.[1]

Besides the development and characterization of piezoelectric materials, most of the recent and past work has focused on investigation of several shunt circuits (Hagood and von Flotow, 1991; Corr and Clark, 2002, 2003; Behrens et al., 2003), of the structural integrity of the piezo-augmented structure (Singh and Vizzini, 1994; Hansen and Vizzini, 2000; Melnykowycz, 2008), and the optimization of their size and placement (Belloli and Ermanni, 2007). New finite element formulations (Becker et al., 2006; Thomas et al., 2009; Côté et al., 2004) and numerical models including the controllers or the shunt circuits (Herold et al., 2004; Larbi et al., 2010) have been presented in the last decade.

1 A deeper and more comprehensive explanation of the working principle of piezoelectric shunt damping is presented in the next chapter.

However, little work done by the adaptive structures community has focused on development of formal design methodologies specifically for adaptive structures (Frecker, 2003).

The analysis of the damped response of structures with shunted piezoelectric elements has been object of different studies, mainly focused on linear shunting techniques: Davis and Lesieutre (1995) proposed a modal strain energy approach to predict the added damping produced by resistive shunts, while Plagianakos and Saravanos (2003) and Saravanos (1999) focused on analytical models for composite plates with resistive shunted piezo layers. Recently, Thomas et al. (2012) presented a closed-form solution for estimating the vibration reduction of resistive and resonant shunts, while Lesieutre et al. (2004) studied the damping associated with a piezoelectric energy harvesting system. In all the cited studies the obtained damping is shown to depend on the electromechanical coupling and some characteristics of the electrical circuit. However, a unifying approach that allows for comparing the damping performance of different shunts and ultimately also other vibration reduction techniques cannot be counted to the state of the art at the beginning of the present project.

State of research on periodic systems and electromechanical metamaterials

While conventional damping techniques are based on dissipating the energy only once it has been accepted in the structure, shunted piezoelectric elements can also be used to obtain structures where the energy is not even admitted in specific frequency ranges, so that large amplitude vibrations are precluded. In conventional materials these stop bands appear at too-high frequencies to be interesting for structural applications. On the other hand, periodic systems and micro-structured mechanical metamaterials have recently received increasing attention for the possibility to design and tune their wave propagation properties also at lower (Hz and kHz) frequency ranges, so that they represent an interesting opportunity also for structural applications (Baravelli and Ruzzene, 2013; Yilmaz and Hulbert, 2010). The term *metamaterials* has been introduced by the electromagnetic community to describe artificially-made media with carefully-designed and periodically-arranged small-scale building blocks, whose macro-scale physical properties can be controlled by

the structural hierarchy and topology across micro- and meso-scales. The study of electromagnetic metamaterials has led to completely new prospective in terms of achievable effective materials properties and applications, such as materials with negative refraction index (Smith et al., 2000) and electromagnetic cloaking (Pendry et al., 2006).

A collective behavior emerges from the interactions between the constituting elements at the micro-scale level

The peculiarity of metamaterials is that the effective properties of the collective system emerge from the interactions between the building blocks at the micro-scale level and from the way electromagnetic or mechanical waves propagate through them. The building block of the periodic system can be designed so that the resulting interference between the propagating waves leads to a desired way in which energy propagates through the material. In other words, the band structure of the metamaterial can be tailored by an appropriate design of its building blocks.

The metamaterial concept has been recently extended to the mechanical domain. Liu et al. (2000) experimentally verified the presence of low frequency bandgaps as result of a periodic arrangement of locally resonating units: the mechanical impedance mismatches resulting from the local resonators alter the band structure so that waves are prevented to propagate in certain frequency ranges, called *bandgaps*.

The metamaterial approach to the tailoring of the wave propagation properties of structures is based on the same physical principles that govern the band structures of crystalline solids. A consequence of the manipulation of the band structure is a modified dynamic behavior of the periodic structure that can be described in terms of effective medium parameters. Other interesting examples have demonstrated, for instance, negative Poisson effects (Bueckmann et al., 2012), negative dynamic bulk modulus and effective density (Li and Chan, 2004) and high specific energy absorption. A comprehensive overview of their characteristics, potential tools for their fabrication and methods for the performance characterization can be found in Lee et al. (2012).

The introduction of adaptive materials in the building blocks can further extend the potentiality of this concept, leading for example to structures with a periodic arrangement of shunted

piezoelectric elements. The metamaterial approach completely differs from the conventional piezoelectric shunt damping, where specific eigenmodes of the host structure are targeted by a discrete number of transducers that are basically used to dissipate the vibration energy. In a metamaterial approach, the piezoelectric elements are used as variable stiffness elements within the unit cell to alter the band structure in such a way that the propagation of energy is inhibited for certain frequency ranges and the combination of wave propagation and boundary conditions cannot lead to the creation of structural vibrations. Instead of exploiting the electrical degrees of freedom at the structural level, in the metamaterial approach this is done at a lower (material) level, so that the resulting properties are intrinsic to the metamaterial and independent from the geometry and boundary conditions of the final structure.

A first application of this concept has been presented by Thorp et al. (2001) on a periodic rod and implemented by Casadei et al. (2010) on a plate with a periodic distribution of shunted piezoelectric patches to achieve broadband vibration reduction. In this periodic configuration, the shunted piezoelectric elements introduce sources of mechanical impedance mismatch in the structure and are responsible for the creation of bandgaps. Compare to conventional shunt damping, this approach exploits the unique properties of broadband wave attenuation of periodic structures. The variable effective stiffness of shunted piezoelectric elements is used to modify the ability of the periodic structure to transmit waves, and therefore the establishment of high amplitude vibrations is inhibited.

1.3 RESEARCH NEEDS

In spite of the advances made in the understanding of adaptive damping technologies, a very limited number of applications of adaptively damped structures can be found on the market. This situation is in clear contrast with the intensity and length of research performed in the field of vibration damping based on adaptive approaches. While the potential of these devices is acknowledged, the additional complexity is not perceived

as being offset by the increase in performance offered by this approach. Additionally, the damping properties of the materials employed in the fabrication of the structures are generally not considered in the design phase. The conventional approach to the dynamic dimensioning of structures is to consider resonance phenomena as leading to malfunction or even to catastrophic failure, with a consequent general trend in the direction of stiffening the structures. To date, shunted piezoelectric devices are treated as an add-on to structures that are designed according to well established procedures based on conventional (i.e. non-adaptive) materials. This approach limits the potentiality of the adaptive material mainly for the following two reasons:

A. While in most cases, the intuitive solution of a stiffness increase brings benefit to the mechanical system, there are cases, such as piezo-augmented structure, where a higher stiffness results in subsequent difficulties in improving the damping properties of the system.

B. The only increase in performance considered when evaluating the use of piezo-devices is the reduction of vibration amplitudes of the structures thanks to the additional damping. This argument alone is not considered as sufficient to justify the introduction of additional elements that are viewed as source of increased complexity and cost.

Need for a deeper integration of adaptive elements in the host structures

Here, a need for a design approach where shunted piezoelectric elements are considered since the beginning of the design process of the structure becomes evident. This approach should (A) avoid the design of too-stiff-to-be-damped structures, and (B) it might extend the design space to solutions that, by reducing the vibration amplitudes, can promote a cascade of beneficial effects, like a reduction in their mass or increase in their functionality.

The high degree of integrability of adaptive elements in the host structure is considered by the research community a strong advantage compared to traditional transducers, and many research activities have focused on their integration in the structural manufacturing and geometry. However, besides the need for a deeper integration of the adaptive elements in the

design of the host structure, we can expect that the integration of adaptive elements even at a lower level, i.e. the (meta)material level, will further their exploitation. The application of adaptive elements in the building blocks of metamaterials opens up an enormous number of research possibilities. For instance, shunted piezoelectric transducers behave as time-dependent stiffness elements that can be exploited to modify the wave propagation properties of the metamaterial. While a few works in which a periodic arrangement of shunted piezos is used for obtaining broad vibration reduction capabilities have been presented, there is the need for a deeper investigation on how their adaptive qualities may be used for tuning the propagation of energy in the metamaterial.

1.4 GOALS AND APPROACHES

Object of this work

The focus of this thesis is set on shunted piezoelectric elements and their applications for altering the dynamic behavior of the host structure. The implications of including adaptive materials in the design of structures are considered beyond their immediate intended purpose. In particular we are addressing the *fundamental question* about the extent to which the additional degrees of freedom introduced in the design space can lead to a qualitative improvement in the dynamic performance of the systems, compared to the plain mechanical one.

First approach

The first approach presented in this thesis focuses on vibration reduction using shunted piezoelectric devices. The *goal* is to verify if the consideration of damping based on piezoelectric elements can allow for the design of systems able to fulfill more stringent requirements than the simply passive structure, or fulfill all the requirements with a minor weight, and increase its functionality. Such a design approach cannot be pursued without a certain degree of robustness of the shunt damping techniques and of their modeling, which represent therefore important intermediate goals of this work.

An example

To illustrate the idea of the far reaching implications of the use of adaptive materials, we shall briefly consider a simple example of the design of a structure, such as a rotating disk with

blades. A limiting factor to the design of large diameter bladed disks is given by the tensile strength of the materials used for the blades. The static load at the root due to centrifugal forces limits the maximum length of the blade for any given material. A structure of the blade, which reduces the centrifugal stresses at the root of the blade, typically corresponds to a lightweight solution that, on the other hand, has the tendency to be subjected to large amplitude vibrations and may be not acceptable if not properly damped. While the use of adaptive materials cannot directly solve the strength problem encountered due to the centrifugal load, they may allow for the implementation of different solutions that might otherwise be rejected because incompatible with dynamic requirements.

Second approach

The second approach presented in this thesis focuses on the possibility to alter the wave propagation properties of electromechanical metamaterials. The main idea is to exploit adaptive elements to directly *control the dynamic properties of materials*, rather than the vibration response of structures. This approach is based on the combination of the opportunities offered by the metamaterial concept and the additional freedom related to the use of adaptive materials. In case of piezoelectric materials, for instance, the energy exchange between the mechanical and the electrical domain can be applied in a metamaterial context to obtained materials, whose mechanical properties are controlled by simple electrical circuits.

In this work, the effective stiffness of shunted piezoelectric elements is used to control the wave dispersion in periodic media, with focus on tunable bandgaps. Bandgaps are particularly significant because they represent forbidden energy states that in a mechanical structure would lead to frequency ranges free from vibrations. The *goal* is to investigate how the additional degrees of freedom offered by shunted piezoelectric transducers can be used to create, cancel or shift the frequency of the bandgaps in mechanical metamaterials.

1.5 DETAILED RESEARCH OBJECTIVES

In order to address the aforementioned fundamental question and goals, this work has been organized according to the following research objectives:

A. To develop and experimentally verify a common design framework for comparing the damping performance of different shunting techniques.

B. To implement a shunting strategy with focus on the robustness of its vibration reduction performance, so that it represents a reliable source of damping for the host structure.

C. To define a performance index for comparing the dynamic response of passive and adaptive structures.

D. To develop a design strategy that exploits the adaptive elements in order to enlarge the design space to lighter or more functional solutions.

E. To investigate how a periodic arrangement of adaptive elements can be used to create or modify acoustic bandgaps in the wave propagation properties of the host structure.

1.6 NOVEL CONTRIBUTIONS

Despite the comprehensive research on piezoelectric shunt damping, the novelty of this work lies in the investigation of design approaches that are specific to adaptive structures. In details, the original contributions of this dissertation are:

A. A design strategy based on finding a compromised between structural stiffness and damping has been proposed for adaptive structures and applied to a realistic case study.

B. A novel autonomous shunt with a strong robustness with respect to both the amplitude and the frequency of the structural vibrations has been proposed, and its performance has been experimentally verified.

C. A robust method for the measurement of the electromechanical coupling of piezo-augmented structures has been proposed and applied to experimentally verify the effect of relevant electrical and mechanical parameters on the damping performance of selected shunting techniques.

D. A tunable acoustic waveguide has been implemented within a two-dimensional phononic crystal. It demonstrates how a fairly small amount of adaptive material can produce remarkable effects on the wave propagation and dynamic properties of the host structure thanks to the exploitation of the periodicity.

E. Adaptive materials have been applied for the first time as variable-connectivity elements between the constituting elements of a phononic crystal with the final goal of controlling its properties. The originality of the approach lies in the way the properties of the phononic crystal are controlled: the modification of the dispersion relation is obtained neither by changing the bulk material properties nor the geometry of the constituting elements, but the connectivity of the crystal structure. Indeed, the effective stiffness of the shunted piezoelectric transducers has been exploited to manipulate the ability of neighboring elements to interact. This implies an actual control of the crystal periodicity and therefore also of its macroscopic properties.

1.7 STRUCTURE OF THE THESIS

This thesis consists of 9 chapters organized in 4 parts, as described in the following:

PART I The first introductory part consists of this chapter presenting an overview of the motivations and goals of this work, and a second chapter collecting the theoretical fundamentals. In particular, the second chapter presents the basis of the piezoelectric effect while focusing on the origins and implications of the time-dependent effective stiffness of shunted piezoelectric transducers.

PART II The second part is dedicated to vibration reduction using shunted piezoelectric devices. Chapter 3 focuses on modeling different shunt damping strategies. An in-depth investigation of the effects of the electromechanical parameters on the damping performance allows for a comparison of the different strategies. Among the investigated shunting strategies, one is selected and improved for obtaining a reliable, autonomous and robust source of damping in chapter 4. The acquired knowledge is then applied in chapter 5 to a case study, where a non-conventional design approach is proposed and applied to the design of a scaled model of an adaptive propeller blade.

PART III The third part focuses on the wave propagation properties of electromechanical metamaterials. Chapter 6 introduces the peculiarities of a design based on the metamaterial approach, where the final properties emerge from the organization of the building blocks and the resulting band structure. The following two chapters present two extreme ways on how shunted piezoelectric transducers can interfere with the presence of bandgaps in the band structure of periodic systems. In chapter 7, resonant shunted discs are used to create and tune a bandgap in a two dimensional waveguide. In chapter 8, resonant shunted discs are used as tunable connecting elements to open a tunable passband in the middle of a bandgap in a phononic crystal.

PART IV In the last part, a brief summary, closing statements and implications of the research findings are presented.

2 FUNDAMENTALS OF PIEZOELECTRIC SHUNT DAMPING

This chapter presents the fundamentals of piezoelectricity and the principles of piezoelectric shunt damping. Particular attention is placed on the definition of the time-dependent effective stiffness of shunted piezoelectric transducers, since it is responsible for both (i) the dissipation of energy in piezoelectric shunt damping and (ii) the mechanical impedance mismatch that is exploited in last chapters of this work with the metamaterial approach.

2.1 PIEZOELECTRIC MATERIALS

Piezoelectricity was first observed by Pierre and Jacques Curie in the late nineteenth century in some natural materials. It is the property of certain materials that exhibit a reciprocal electromechanical coupling: on one side, a mechanical deformation causes an electrical displacement *(direct piezoelectric effect)*; on the other side, a mechanical strain arises when an electric field is applied *(converse piezoelectric effect)*.

2.1.1 *Physical basis of the piezoelectric effect*

One of the most important material properties in relation to the piezoelectricity is the *electric polarization*. In a *dielectric* material, the application of an external electric field E leads to electric dipoles, which can be visualized by thinking of a positive and a negative charge separated by a certain distance. When the structure of the material is such that in absence of external electric fields the centers of positive and negative electrical charges do not coincide, the material is said to exhibit a *spontaneous polarization*. Moreover, if the domains with spontaneous

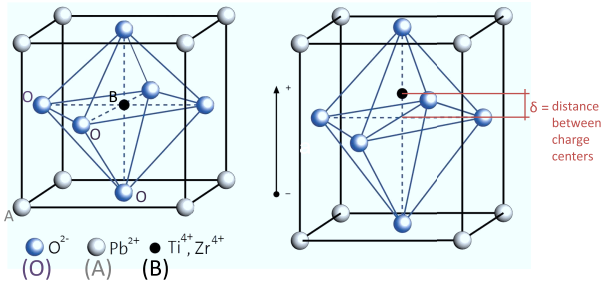

Figure 2.1: PZT crystal structure (ABO_3) above (left) and below (right) the Curie temperature T_C.

polarization can be oriented by an external electric field, the material is said to be *ferroelectric*.

Ferroelectricity is not enough to enable the piezoelectric effect. In their original state, these materials are isotropic in the sense that the electric dipoles are randomly distributed and do not show any macroscopic polarization. In order to exhibit a piezoelectric effect, the electric dipoles have to be aligned and parallel along a dominant polarization direction in the material microstructure. Piezoelectricity can be found in natural crystals, such as quartz and Rochelle salt, synthetic ceramics, as the well-known lead-zirconium-titinate (PZT), but also in polymers, such as polyvinylidene fluoride (PVDF).

Most of the current piezoelectric materials belong to a class of ceramics with a crystalline structure of the *perovskite* type, ABO_3. In the idealized unit cell of such a compound, type 'A' atom sits at corner positions, type 'B' atom sits at body center position and oxygen atoms sit at face centered positions. A classic example of *perovskite*-type materials is the PZT ($Pb[Zr_xTi_{1-x}]O_3$, with $0 \leqslant x \leqslant 1$), whose crystal structure is schematically shown in figure 2.1. Above the Curie temperature, the PZT has a cubic lattice whose charge centers coincide and no electric dipoles are present. On cooling down below the Curie temperature, the crystalline structure of the PZT passes through a lattice distorting phase transformation which causes the formation of electric dipoles.

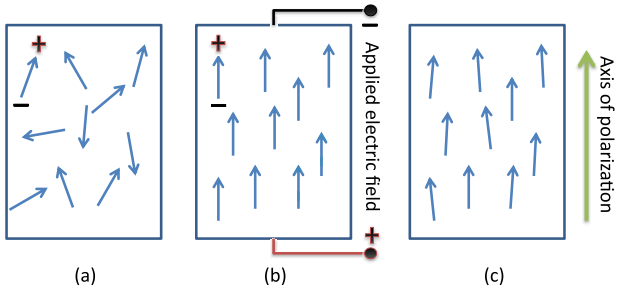

Figure 2.2: Poling process of piezoelectric materials: (a) randomly distributed electrical dipoles due to the crystal structure, (b) polarization in DC electric field, (c) residual polarization after electric field is removed (Leo, 2007).

PZT is a synthetically produced ceramic that, after sintering, is generally isotropic, since the electrical dipoles due to the crystal structure are randomly distributed. It is the *poling process* that is therefore responsible for the appearance of piezoelectric properties (see figure 2.2). This process can take place either at room temperature or just below the *Curie temperature* so that the dipoles can freely rotate. If the material is placed in a strong static electric field (typically 2 kV/mm), the dipoles are aligned along the direction of the electric field. After reducing the temperature and switching off the electric field, the majority of the dipoles will remain oriented.

After the poling process, when an electric field is applied to the piezoelectric material, the electric dipoles will be attracted by the opposite charges, causing a movement of the dipoles and a corresponding strain in the surrounding material. This is the physical basis for the *converse piezoelectric effect*. Similarly, if a mechanical strain is applied to the piezoelectric material, the electric dipoles will be forced to move, and this motion of charges will produce a charge flow at the faces of the material. This is the physical basis for the *direct piezoelectric effect*.

2.1.2 *Linear constitutive equations*

The basic properties of piezoelectric materials are expressed mathematically as a relationship between two mechanical variables, the stress and the strain tensors, and two electric variables, the electric field and electric displacement vectors. In this work the Voigt notation is used, so that the stress and strain tensors are represented respectively by the one-dimensional arrays $\underline{T}$ and $\underline{S}$ (size 6×1), and the electric field and electric displacement are represented by the one-dimensional arrays $\underline{E}$ and $\underline{D}$ (size 3×1), respectively. Even though the presence of a hysteretic behavior is an inherent property of ferroelectric and piezoelectric materials, when the strain and the electric field are small, both the direct and converse piezoelectric effects are considered linear and can be described by a matrix expression:

$$\left\{ \begin{array}{c} \underline{T} \\ \underline{D} \end{array} \right\} = \left[\begin{array}{cc} \underline{\underline{c}}^{E} & -\underline{\underline{e}}' \\ \underline{\underline{e}} & \underline{\underline{\epsilon}}^{S} \end{array} \right] \left\{ \begin{array}{c} \underline{S} \\ \underline{E} \end{array} \right\} \tag{2.1}$$

where $\underline{\underline{c}}^{E}$ is the mechanical stiffness matrix at constant electric field (size 6×6), $\underline{\underline{e}}$ is the piezoelectric stress coupling matrix (size 3×6) and $\underline{\underline{\epsilon}}^{S}$ is the permittivity matrix at constant strain (size 3×3) (ANSI/IEEE, 1988). On the diagonal we can see the constitutive equations of a mechanical and electrical material respectively. The electromechanical coupling is represented by the off-diagonal terms. The relationship is symmetric, representing the reciprocity between the electromechanical transductions mechanism in the material. The first 6 lines of the linear system describe the converse piezoelectric effect (actuator equation), while the last 3 lines describe the direct piezoelectric effect (sensor equation).

The same relationships can be written with different combination of independent/dependent variables. For example, an equivalent formulation could be:

$$\left\{ \begin{array}{c} \underline{S} \\ \underline{D} \end{array} \right\} = \left[\begin{array}{cc} \underline{\underline{s}}^{E} & \underline{\underline{d}}' \\ \underline{\underline{d}} & \underline{\underline{\epsilon}}^{T} \end{array} \right] \left\{ \begin{array}{c} \underline{T} \\ \underline{E} \end{array} \right\} \tag{2.2}$$

where $\underline{\underline{s}}^E$ is the mechanical compliance matrix at constant electric field, $\underline{\underline{d}} = \underline{\underline{e}}\,\underline{\underline{s}}^E$ is the piezoelectric strain coupling matrix and $\underline{\underline{\epsilon}}^T = \underline{\underline{\epsilon}}^S + \underline{\underline{e}}\,\underline{\underline{d}}'$ is the permittivity matrix at constant stress.

2.1.3 *Electromechanical boundary conditions*

Mechanical compliance and electrical permittivity depend on the boundary conditions

The relationships described by equations 2.1 or 2.2 alone do not allow for a complete definition of the electromechanical response of a piezoelectric device. The electromechanical coupling implies that the response of the material depends on both the mechanical and electrical boundary conditions. For instance, the mechanical stiffness of a piezoelectric device depends on the electrical boundary conditions (open circuit or short circuit), and the electric permittivity at constant stress (ϵ^T) differs from the one at constant strain (ϵ^S).

The difference between the mechanical compliance (or electric permittivity) in the open and short circuit state (stress-free and strain-free condition) is related to the piezoelectric coefficients and is normally used to describe the electromechanical coupling of a piezoelectric material. The ANSI/IEEE Standard on Piezoelectricity (ANSI/IEEE, 1988) defines the *coupling factors* k_{ij} as:

> *"The coupling factors are non-dimensional coefficients which are useful for the description of a particular piezoelectric material under a particular stress and electric field configuration for conversion of stored energy to mechanical or electric work. The coupling factors consist of particular combinations of piezoelectric, dielectric, and elastic coefficients. Since they are dimensionless, it is clear that the coupling factors serve to provide a useful comparison between different piezoelectric materials independent of the specific values of permittivity or compliance, both of which may vary widely."*

Under specific assumptions associated with the considered problem, the full constitutive equations (equations 2.1 or 2.2) can be reduced to a subset of relationships. Among others, the two most common operating modes of a piezoelectric transducer are the

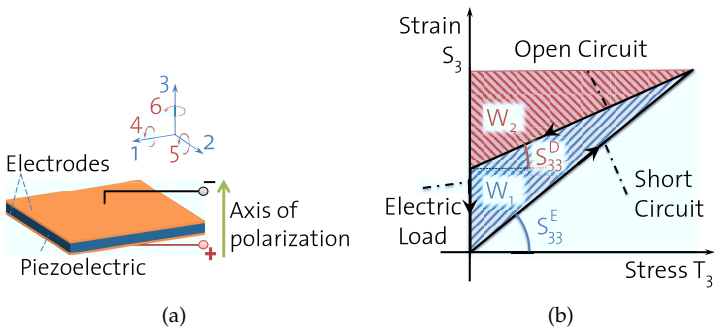

Figure 2.3: Piezoelectric plate (a) and graphic illustration of conversion from mechanical to electrical work (b).

31 and the 33 operating modes. Assume we have a small plate of piezoelectric material, as the one shown in figure 2.3a. The 33 operating mode corresponds to the condition where the only non-zero stress and electric field are in the 3 direction. Under these assumptions, the constitutive equations can be reduced to:

$$\begin{Bmatrix} S_3 \\ D_3 \end{Bmatrix} = \begin{bmatrix} s^E_{33} & d_{33} \\ d_{33} & \epsilon^T_{33} \end{bmatrix} \begin{Bmatrix} T_3 \\ E_3 \end{Bmatrix} \tag{2.3}$$

The mechanical compliance in the short circuit case ($E_3 = 0$) is S^E_{33}, while the open circuit one (obtained by setting $D_3 = 0$ in Eq. 2.3) is $s^D_{33} = s^E_{33}\left(1 - \frac{d^2_{33}}{s^E_{33}\epsilon^T_{33}}\right)$. The term $\frac{d^2_{33}}{s^E_{33}\epsilon^T_{33}}$ represents the change of compliance/stiffness, and it is the square of the piezoelectric coupling factor for the 33 mode:

$$k_{33} = \frac{d_{33}}{\sqrt{s^E_{33}\epsilon^T_{33}}} \tag{2.4}$$

Mathematically, this factor is related to all three piezoelectric material properties: mechanical compliance, dielectric permittivity and piezoelectric strain coefficient. Physically, this factor can be related to the amount of energy exchanged between the mechanical and the electrical domain, as illustrated in figure 2.3b.

Consider the same piezoelectric plate of figure 2.3a in a short circuit condition, so that the mechanical compliance is s_{33}^E. The application of a stress T_3 results in strain field and, since the element is free to expand in the plane 1−2, T_3 is the only nonzero stress component. At this point in the cycle, the piezoelectric plate is switched to an open circuit condition, the applied stress is reduced to zero, and the mechanical work W_2 is released. It is then connected to an ideal electric load to complete the cycle. As work is performed on the electric load, the strain returns to its initial state. The square of the coupling factor represents the ratio between the work W_1, done on the electric load, and the initial mechanical work done on the piezoelectric element $W_1 + W_2$. For the illustrated operating mode, the square of the coupling factor k_{33} is:

$$(k_{33})^2 = \frac{W_1}{W_1 + W_2} = \frac{s_{33}^E - s_{33}^D}{s_{33}^E} = \frac{d_{33}^2}{s_{33}^E \epsilon_{33}^T} \tag{2.5}$$

2.2 SHUNTED PIEZOELECTRIC TRANSDUCERS

Several shunting strategies have been proposed in the past years

The so-called piezoelectric shunt damping consists in connecting an electrical shunt to the terminals of a piezoelectric transducer, with the goal of reducing the structural vibrations with a lightweight and integrable method. This method takes advantage of the relatively strong electromechanical coupling exhibited by piezoelectric ceramics. As the piezoelectric element - bonded on or embedded in the structures - strains, a portion of the mechanical vibration energy is converted into electrical energy and dissipated in the electrical circuit.

The technique was firstly introduced by Forward (1979) and, after his pioneering work, many different electrical shunt topologies have been proposed. These shunts can be categorized into passive and active[1], as well as in linear and nonlinear shunts, as shown in table 2.1.

1 In the context of piezoelectric shunt damping, the terms 'active' and 'passive' refer to techniques that add or do not add external energy to the system, respectively (Niederberger, 2005).

Active	Linear	Negative capacitance shunts
		Active-passive shunts
	Non-linear	Switching shunts
Passive	Linear	Resonant shunts (single or multi mode)
		Resistive shunts
		Capacitive shunts
	Non-linear	State switching shunts
		Synchronized switching shunts
		Variable resistor shunts

Table 2.1: Different types of shunt networks for damping (Niederberger, 2005)

Active and passive shunts

Active shunts are generally quite effective but, like all the active techniques, they often require complex systems and a large amount of external energy. Moreover, since external energy is injected into the system, stability is not guaranteed. On the other hand, passive piezoelectric damping is usually appreciated because of its simplicity and the fact that the system is always stable. The simplest passive shunt consists in connecting the piezoelectric element to a resistor, even if it is not very effective in damping the vibrations. Better performance can be achieved with the resonant shunt (Hagood and von Flotow, 1991), in which an electrical oscillation is created by the capacity of the piezoelectric patch combined with a resistor and an inductor arranged in a series connection. Although excellent damping performance can be achieved, this shunt requires an accurate tuning between the mechanical and the electrical frequencies, and thus it suffers from high sensitivity to changes in the mechanical and electrical parameters (Andreaus and Porfiri, 2007). Moreover, the tuning at low frequencies implies the need for large inductance (tens or hundreds of Henrys) that, for a purely passive implementation, would require unacceptably large and heavy coils.

Semi-passive shunts

To tackle the aforementioned drawbacks, several semi-passive implementations have been proposed. In semi-passive methods

some external energy is required by the components of the system to operate (for instance, the power required by the electronic components of a circuit), but this external energy is not injected into the host structure so that they should not be categorized as purely active methods. In a first family of these systems, the coil required by the resonant shunt is substituted by a synthetic inductor that can be also adaptively tuned (Niederberger et al., 2004). Another family of semi-passive shunts is represented by the non-linear switching techniques, based on the idea of repeatedly changing the stiffness of the structure in order to dissipate energy.

The implementations of shunting strategies that use electronic components in the circuits is categorized as semi-passive when the external power required for their operation is not injected in to the system. Compared to the active methods, the semi-passive systems turn out to be unconditionally stable. Compared to the passive methods, they are less sensitive to changes in the mechanical structure characteristics. Moreover, since the energy required by the semi-passive shunts can be very small, some of them are suitable for a self-powered implementation.

2.2.1 *Equivalent model of a piezoelectric transducer*

Consider a piezoelectric transducer working in the 33 operation mode, like the one introduced in the previous section. The material constitutive equations 2.3 can be rewritten using S_3 and E_3 as independent variables:

$$\begin{cases} T_3 = \frac{1}{s_{33}^E} S_3 - \frac{d_{33}}{s_{33}^E} E_3 \\ D_3 = \frac{d_{33}}{s_{33}^E} S_3 + \left(\epsilon_{33}^T - \frac{d_{33}^2}{s_{33}^E} \right) E_3 \end{cases} \tag{2.6}$$

If the transducer has a surface A and a thickness L, the equations describing the relations between the force on the transducer $F_p = AT_3$, its elongation $u = LS_3$, the voltage $V = LE_3$ and the current $I = A\dot{D}_3$ can be obtained by integrating over the surface A both the previous equations, and differentiating in time the second one:

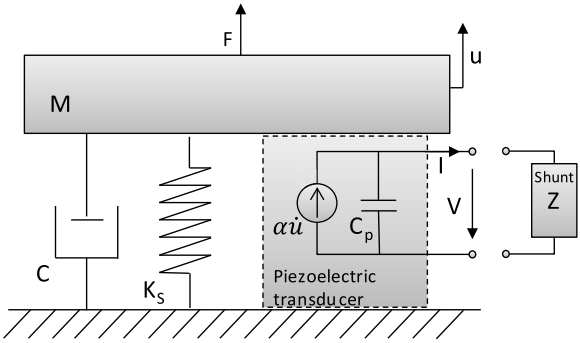

Figure 2.4: SDOF system with a piezoelectric transducer and a generic shunt

$$\begin{cases} F_p = K_p u - \alpha V \\ I = \alpha \dot{u} + C_p \dot{V} \end{cases} \tag{2.7}$$

where $K_p = \frac{AL}{s_{33}^E}$ is the stiffness at constant electric field, $\alpha = \frac{A d_{33}}{s_{33}^E L}$ is the electromechanical coupling and $C_p = \left(\epsilon_{33}^T - \frac{d_{33}^2}{s_{33}^E}\right)\frac{A}{L}$ is the capacity of the transducer at constant strain. The first equation describes the force acting on the transducer as the sum of an elastic and an actuating contributions, while the second one represents the parallel of a current source and a capacitor, as shown in figure 2.4.

2.2.2 *Time dependent effective stiffness*

The generic Single Degree Of Freedom system depicted in figure 2.4 has a mass M, a damping element C and a stiffness K_S and is described by the following equation

$$s^2 M u + s C u + K_s u = F - F_p \tag{2.8}$$

where s is the Laplace variable, u is the displacement of the mass and F is an external force acting on the structure. This simple

example can be representative of each eigenmode of a more complex structure by reducing the finite element model of the structure with a modal condensation, as explained in (Thomas et al., 2009).

By replacing the expression of F_p from equation (2.7) in equation (2.8), the following set of equations is obtained:

$$\begin{cases} s^2 M u + s C u + K u = F + \alpha V \\ I = s\alpha u + s C_p V \end{cases} \tag{2.9}$$

where $K = K_S + K_p$. In an analogous way to how the concept of coupling factors was introduced in the previous section, the dynamic of the system is undefined until a relation between I and V is specified. This relation can depict a situation of short circuit ($V = 0$), open circuit ($I = 0$), or more in general

$$V = -Z(s, u) I \tag{2.10}$$

where Z is a generalized impedance that describes the shunt connected to the piezo. This relation allows for closing the loop, leading to the following equation:

$$\left(s^2 M + s C + K + \frac{s\alpha^2 Z(s, u)}{1 + s C_p Z(s, u)} \right) u = F \tag{2.11}$$

Equation (2.11) is strictly valid only for linear shunts, i.e. when Z is a complex impedance in the Laplace domain (such as for the resonant shunt). On the other hand, in the case of non linear shunts (i.e. when the relation between V and I is not linear, like for the switching shunt discussed in chapter 4), Z has to be considered a symbol representing the electrical behavior of the shunt that results in an additional time-variable stiffness.

The shunted piezo behaves as a time-variable stiffness element

The effect of the shunted piezo on the structure is therefore to add a time-variable term to the stiffness. This contribution depends on the size and position of the piezoelectric element (represented by the factor α in equation 2.11) and on the impedance of the electrical circuit. For example, in the short circuit configuration $Z = 0$ and the corresponding stiffness is $K_{SC} = K$. In the open circuit case, $Z \to \infty$ and the resulting

stiffness $K_{OC} \rightarrow K + \frac{\alpha^2}{C_p}$. This change of stiffness allows introducing the *generalized electromechanical coupling coefficient* as an indicator of the authority of the piezoelectric patches on the structures (in a similar way to the coupling factors previously introduced for describing the piezoelectric material properties). It is defined as

$$K_{ij}^2 = \frac{K_{OC} - K_{SC}}{K_{SC}} = \frac{\alpha^2}{KC_p} \tag{2.12}$$

If the force applied on the structure (F) is represented in a force-displacement diagram, damping is achieved when the generalized impedance Z is such that the corresponding variable stiffness creates a hysteresis in the same diagram. The electric shunt can then be designed in order to obtain a certain shape or maximize this hysteresis. The damping energy can be calculated by multiplying the force applied by the piezo (αV in Equation (2.9)) by the velocity and integrating over the time. If a periodic response of the structure is assumed, the energy per cycle D that is transferred from mechanical energy to electrical energy and then dissipated corresponds to the area of the hysteresis in the force-displacement diagram:

$$D = \int_0^T \alpha V \dot{u} dt = \oint \alpha V dq \tag{2.13}$$

The loss factor η is obtained as the ratio between the dissipated energy D and the elastic energy of the structure E:

$$\eta = \frac{D}{2\pi E} = \frac{\oint \alpha V dq}{\pi K u^2} \tag{2.14}$$

In chapter 3, the integral of equation (2.13) is solved for different shunting strategies.

2.2.3 *Resonant shunt*

The resonant shunt is a type of linear, passive shunt that consists of a series of a resistor R and an inductor L connected in parallel to a piezoelectric transducer. Besides its application for vibration reduction purposes, the extreme values of the resulting

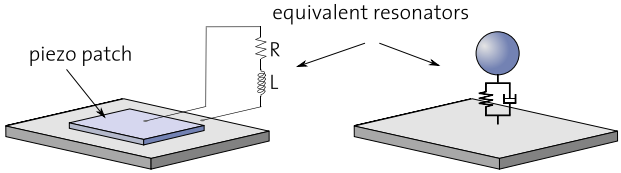

Figure 2.5: Analogy between electrical and mechanical resonators

piezoelectric effective stiffness are well suited to modify the wave propagation properties of periodic systems.

The complex electrical impedance of the resonant shunt is:

$$Z(s) = R + sL \tag{2.15}$$

Its working principle is the same of the well-known tuned mass damper, where an electrical oscillation is added to the system instead of a mechanical one, see Fig. 2.5. The combination of the inductance with the capacity of the piezoelectric patch C_p creates an electrical oscillator with a resonance frequency $\omega_{LC} = \frac{1}{\sqrt{LC_p}}$. Damping is achieved when this frequency is tuned to the frequency of the eigenmode to be damped: the electrical resonance amplifies the value of voltage acting on the transducer and creates a phase lag between the same voltage and the displacement, which results in an elliptical hysteresis in the force-displacement diagram. Like in a mechanical tuned mass damper, the vibration energy is transferred from the targeted eigenmode to the resonating auxiliary system, where it is then dissipated.

When substituting equation 2.15 in 2.11, the effective stiffness of the resonant shunted piezo (see figure 2.6) can be written as:

$$K_{RL}(s) = K\left(1 + K_{ij}^2 \frac{sR/L + s^2}{\omega_{LC}^2 + sR/L + s^2}\right) \tag{2.16}$$

As in a purely mechanical oscillator, the real part of the effective stiffness of the piezoelectric resonator is strongly reduced (approaching zero, depending on the value of electrical resistance in the circuit) just before resonance and exhibits a maximum just

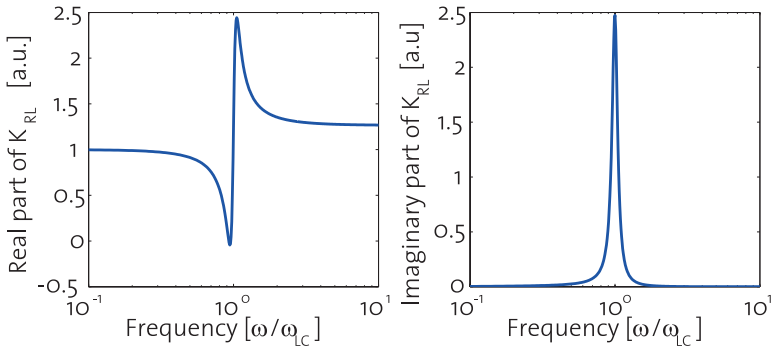

Figure 2.6: Real and imaginary part of the effective stiffness of a piezoelectric transducer connected to a resonant shunt

after. When shunted piezoelectric transducers are arranged in a periodic configuration, these extreme variations in the stiffness can be tuned to obtain a controllable modification of the wave propagation properties of the periodic system. This concept is at the basis of the investigation presented in part iii. On the other hand, the imaginary part is related to the out-of-phase response and indicates the amount of dissipated energy. The sharp peak in correspondence of the resonance frequency highlights the poor robustness of this technique with respect to changes in the tuning frequencies. A deeper study on the dissipated energy and the damping properties is discussed in part ii.

Part II

PIEZOELECTRIC SHUNT DAMPING: MODELING, IMPLEMENTATION AND DESIGN

3

MODELING OF PIEZOELECTRIC SHUNT DAMPING

This chapter presents an in-depth investigation into the modeling of piezoelectric shunt damping and the electromechanical parameters that defines its damping performance. A robust method for the measurement of the electromechanical coupling is proposed and applied to experimentally verify the accuracy of the presented model in predicting the loss factor. An outcome of this method is the possibility to describe the attainable damping as a function of a specific damping, distinctive for each shunt type, and the ratio between the modal strain energies in the piezoelectric transducer and the whole system. The results presented in this chapter have been summarized and published in the following journal paper:

> T. Delpero, A. Bergamini, and P. Ermanni, "Identification of electromechanical parameters in piezoelectric shunt damping and loss factor prediction," *J. Intell. Mater. Syst. Struct.* **2013**, 24 (3), 287-298

3.1 AN ENERGY-BASED APPROACH

The piezoelectric shunt damping method takes advantage of the possibility to modify the effective mechanical stiffness of the structure by changing the electrical boundary conditions, as explained in chapter 2. The state switching strategy, for instance, exploits the change of stiffness between the open and short circuit configuration (Clark, 2000). In each cycle of the vibration, the state of the electrical circuit is switched four times in order to obtained an hysteresis in the force-displacement diagram and, therefore, to dissipate energy. When the piezoelectric element is in the open circuit state, electric charges are displaced between the electrodes by the direct piezoelectric effect; the energy is

dissipated by Joule heating once the circuit is closed and the accumulated charges flow through a resistor.

The analysis of the damped response of structures with shunted piezoelectric elements has been object of different studies (Davis and Lesieutre, 1995; Thomas et al., 2012; Ducarne et al., 2010) that showed how the obtained damping is shown to depend on the electromechanical coupling and the characteristics of the electrical shunt, independently of the materials and the dimensions of structure. In the following, a unifying approach based on energy considerations is proposed. The aim is the development of a common framework that allows for comparing the damping performance of different shunts and ultimately also other vibration reduction techniques.

3.1.1 *Switching shunt techniques*

State and synchronized switching shunts

Among the non-linear shunts, the family of the switching techniques is promising because of its robustness and possible self-powered implementation. State switching (SS) (Clark, 2000) and synchronized switching damping (SSD) (Corr and Clark, 2002; Lefeuvre et al., 2006; Richard et al., 2000) fall into this category. Concerning the former, the piezoelectric patch is switched from an open to a short circuit state at specific times of the vibration cycles (see figure 3.1a). In the latter the piezoelectric patch is cyclically switched from an open circuit state to a specific electric impedance in order to get a fast change in the voltage across the piezo and immediately opened again (see figure 3.1b). This impedance can be a simple resistor (in the case of the SSDS), or inductance (SSDI) or a voltage source (SSDV). Different switching strategies reflect in different hysteresis in the voltage-displacement diagram and in the relative force-displacement diagram, as shown in figure 3.2.

The synchronized switching techniques allow for a larger hysteresis, and thus more damping, than the state switching. The voltage on the piezo is in anti-phase with the velocity, and the resulting force counteracts the vibrations of the system. The switch occurs therefore when the displacement reaches a maximum or a minimum (i.e. the velocity is zero).

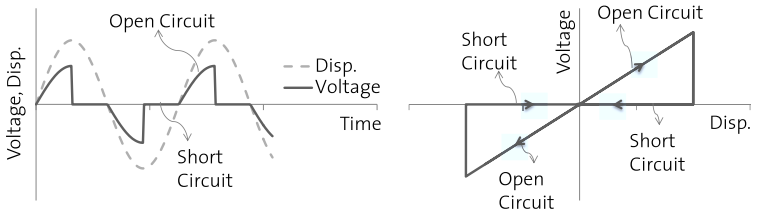

(a) State switching shunt

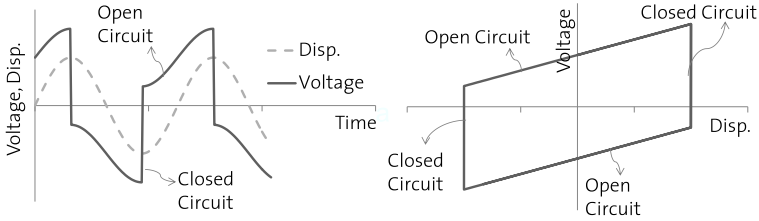

(b) Synchronized switching shunt

Figure 3.1: Qualitative behavior of the state (a) and synchronized (b) switching shunts when the structure is forced to a sinusoidal response. For both the shunting strategies, the voltage on the piezoelectric actuator is plotted as a function of time and displacement.

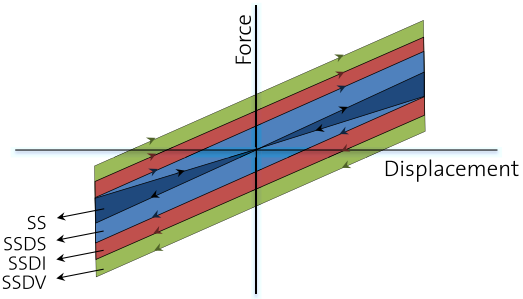

Figure 3.2: Qualitative representation of the hysteresis in the force-displacement diagram obtained with different switching shunting techniques: SS, SSDS, SSDI and SSDV. The area of the hysteresis is proportional to the dissipated energy.

Quality factor γ

In the case of the SSDS the circuit is closed on a small resistor and the voltage drops from the open circuit value to zero. If the switch occurs on an inductance (SSDI), a partial voltage inversion is obtained through an electrical oscillation due to the combination of the capacitor of the piezo and the inductance. The overshoot of the voltage inversion is characterized by the quality factor of the shunt $\gamma = V_m/V_M$ (described in figure 3.3), where V_M and $-V_m$ are the values of the voltage respectively before and after the switch. The absolute value of the voltage after the inversion is lower than the initial value, because a part of the energy stored on the piezoelectric elements capacitance is lost in the parasitic resistance of the switching network.

Since the resulting force acting on the structure is proportional to the voltage and the area of the hysteresis is directly related to the voltage inversion, the factor γ should be as large as possible in order to increase the dissipated energy. The SSDS can be considered a particular case of the SSDI when γ is null, while the SSDV is as an active technique for improving the quality factor, since a voltage source V_s is added in series with the inductance in order to increase the voltage drop.

Dissipated energy per cycle

The resulting dissipated energy per cycle D can be calculated as the area of the hysteresis in the force-displacement diagram, and it can be analytically solved for the different switching shunting techniques if a sinusoidal displacement is assumed (Badel et al., 2006), using equations 2.13 and 2.14. The results are reported in table 3.1, where α, C_p and u_{max} are respectively the electromechanical coupling, capacity of the piezo and the maximum displacement of the structure in the cycle as introduced in section 2.2.

Table 3.1: Dissipated energy per cycle and loss factor for different switching shunt techniques

	Dissipated energy per cycle D	Loss factor η
SS	$\frac{\alpha^2}{C_p} u_{max}^2$	$\frac{K_{ij}^2}{\pi}$
SSDS	$4\frac{\alpha^2}{C_p} u_{max}^2$	$4K_{ij}^2$
SSDI	$4\frac{\alpha^2}{C_p} u_{max}^2 \frac{1+\gamma}{1-\gamma}$	$\frac{4K_{ij}^2}{\pi}\frac{1+\gamma}{1-\gamma}$
SSDV	$\left(4\frac{\alpha^2}{C_p} u_{max}^2 + 4\alpha u_{max} V_s\right)\frac{1+\gamma}{1-\gamma}$	$\frac{4K_{ij}^2}{\pi}\left(1+\frac{V_s C_p}{\alpha u}\right)\frac{1+\gamma}{1-\gamma}$

These analytical expressions for the loss factor are only valid under the assumption of a periodic single-tone response. Since the switching shunt introduces a step input every time the circuit is closed, this assumption may be violated depending on the amplitude of the voltage change and the authority of the piezo on the structure. Indeed, Ducarne et al. (2010) studied the response of the SSDI without the assumption of a periodic response and showed that, for a given value of the generalized coupling coefficient, there is a maximum value of γ that allows to maximize the damping while, if it is exceeded, the step input causes a beating phenomenon to appear with consequent irregular switching times and poor damping performance. However, this limit corresponds to very high value of quality factor that are not likely to be exceeded in passive or semi-passive implementations, since the inherent electrical losses of the circuit restrict the quality factor. Moreover, the assumption of a periodic response is still acceptable when this limit is not exceeded (Ducarne et al., 2010), and the analytical expressions of the loss factor previously explained are valid.

In the case of the SSDI, the performance of the shunt is described by the quality factor γ, and further qualified by the synchronization of the switch. In order to maximize the area of the hysteresis and the damping, the switch should occur in correspondence of a maximum or minimum of the displacement. In the case of a periodic response of the system, if δ is the

difference in radiant between a maximum of the displacement and the switch, as shown in figures 3.3, the resulting loss factor is:

$$\eta_{SSDI} = \frac{4K_{ij}^2}{\pi}\frac{1+\gamma}{1-\gamma}\cos^2(\delta) = \lambda K_{ij}^2 \tag{3.1}$$

where the factor λ includes all the electrical performance factors of the shunt, both in terms of quality factor and synchronization of the switch.

Maxima and minima detection

The detection of the maximum and minimum is therefore a critical aspect, especially in the case of multi-modal or random response. When the response of the structure is dominated just by a single eigenmode, the maximum and minimum detection is not an issue since it can be obtained by detecting the change of the sign of a signal that is $\pi/2$ out of phase with the displacement. This can be easily implemented with an additional piezoelectric patch bonded on the structure (Niederberger and Morari, 2006) which generates a signal proportional to its strain and, thus, to the displacement of the structure: this signal, if processed by a low pass filter that introduces the desired phase lag, can be then used for controlling the switch. On the other hand, when the response of the structure involves more than one eigenmode, different strategies have been proposed in literature (Lallart et al., 2008) that can be used for the detection of global maxima and minima. For instance, a possibility is given by placing the additional piezoelectric patch in such a way that it responds only to the eigenmode to be damped.

3.1.2 *Resonant shunt*

Tuning of the electrical parameters

The resonant shunt (denoted here as RL shunt) consists of a series of a resistor R and an inductance L. As introduced in section 2.2, it leads to an elliptical hysteresis in the force-displacement diagram. Different strategies for the tuning of resonant shunt circuits have been developed, either based on maximum damping in a root locus or pole placement context, or by minimization of the frequency response magnitude (Hagood and von Flotow, 1991). Optimal values for the resistor and the

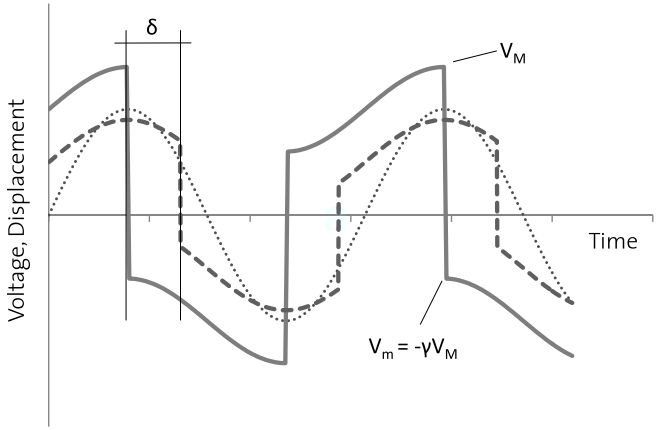

(a) Time history of displacement (thin dotted line), voltage with non-synchronized switch (dashed line) and voltage with synchronized switch (thick continuous line)

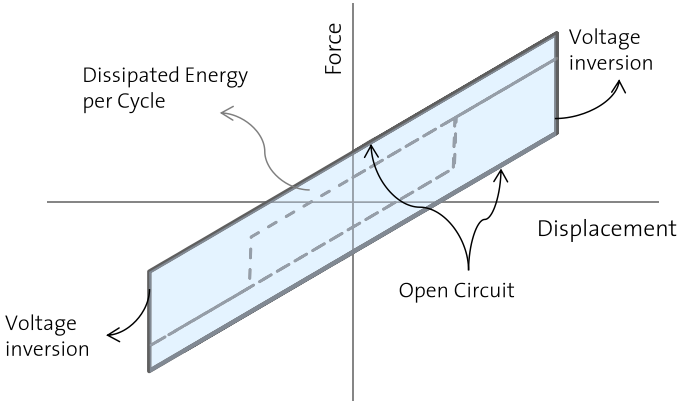

(b) Force-Displacement diagram for synchronized switch (continuous line) and non-synchronized switch (dashed line)

Figure 3.3: Qualitative illustration of the SSDI principle: comparison between a synchronized and non-synchronized switch.

inductance obtained by minimization of the frequency response amplitude are:

$$L_{opt} = \frac{1}{\omega_n^2 C_p (1 + K_{ij}^2)} \tag{3.2a}$$

$$R_{opt} = \frac{\sqrt{2} K_{ij}}{(1 + K_{ij}^2) \omega_n C_p} \tag{3.2b}$$

where ω_n denotes the structure resonance frequency to be damped. The value of the inductance is chosen in order to tune the electrical resonance frequency, while the value of the resistor represents the damping of the electrical circuit. This closed-form solution has been obtained neglecting the inherent damping, but Hollkamp (1994) showed that for lightly damped structures, the undamped optimal solution assumptions are still valid.

Loss factor

The linear complex impedance of the resonant shunt allows for an explicit expression of the effective stiffness of the shunted piezo (see equation 2.16). Due to the elliptical shape of the hysteresis in the force-displacement diagram, the loss factor (equation 2.14) corresponds to the ratio between the imaginary and real part of the complex effective stiffness (Ungar and Edward M. Kerwin, 1962). The optimal values of R and L for the complex impedance Z lead to the following expression of the loss factor:

$$\eta_{RL} = \left. \frac{\mathrm{Im}\left(K_{RL}(s)\right)}{\mathrm{Re}\left(K_{RL}(s)\right)} \right|_{s=j\omega_{SC}} = \frac{K_{ij}}{\sqrt{2}} \tag{3.3}$$

3.2 ELECTROMECHANICAL COUPLING AND STRAIN ENERGY

The generalized electromechanical coupling coefficient K_{ij} has been introduced in section 2.2 as a measure of the energy exchanged between the mechanical and the electrical domain for a single-degree-of-freedom system. In the case of a generic structure with multiple transducers and eigenmodes, equations 2.8 and 2.11 are still valid if the response of the structure is mainly governed by a single eigenmode that is well separated from the others. In this case, the coefficient K_{ij} refers to the authority of the jth transducer on the ith eigenmode, and the mass, damping

and stiffness coefficients have to be considered as modal coefficients. The generalized electromechanical coupling coefficient can be defined using the values of the resonance frequency $\omega_{SC,i}$ of the ith eigenmode with short-circuited transducers, and the frequency $\omega_{OC,ij}$ of the same mode with the jth transducer in open-circuit configuration:

$$K_{ij}^2 = \frac{\omega_{OC,ij}^2 - \omega_{SC,i}^2}{\omega_{SC,i}^2} \tag{3.4}$$

An alternative expression for the generalized coupling coefficient is (Hagood and von Flotow, 1991):

$$K_{ij}^2 = \frac{K_{piezo}}{K_{structure} + K_{piezo}} \frac{k_{mn}^2}{1 - k_{mn}^2} = \overline{K} \frac{k_{mn}^2}{1 - k_{mn}^2} \tag{3.5}$$

where $\overline{K}$ is the ratio between the modal stiffness of the short-circuit piezoelectric patch and the modal stiffness of the whole system, and k_{mn} is the electromechanical coupling coefficient of the piezoelectric material. While the generalized coupling coefficient K_{ij} refers to the whole electromechanical system (ith eigenmode of the host structure and jth piezoelectric transducer), the k_{mn} is used for the description of the piezoelectric material under a particular stress (m index) and electric field (n index) configuration for conversion of stored energy to mechanical or electric work. Equation 3.5 reflects the fact that the piezoelectric is arranged in parallel with the host structure stiffness and, thus, just a portion of the total modal strain energy is available in the piezoelectric material to be transformed in electrical energy. In fact, $\overline{K}$ does not only represent the ratio between the modal stiffness of the piezoelectric patch and the whole system, but also between the modal strain energies U:

The piezoelectric is arranged in parallel with the structural stiffness

$$K_{ij}^2 = \overline{K} \frac{k_{mn}^2}{1 - k_{mn}^2} = \frac{U_{piezo}}{U_{total}} \frac{k_{mn}^2}{1 - k_{mn}^2} \tag{3.6}$$

Equations 3.5 and 3.6 show how a stiffer structure will results in a smaller portion of strain energy available in the piezoelectric material to be transformed in electrical energy, and consequentially in a smaller electromechanical coupling and

lower damping. If the expression of the generalized coupling coefficient in equation 3.6 is substituted in the expressions of the loss factor reported in table 3.1, the loss factor can be expressed as a function of the modal strain ratio and of a specific damping η_{sp} characteristic of the piezoelectric material properties and the applied shunt. For example in the case of the SSDI:

$$\eta_{SSDI} = \frac{4}{\pi}\frac{1+\gamma}{1-\gamma}\cos^2(\delta)\frac{k_{mn}^2}{1-k_{mn}^2}\frac{U_{piezo}}{U_{total}} = \eta_{sp}\frac{U_{piezo}}{U_{total}} \tag{3.7}$$

This is a valuable approach for designing structures with shunted piezoelectric patches for mainly two reasons:

A. It suggests the need for a compromise between the stiffness of the structure and the piezoelectric in order to satisfy both the classical strength/stiffness requirements and the damping or dynamic ones.

B. A similar method based on the modal strain energy ratio is typically used for predicting the damping levels in structures comprising layers of elastic and viscoelastic elements and, thus, a comparison between different damping techniques (with viscoelastic layers, passive, active or semi-active shunted piezoelectric) can be performed.

3.3 EXPERIMENTAL ANALYSIS

Aim of the experimental analysis

Vibration tests are conducted on different structures in order to measure the generalized coupling coefficient K_{ij} and the loss factor η attained with RL and SSDI shunts. The aim of these measurements is to verify the analytical expressions of the loss factor presented in the previous section for different combinations of (i) structural stiffness, (ii) size of the piezoelectric transducers and (iii) type of shunting circuit. In particular, the first and the second bending mode of aluminum cantilever beams with piezoelectric patches are investigated. The dimensions and characteristics of the six different configurations used for the tests are reported in table 3.2.

Two different types of piezoelectric transducers are used during the tests. A first one is an in-house manufactured ac-

Table 3.2: Geometric characteristics of the specimens

Test #	Plate [mm]	Piezo [mm]	Eigenmode	ω_{SC} [Hz]
1	200 × 60 × 2	50 × 30 × .1**	2nd bending	240.3
2	200 × 60 × 2	100 × 30 × .2*	2nd bending	238.6
3	140 × 60 × 2	50 × 30 × .1**	1st bending	82.7
4	200 × 60 × 2	50 × 30 × .1**	1st bending	41.2
5	200 × 60 × 2	50 × 30 × .2*	1st bending	43.6
6	200 × 60 × 2	100 × 30 × .2*	1st bending	44.7

*In-house manufactured actuator with PIC255

**Commercial actuator P-876.A11 from PI

tuator (Bachmann and Ermanni, 2010) whose basic piezoelectric material is PIC255 (see the material properties in table 3.3) and has a thickness of 0.2 mm. The second type of transducer is a commercially available actuator P-876.A11 from Physik Instrumente (PI) GmbH & Co, in which the piezoelectric material is PIC 252 (a low-sintering modification of PIC 255) with a thickness of 0.1 mm.

Experimental setup

The block diagram of the experimental setup is shown in figure 3.4: the specimen is excited near the clamping by an electrodynamic shaker, and the force introduced in the structure is measured by an impedance head fixed on the tip of the shaker stinger. The displacement at the tip of the structure is measured by a laser displacement meter. The stimulus signal for the shaker, as well as the response signals in terms of displacement and force, is processed by a PXI system. The stimulus signal is a stepped frequency sweep, and the transfer function between the stimulus and the systems response is calculated by a Lab-View subroutine using the Root Mean Square of the measured signals. Furthermore, in order to measure the quality factor γ and verify

Table 3.3: PIC 255 material properties

Density	ρ	$[kg/m^3]$	7800
Permittivity	$\epsilon_{33}^T/\epsilon_0$	-	1750
Piezoelectric constants	d_{31}	$[10^{-12}\ C/N]$	−180
	d_{33}	$[10^{-12}\ C/N]$	400
	d_{15}	$[10^{-12}\ C/N]$	550
Elastic compliance	S_{11}^E	$[10^{-12}\ m^2/N]$	16.1
	S_{33}^E	$[10^{-12}\ m^2/N]$	20.7

Source: www.piceramic.com

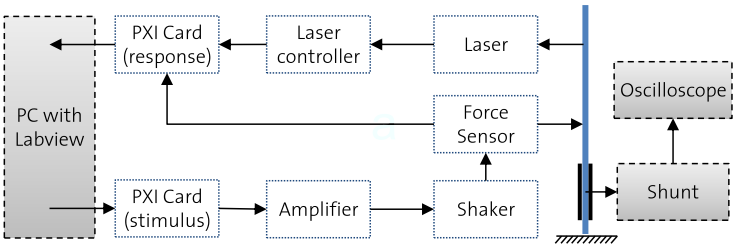

Figure 3.4: Block diagram of the experimental set up.

the correct behavior of the shunt, the values of the voltage on the actuator are measured with an oscilloscope.

The implementation of the SSDI technique requires an additional piezoelectric patch to be bonded on each structure. The patch works as a sensor for detecting the maxima and minima of the strain and displacement, in order to control the switch in the SSDI shunt. It does not contribute to the damping of the vibration, since it is not used as an actuator. During the tests with the resonant shunt, this additional piezoelectric patch is kept in a open circuit configuration.

3.4 ELECTROMECHANICAL COUPLING MEASUREMENTS

The analytical expressions for the loss factor discussed in section 3.1 refer to the generalized coupling coefficient as a key parameter in determining the performance of shunt damping. A reliable experimental identification of this fundamental parameter is essential for developing analytical or numerical models that can be used in the design of shunted-piezo-augmented structures.

Identification by open/short-circuit frequencies

The generalized coupling coefficient may be determined by exploiting the effect of the electric coupling on the mechanical stiffness. In this method, denoted here as OS method, the K_{ij} is identified by using its definition (equation 3.4). The main drawback is that this method is very sensitive to errors in the measure of the resonance frequencies, especially for low value of the coupling coefficient, since the difference between the resonance frequencies may be very small (Porfiri et al., 2007).

Identification by resonant shunt

Another possible approach is related to the use of a resonant shunt. Figure 3.5a reports the mobility functions[1] measured for different values of the resistance of the resonant shunt. As explained by Den Hartog (1956) for a generic tuned mass absorber, all the mobility functions obtained with different levels of damping of the auxiliary system intersect at two points (indicated with S and T in figure 3.5a), and the difference between their corresponding frequencies depends on the coupling between the oscillating systems. Porfiri et al. (2007) showed that, in the case of a resonant shunt where the resistance and the inductor are in parallel and the electrical and the mechanical frequencies match, the difference between the frequencies ω_S and ω_T is directly proportional to the coupling coefficient with the following relationship:

$$K_{ij} = \sqrt{2}\frac{\omega_T - \omega_S}{\omega_{SC,i}} \tag{3.8}$$

This method, denoted here as ST, is much less sensitive to error in the frequencies measurement than the OS one, but it

1 A mobility function is defined as the transfer function between the velocity of the system and the applied force.

requires a very accurate tuning of the electrical frequencies and it is strictly valid only if there is no mechanical damping in the host structure (Hollkamp, 1994). If mechanical damping is present, the mobility functions obtained for different values of the resistance do not intersect anymore in the two points S and T, but in small areas whose size depends on the amount of mechanical damping. For these reasons, the detection of the frequencies ω_S and ω_T can be inaccurate, and the ST method is not always applicable. For example, in a structure with a coupling coefficient of $K_{ij} = 0.06$, a mechanical damping of $\eta_m = 0.01$ will result in an uncertainty of the frequencies of $\frac{\sigma_\omega}{\omega_{SC}} \simeq 0.6\%$ and in a corresponding uncertainty of the estimated coupling of $\frac{\sigma_{K_{ij}}}{K_{ij}} = \frac{2}{K_{ij}} \frac{\sigma_\omega}{\omega_{SC}} \simeq 20\%$.

A fitting procedure

In this work, the generalized coupling coefficient is still measured exploiting the resonant shunt but, instead of trying to identify the frequencies ω_S and ω_T, the whole transfer function $H(j\bar{\omega})$ between the displacement $Y(j\bar{\omega})$ and the force $F(j\bar{\omega})$ is analyzed in a range of frequencies about the resonance. The analytical expression of the transfer function can be obtained from equation 2.11 and equation 2.15:

$$H(j\bar{\omega}) = \frac{Y(j\bar{\omega})}{F(j\bar{\omega})} = \mu \frac{\beta + j\bar{\omega}\delta - \bar{\omega}^2}{(1 + j\eta_m - \bar{\omega}^2)(\beta + j\bar{\omega}\delta - \bar{\omega}^2) + K_{ij}^2 (j\bar{\omega}\delta - \bar{\omega}^2)} \tag{3.9}$$

where $\bar{\omega} = \frac{\omega}{\omega_{SC}}$ is the non-dimensional frequency, μ is the static response of the system, $\beta = \frac{1}{\omega_{SC,i}^2 LC}$ represents the tuning of the electrical circuit, $\delta = \frac{R}{L\omega_{SC,i}}$ is the electrical damping. In the proposed method the amplitudes of the measured transfer function are fitted to the analytical expression, and the value of the generalized coupling coefficient K_{ij} is chosen in order to minimize the least mean square error between the experimental data and the fitted values. Also the electrical parameters β and δ are obtained with the fitting, while the resonance frequency $\omega_{SC,i}$ and the mechanical damping η_m are measured on the same structures when short-circuited.

Table 3.4: Results of the fitting procedure (δ_{fit}, β_{fit} and K_{ij}^{fit}); measurements of the electrical parameters (R, L and C_p)

Test	R	L	C_p	$\frac{R}{L\omega_n}$	δ_{fit}	$\frac{1}{\omega_n^2 L C_p}$	β_{fit}	K_{ij}^{fit}
#	[Ω]	[H]	[nF]	[–]	[–]	[–]	[–]	[–]
1	220	4.3	102	0.034	0.031	1.001	1.001	0.025
2	380	2.9	154	0.088	0.079	0.997	0.997	0.044
3	1.2k	33	105	0.068	0.084	1.070	1.004	0.070
4	4.3k	141	104	0.117	0.136	1.019	1.009	0.073
5	2.9k	161	79	0.064	0.066	1.078	1.007	0.093
6	2.9k	82	154	0.126	0.125	1.005	1.036	0.102

The shape of the two peaks of an ideal RL-shunt response, as the one shown in figure 3.5a, is mainly determined by the parameters K_{ij}, β and δ. The coupling coefficient K_{ij} determines the distance between the intersection areas S and T, while the electrical damping δ defines the amplitude and the sharpness of the two peaks. The tuning parameter β determines whether the two peaks are symmetric with respect to the eigenfrequency of the structure. Its optimal value can be obtained from equation 3.2a as $\beta_{opt} = \frac{1}{1+K_{ij}^2}$. In the experimental tests, however, the value of the inductance L has been simply chosen such that β is as close as possible to unit, since the values of the square of coupling coefficient are of the order of 10^{-4} for the considered structures. The fitting procedure is lightly affected by errors in measurements of the two parameters ω_{SC} and η_m. The inherent mechanical damping η_m affects only the size of the areas of intersection (S and T) between the mobility functions obtained with different values of the electrical damping, while an error in the measure of the ω_{SC} will simply cause a shift on the frequency axis. The results of the fitting procedure are reported in table 3.4.

3.5 LOSS FACTOR MEASUREMENTS

The vibration reduction obtained with the shunted piezo is measured as the difference of the dynamic response at the resonance frequency between the open circuit state and the shunted configuration. In forced harmonic vibration tests, a dB reduction factor is generally used to assess the damping performance. The amount of this reduction depends on both the values of the inherent mechanical damping of the structure and the additional damping attained with the shunting techniques. Therefore, a general comparison between different damping techniques requires the definition of an equivalent loss factor that does not depend on the inherent damping of the structure.

The inherent mechanical damping η_m is mainly due to the clamping of the plate between the supports and is calculated with the half-power method based on the dynamic response of the structure in an open circuit configuration. On the other hand, the total loss factor η_{TOT} can not be calculated with the the half-power method, since the single degree of freedom model is not suitable for the shunted structures: in the case of the resonant shunt, the system must be modeled with two degrees of freedom (the mechanical and the electrical one), while in the case of the non-linear SSDI this is not possible. An equivalent loss factor η_{TOT} is defined as the one that would achieve the same vibration reduction in a single degree of freedom system at the resonance frequency. It is calculated at the resonance frequency as:

$$\eta_{TOT} = \eta_m \frac{max\left(|H_{OC}\left(j\omega\right)|\right)}{max\left(|H_{SH}\left(j\omega\right)|\right)} \tag{3.10}$$

where $|H_{OC}\left(j\omega\right)|$ and $|H_{SH}\left(j\omega\right)|$ are respectively the amplitude of the transfer function in the open circuit and shunted configuration. The loss factor η associated to the shunting is considered to be the difference between the aforementioned value and the total one measured with the shunting technique.

$$\eta = \eta_{TOT} - \eta_m = \eta_m \left(\frac{max\left(|H_{OC}\left(j\omega\right)|\right)}{max\left(|H_{SH}\left(j\omega\right)|\right)} - 1 \right) \tag{3.11}$$

3.6 EXPERIMENTAL RESULTS

Table 3.2 summarizes the characteristics of the specimens, and the values of the generalized electromechanical coupling coefficient are reported in table 3.4. Six different values of the K_{ij} have been measured in a frequency range between 40 Hz and 240 Hz. The values of the K_{ij} are always larger for the first bending mode than the second one since the piezoelectric transducers are bonded in an area closed to the clamping and, therefore, have a higher modal strain energy ratio in the first bending mode than the second one.

Figure 3.5a shows the amplitude of the frequency response function between displacement and force measured in test #5 with the piezoelectric transducer connected to the resonant shunt. These measurements are used for both calculating the K_{ij} and assessing the damping performance of the resonant shunt. In this particular case, a vibration reduction of 20dB is obtained with the shunted configuration with respect to the open circuit state.

Figure 3.5b shows the amplitudes of the frequency response functions obtained on the same structure with the SSDI. In order to verify the effect of the factor λ on the damping performance of the shunt, four different settings of the electrical circuit are obtained by adding a potentiometer in series to the switch, so that tunable electrical losses are introduced into the system. Lower values of the resistance correspond to higher factor λ and to better damping performance of the shunt, as shown in equation 3.7. In the test #5 with SSDI, a maximum vibration reduction of 14dB is obtained.

Comparison of analytical and experimental results

The same vibration tests have been performed for all the six configurations reported in table 3.2. The results are summarized in figure 3.6, where the loss factor is presented as a function of the square of the generalized coupling coefficient and the shunt design. Each configuration corresponds to a specific value of the K_{ij} and has been tested with five different electrical connections: open circuit state, connected to the resonant shunt and connected to the switching shunt with three different values of the electrical factor λ. With both the RL and SSDI shunting techniques, a

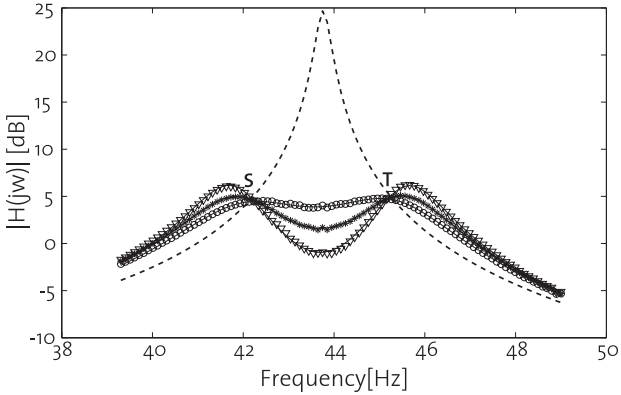

(a) Open circuit state (dashed line), Resonant Shunt with $R = 4.9k\Omega$ ($^\circ$), $R = 3.9k\Omega$ (*) and $R = 2.9k\Omega$ ($^\nabla$). The solid lines are the results of the fitting used for calculating the K_{ij}.

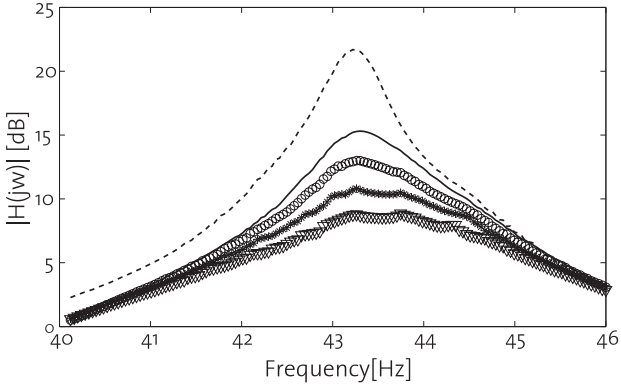

(b) Open circuit state (dashed line), SSDI with $\lambda = 2.7$ (solid line), $\lambda = 4.3$ ($^\circ$), $\lambda = 5.9$ (*), $\lambda = 7.5$ ($^\nabla$).

Figure 3.5: Amplitude of the Frequency Response Functions between displacement and force measured in test #5: **(a)** Resonant Shunt; **(b)** SSDI.

significant level of damping has been measured: for example, in the case test #6, the one with the largest value of K_{ij}, a loss factor of 7% and 6% has been obtained respectively with the RL and SSDI shunt.

In the same diagram, the lines represent the value of the loss factor predicted by the analytical expressions discussed in Section 3.1, as a function of the electromechanical coupling. In particular, the solid line describes the loss factor obtained with a resonant shunt (equation 3.3), while the other three lines describe the loss factor for the SSDI with three different values of the electrical factor λ (equation 3.1). An extremely good agreement can be observed between the experimental and the theoretical values, for both the resonant and the switching shunts.

The diagram reported in figure 3.6 reflects the basic idea of this chapter related to the possibility of assessing the damping performance of piezoelectric shunt damping by simply referring to two non-dimensional parameters: the electromechanical coupling and the shunt type. The analytical expressions for the loss factor have been validated on geometrically simple structures by measuring both the electromechanical coupling and the added loss factor, but they are intended to be also used to predict the damping performance of the same shunts on more complex structures with different sizes. A finite element model may be used to accurately determine the K_{ij} of a vibrating mode of a generic structure and, using the analytical expressions discussed in this work, the predicted loss factor may be found as a function of the Kij and the shunt design. Moreover, other shunting circuits or active piezoelectric strategies could be represented in the same diagram, leading to an extremely useful tool for comparing different damping strategies.

3.7 CONCLUSIONS

In this chapter, the electromechanical parameters describing the performance of different piezoelectric shunt damping techniques have been investigated. An analytical study based on an energy approach has shown how the damping can be related to two main contributions that respectively reflect the authority of the

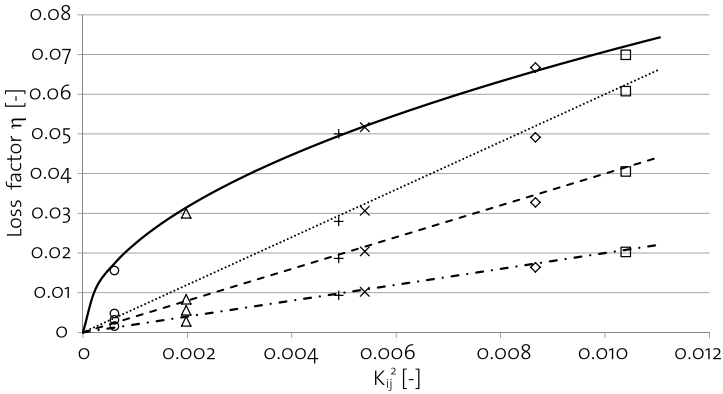

Figure 3.6: Comparison between experimental (points) and theoretical (lines) values of the loss factor expressed as a function of the square of the generalized coupling coefficient: RL shunt 'solid line', SSDI with shunt performance factor $\lambda = 6$ 'dotted line', SSDI with $\lambda = 4$ 'dashed line', SSDI with $\lambda = 2$ 'dash-dot line'.

piezoelectric transducers on the host structure and the behavior of the electrical circuit. This approach allows for a prediction of the damping performance of shunted piezoelectric transducers simply starting from global information of the system, like the generalized electromechanical coupling coefficient and the shunt type.

A robust experimental method for the measurement of the generalized electromechanical coupling coefficient has been proposed and applied to specimens with different sizes and piezoelectric transducers. Vibration tests have been carried out on the same structures and the damping performance of resonant and switching shunt has been assessed. The experimental results show an excellent agreement with the analytical prediction of loss factor and have been summarized in a diagram where the loss factor is expressed as a function of the electromechanical coupling and the shunt design. This diagram can be used for the prediction of the damping of structures with more complex shapes and different sizes than the ones used in this work, since

it is based on non-dimensional parameters. Moreover, other shunting techniques (besides RL and SSDI) or active piezoelectric damping strategies can be represented in the same diagram, leading to a common base for a comparison of different piezo-based damping techniques.

An additional outcome of this work is the possibility to describe the attainable damping of shunted piezoelectric actuator as a function of a specific damping coefficient, representative of the piezoelectric material properties and the type of shunt, and the ratio between the modal strain energies in the piezoelectric transducer and the whole system. A similar approach, based on the modal strain energy ratio and specific damping, is also typically used in the analysis of classical passive viscous damping. The importance of this outcome lies in the fact that a common design environment has been identified to compare the performance of different damping techniques, both passive and adaptive, and it can result in a comprehensive tool to develop design strategies for adaptive structures.

The model validated in this chapter is applied in the design case study of chapter 5 to calculate the damping obtained with adaptive design solutions. Moreover, the relationship between the damping performance and the modal stiffness ratio, expressed in equation 3.7, highlights the importance of the concurrent approach that is at the base of the strategy proposed in this thesis for the design of adaptive structures. While in most cases the intuitive solution of a stiffness increase brings benefit to the mechanical system, there are cases–such as piezo augmented structures–where increasing the stiffness may not be the optimal strategy to achieve the desired dynamic behavior and a compromise between the stiffness of the structure and the piezoelectric is required in order to satisfy both the classical strength/stiffness requirements and the damping or dynamic ones.

The knowledge developed in this chapter about the effects of the electrical parameters on the damping performance of switching shunting techniques are exploited in the next chapter to develop and implement a robust and autonomous shunt.

4

A NOVEL AUTONOMOUS SHUNT

The autonomous implementation and robustness of switching shunt strategies play a key role in defining the reliability of shunt damping in adaptive structures. This chapter presents a new technique for improving the damping performance of autonomous switching shunts, based on the application of an energy harvesting module. An experimental validation of the proposed shunting technique is carried out in order to assess its robustness in both the cases of a single tone and multimodal response of the structure. The results presented in this chapter have been summarized and published in the following journal paper:

> T. Delpero, L. Di Lillo, A. Bergamini, and P. Ermanni, "Energy harvesting module for the improvement of the damping performance of autonomous synchronized switching on inductance," *J. Intell. Mater. Syst. Struct.* **2013**, 24 (7), 837-845

4.1 INTRODUCTION

Vibration suppression approaches via piezoelectric elements can be distinguished in active, passive and semi-passive methods, as described in section 2.2. In all the semi-passive methods, a small power is required by the electronic components. Compared to active methods, semi-passive systems are known to be unconditionally stable—as no power is injected into the system. Compared to passive methods, they are less sensitive to changes in the mechanical structure characteristics. Moreover, since the energy required by the semi-passive ones can be very small, some of them are suitable for a self-powered implementation. Examples of autonomous implementation can be found in Niederberger and Morari (2006), who proposed an autonomous shunt for the

implementation of the SSDI technique, while Shen et al. (2010) implemented an SSDV where the energy for the voltage source is harvested from an additional vibrating structure. In this study a new implementation for improving the damping performance of the self-powered SSDI technique is proposed.

As explained in section 3.1, the rationale of the SSDI consists in applying a voltage V on the piezo that is in anti-phase with the velocity, in order to get a force that counteracts the vibrations of the system (Corr and Clark, 2002). This principle is implemented by a synchronized switch on an inductance L: when the displacement u reaches a maximum (the velocity is zero), the circuit is closed for a short period of time in order to reverse the voltage on the piezo and successively it is opened again (see figure 3.3).

The voltage inversion is obtained through an electrical oscillation due to the combination of the capacitor of the piezo C_p and the inductance L, and it is characterized by the quality factor $\gamma = V_m/V_M$, that describes the electrical losses of the circuit. Since the resulting force acting on the structure is proportional to the voltage and the area of the hysteresis is directly related to the voltage inversion, the factor γ should be as large as possible in order to increase the damped energy.

In section 3.1, the analytical expression of the damped energy is derived and the loss factor η is expressed as:

$$\eta = \frac{4K_{ij}^2}{\pi}\frac{1+\gamma}{1-\gamma}\cos^2(\delta) \tag{4.1}$$

where K_{ij}^2 is the square of the generalized coupling coefficient and δ takes into account the synchronization of the switch, as shown in figure 3.3. Equation 4.1 shows a singularity for $\gamma = 1$, which represents the unrealistic situation of no electrical losses in the circuit. The quality factor is limited by three factors: the resistance of the piezo itself, the resistance (small) of the electric circuit and the resistance due to a non-ideal switching mechanism.

This brief introduction on the SSDI shows that the quality factor is a critical parameter in determining the damping performance of the shunt. This is particularly true in the case of

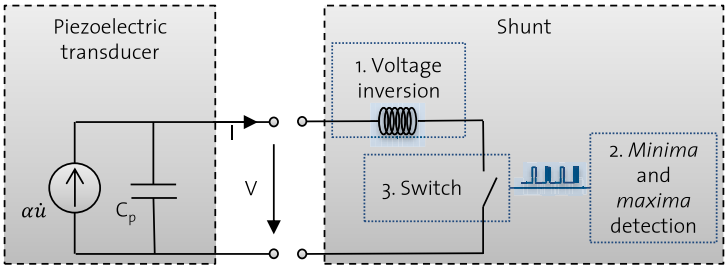

Figure 4.1: SSDI functional block diagram

autonomous shunts where the switch process can be inefficient since the power for enabling the switching mechanism is not supplied by an external source but by the vibrating structure itself.

4.2 IMPLEMENTATION

An SSDI shunt can be generally represented by a diagram with three functional blocks, as shown in figure 4.1: the first block is responsible for the voltage inversion and is usually implemented using an inductance that, in combination with the capacity of the piezoelectric transducer, creates an electrical oscillator. The second block is responsible for the detection of the minima and the maxima of the displacement and generates the control signal for the switch (third block).

The second task is typically fulfilled by a processor that receives a measure of the displacement as an input and generates the signal for controlling the switch. These implementations are still semi-passive because no power is supplied to the system, but still the power for controlling the switch is provided by an external source. Niederberger and Morari (2006) proposed an autonomous implementation, where the second task is fulfilled by an additional collocated piezoelectric transducer, whose voltage is proportional to the strain and, thus, to the displacement of the structure. This signal is filtered and then used for controlling and supplying the energy to the switch, as shown in figure 4.2a. The

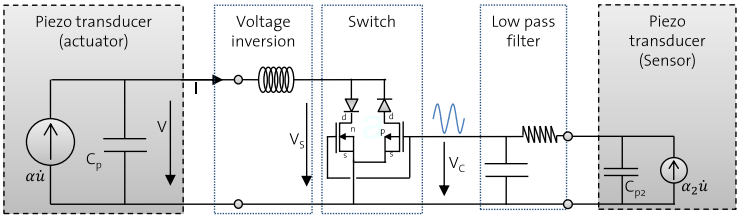

(a) Shunt proposed by Niederberger and Morari (2006)

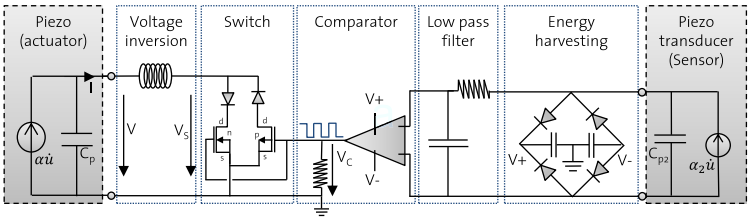

(b) Shunt developed in this work

Figure 4.2: Sketches of the autonomous switching shunts

switch is implemented by arranging a n-channel and a p-channel field-effect transistors (MOSFETs) and two diodes: each MOSFET closes the circuit alternatively when the control voltage V_C is positive or negative, while the diodes open again the circuit as soon as there is a current inversion. Since the switch should occur when the strain reaches a maximum, a $\pi/2$ phase shift between V_C and the output voltage provided by the additional piezo is required. This phase lag is implemented with a low pass filter.

Further improvement to the self-powered SSDI has been proposed by Lallart et al. (2008), who focused on global extrema detection in order to enhance the broad-band and multimodal application of this technique. However, there is not yet an investigation on how the quality factor γ can be improved without the use of additional voltage source (such as in the case of SSDV, that requires additional power supply and may become unstable).

In the autonomous shunt proposed by Niederberger and Morari (2006), the switch is driven by a low amplitude sinusoidal

voltage (at least 10 times smaller than the one generated by the additional piezo because of the amplitude reduction of the low pass filter) with negative effects on the performance of the shunt. This elegant implementation has however some drawbacks.

Limitations of the current autonomous implementation

A. A low amplitude control voltage causes an inefficient switch with large electrical losses. As a result, there is a strong dependence on the vibration amplitude of the quality factor γ, that will reach high values only with large vibrations of the structure.

B. The switch occurs when the control voltage V_C overcomes the transistor's threshold voltage that is actually different from zero. Since the V_C is sinusoidal, it crosses the threshold voltages at different phases depending on its amplitude: therefore, the synchronization of the switch depends on the amplitude of the vibrations.

The power required for switching is harvested from the structural vibration

In this study, a novel autonomous shunt is proposed in order to address the aforementioned limitations. The simple but effective idea is to control the switch with a square function, instead of a sinusoidal one. The proposed autonomous switching shunt is shown in figure 4.2b and is described in the following. The detection of maxima and minima is still implemented with a low pass filter that provides the proper phase lag, but a nano operational amplifier arranged in a comparator configuration is added to the circuit in order to transform the filtered voltage into a square signal. The power for the comparator is harvested by a bridge of diodes and two capacitors from the same additional piezoelectric transducer, so that the circuit is self-powered. The voltage on the capacitors can be limited by two Zener diodes for protecting the comparator. As a matter of fact, the energy harvested by the bridge rectifier will result in an additional contribution to the damped energy, as explained by Lesieutre et al. (2004).

In the proposed shunt, a key role is played by the use of a high performance nanopower comparator that, together with the MOSFETs, requires just few μW that can be easily harvested from the additional piezoelectric transducer. Main advantages of the

proposed shunt are high efficiency and good synchronization of the switch, even with low vibration amplitudes and without any external power source, that result in a significant increase of the quality factor and of the damping performance.

4.3 EXPERIMENTAL RESULTS

This section shows the experimental results obtained with the self-powered switching shunt proposed in this chapter. Its damping performance is compared to the classical resonant shunt. In the SSDI shunt the voltage inversion is obtained using a 50 mH inductor. The resonant shunt instead, in order to match the electrical and the mechanical resonance frequencies, requires instead an 85 H inductor (three orders of magnitude larger than the one used for the SSDI), which is synthesized using an Antoniou's circuit (Antoniou, 1969).

The experimental setup is the one described in the previous chapter, while the experiments are carried out only on the aluminum plate used for the test #6 (see table 3.2). The input signal is a stepped frequency sweep in a range about the first resonance: at each frequency step, the structure is excited with a single tone sinus for a sufficient number of cycles in order to get a steady state response of the electromechanical system. The response of the structure is measured for different shunting techniques in order to compare the damping performance and verify the effect of the enhanced quality factor of the switch. The transfer function between the stimulus and the systems response is calculated by a LabView subroutine, and the loss factor is measured as described in section 3.5.

Large values of quality factor

Figure 4.3 illustrates the voltage on the piezoelectric actuator, i.e. the one responsible for the damping: the solid line is the voltage obtained by using the proposed self-powered shunt and it is characterized by a larger quality factor than the one obtained with the Niederberger's shunt (dashed line). Moreover, the switch in the dashed line occurs before a maximum or minimum is reached, suggesting that the phase lag introduced by the low-pass filter is not sufficient. Larger values for the resistor or the capacitor of the low-pass filter would increase the phase lag, but

the amplitude of the control voltage, and thus also the quality factor, would be further reduced.

A closer view on the voltage inversion

The better performance of the proposed shunt arises from the extremely short period of time in which the voltage inversion occurs. For a more comprehensive analysis, the measures of the voltage on the switch V_S are presented in figure 4.4. This voltage is a direct indicator of the resistance and the losses related to the switch: when the switch is disabled, the circuit is open, no current is flowing and V_S has the same value of the voltage V on the actuator; when the switch is enabled, the circuit is closed and V_S is proportional to the resistance and the losses of the switch. Figure 4.4 clearly shows that during the voltage inversion, the losses in the switch are much smaller in the proposed shunt than in the shunt without the nanocomparator. The additional losses of the shunt without comparator are due to the fact that the switch is slow compared to the dynamic of the voltage inversion (it takes almost 0.5 ms for closing the circuit), while the switch driven by the comparator is relatively fast. As reported by Niederberger and Morari (2006), the vibration suppression obtained with their autonomous shunt is strictly related to the amplitude of the vibration. If the vibration amplitude is too low, the transistors do not work efficiently because the generated voltages are too small. On the other hand, a high level of quality factor is only obtained with such a large vibration that the hysteresis of the piezoelectric material starts playing a role and the vibration suppression loses efficacy. However, even in the best case scenario, their shunt is far away from matching the vibration suppression obtained by the resonant shunt. By contrast, the vibration reduction of the proposed shunt–even at low vibration amplitude–is comparable to the one of the resonant shunt, as shown in figure 4.5, and does not change significantly with the vibration amplitude. The reason lies in the fact that the amplitude of the control voltage that drives the MOSFETs is fixed by the Zener diodes allowing a large quality factor independently of the vibration amplitude.

Impact on the damping performance

The improved quality factor obtained with the proposed shunt has a noticeable impact on the damping performance of the shunt, as shown in figure 4.5, where the transfer functions relat-

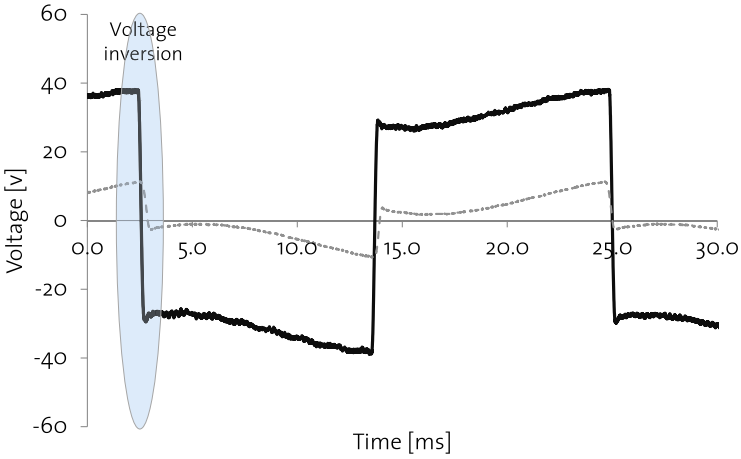

Figure 4.3: Voltage on the actuator measured at the first resonance frequency using Niederberger's shunt (thin dotted line) and the proposed shunt (thick solid line)

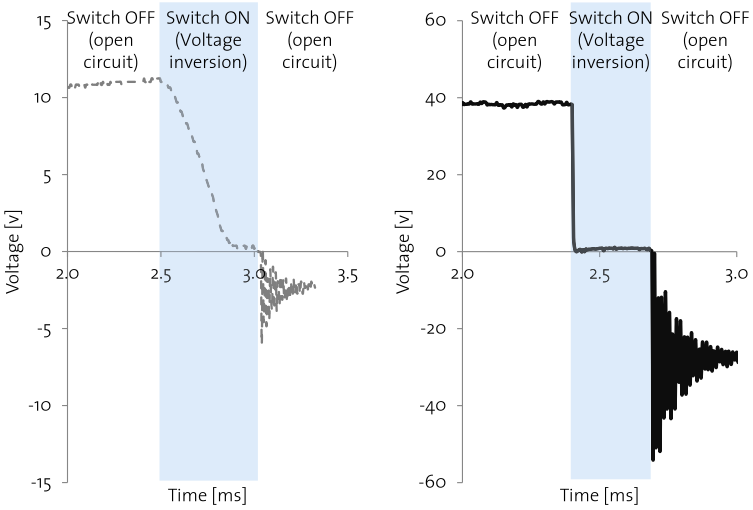

(a) Shunt proposed by Niederberger and Morari (2006)

(b) Shunt developed in this work

Figure 4.4: Voltage on the switch during the voltage inversion

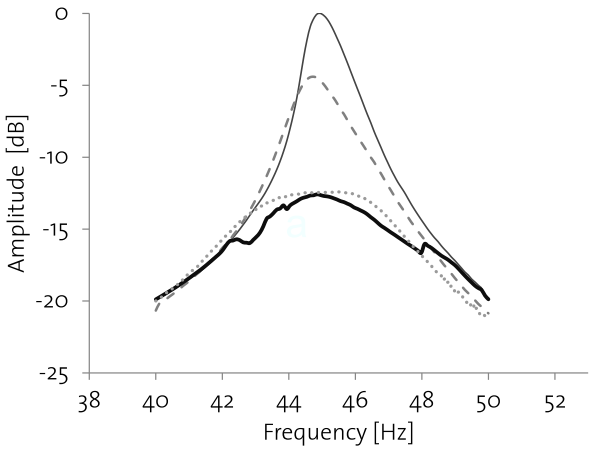

Figure 4.5: Transfer function force-displacement for different shunts: Open circuit (thin solid line), Niederberger's shunt (dashed line), Resonant shunt (dotted line) and proposed shunt (thick solid line)

ing the force/displacement dynamics are compared for different shunts. The reference for the comparison is the transfer function obtained when the piezoelectric transducers are in a open circuit configuration, and the maximum value of this transfer function has been set to 0 dB. The amplitude reduction with the Niederberger's shunt is 4.6 dB (40%), while with the proposed shunt it is 12.5 dB (more than 75%). For an overview of the the experimental results, table 4.1 summarizes the damping performance of the different shunts in terms of amplitude reduction and loss factor. The contribution of the proposed shunt to the loss factor is 7.6%, since it allows to reach a final value of 10% starting from a 2.4% of the structure with the open-circuit transducers. This represents a remarkable result because the proposed shunt yields the same amount of damping as the resonant shunt, that can be considered a reference in terms of damping performance, but it is more robust, since it does not require a fine tuning of the resonance frequency of the electrical circuit, and it is completely self-powered.

Table 4.1: Comparison of the damping performance obtained with different shunts

Shunt	Max amp X	Loss factor η
Open circuit	0 dB	2.4%*
Niederberger's shunt	−4.6 dB	3.9%**
Proposed shunt	−12.5 dB	10.0%**
Resonant shunt	−12.4 dB	9.8%**

* η calculated with the half-power bandwith method

** η calculated as $\eta_{Shunt} = \eta_{OpenCircuited} 10^{(X_{Opencircuited} - X_{Shunt})/20}$

4.4 MULTIMODAL PERFORMANCE

Non-linearity

The inherent non-linearity of the SSDI techniques does not allow applying the superposition principle for establishing the performance of the shunt when more eigenmodes are simultaneously present in the response of the structure. The main issue lies in the identification of the timing for a proper switch: while the detection of the extrema is clearly defined in the case of a single tone excitation, this can be more complex in the case of a multimodal response (Guyomar and Badel, 2006).

This section reports on the multimodal performance of the proposed autonomous SSDI, where the extrema detection is simply obtained by a low-pass filter applied to the signal generated by the additional piezoelectric sensor. In case of a multimodal response of the system, the switch is therefore driven by the eigenmode that results in a larger strain rate of the piezoelectric sensor. The following experimental results show the attenuation obtained when the structure is excited with a double frequency tone burst (obtained as the sum of two sinusoidal signals with different frequencies modulated by a Gaussian window). The frequency spectrum of the stimulus is characterized by two peaks in correspondence of the first two resonance frequencies and allows a simultaneous excitation of both the first and the second bending modes.

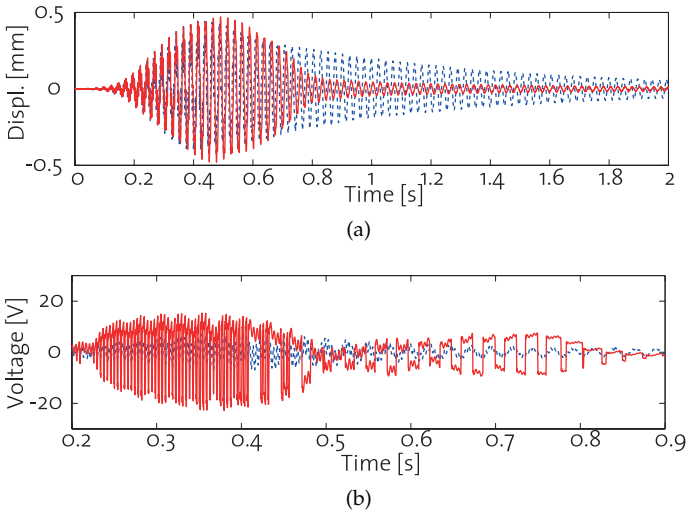

Figure 4.6: Displacement (a) and voltage on the actuator (b) obtained in a open circuit configuration (dashed blue line) and shunted (solid red line)

Figure 4.6a presents the response of the structure excited with the double frequency tone burst. The response measured in the shunted configuration (solid line) clearly shows an important attenuation of the vibration amplitude respect to the response measured in the open circuit case (dashed line). The Power Spectral Density (PSD) of these measures, reported in figure 4.7, gives more information about the frequency spectrum of the response and confirms that the vibration of the structure is reduced at both the eigenfrequencies.

The operation of the proposed shunt can be further analyzed looking at the voltage on the piezoelectric actuator, reported in figure 4.6b. In the first 0.4 seconds the switch occurs at the frequency of the second eigenmode, whose corresponding amplitude is therefore reduced until the first mode prevails. Then, the switch occurs at a lower frequency and the first bending mode is damped.

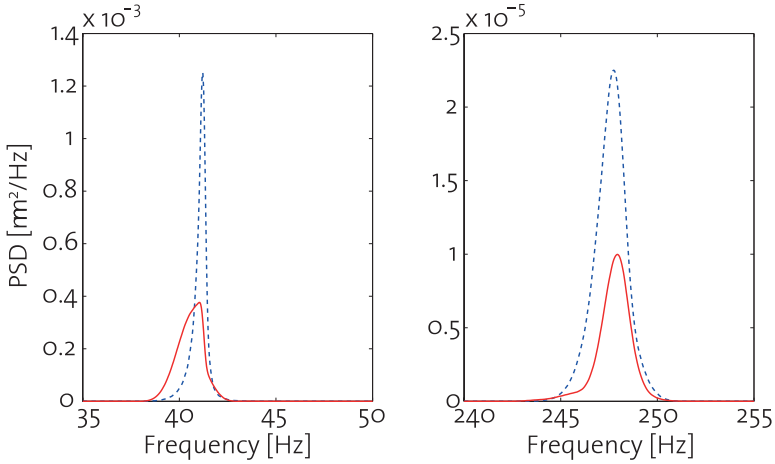

Figure 4.7: Power Spectral Density of the displacement. Open circuit configuration (dashed blue line) and shunted (solid red line)

This simple example shows the robustness of the proposed shunt to perform at different frequencies and also in the case of a multimodal response of the structure. More in general, if the structure is excited by a broadband stimulus, the structure will respond with the eigenmodes included in the frequency range of the excitation and the proposed shunt will reduce the vibrations associated at the predominant modes. Since the multimodal performance is strictly related to the strategy used for the extrema detection, it could be further improved or optimized by implementing more complex techniques than a simple low-pass filter.

Outlook on extrema detection

4.5 CONCLUSIONS

In this chapter, a novel autonomous switching shunt based on the SSDI technique has been proposed. The damping performance of this type of shunts greatly depends on the quality and synchronization of the switch that, in the case of autonomous circuit, can be inefficient, especially at low vibration amplitude. In the proposed shunt a solution that allows for good damping

performance, even with low vibration amplitude, has been developed. The new shunt requires two collocated piezoelectric patches: one used as an actuator, while the other one responsible for harvesting the necessary energy for the electronic components and for controlling the switch.

The vibration reduction and loss factor obtained with the proposed shunt have been compared to the ones obtained with a standard resonant shunt and with another autonomous switching shunt. The experimental results show excellent damping performance: the vibration reduction is much higher than the one obtained with the reference autonomous shunt and comparable to the one obtained with the resonant shunt. Compared to the latter, the proposed shunt does not require any external source of power for the synthetic inductor and is much more robust to changes in the natural frequency of the structure.

The focus of this work was on the improvement of the quality factor of the switch, while the extrema detection is implemented with a simple low pass filter that is optimal only in the case of a sinusoidal excitation of the structure. The proposed shunt has been however tested with a multimodal excitation of the structure and has shown a robust behavior. As an outlook, the application of more complex global maxima and minima detection techniques could further improve the broadband characteristic of this shunt.

5

CONCURRENT DESIGN OF ADAPTIVE STRUCTURE

In this chapter, a new approach to the design of adaptive structures is proposed and applied to a realistic case study. The main outcomes are (i) the definition of a common performance index for comparing the dynamic response of adaptive and passive design solutions, and (ii) a design method that allows to find a compromise between the stiffness of the host structure and the attainable piezoelectric damping. The proposed method opens up the design space of adaptive structures to lighter solutions, which may be rejected by a conventional design approach.

5.1 DEFINITION OF THE PERFORMANCE INDICES

The conclusions of chapter 3 highlight the importance of concurrent design strategies for adaptive structures and suggest the need for a compromise between the stiffness of the structure and of the piezoelectric in order to satisfy both the classical strength/stiffness requirements and the dynamic ones. One of the main challenges related to a concurrent design is the definition of a common ground for comparing adaptive and traditional structures that, additionally, may feature any source of damping. The choice of a common performance index is not trivial, because of the large variety of structural properties (static stiffness, weight, natural frequencies and modal damping, for instance) that interacts in determining the final response of the system.

An elegant approach to the selection of the best *material* for minimizing the deformation of mechanical components caused by vibrational inputs has been proposed by Cebon and Ashby (1994). Different materials are compared using 'material selection charts' (Ashby, 2004) combined with 'performance indices' (combinations of material properties). While their approach is strictly

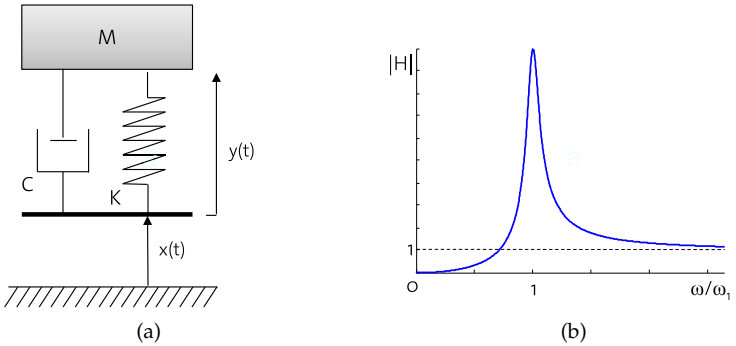

Figure 5.1: Single degree of freedom oscillator subjected to displacement input x (a). Magnitude of the transfer function between the relative displacement y and input x (b).

focused on materials, in this chapter it is applied to compare different structural designs, which may include both adaptive and purely passive solutions. The resulting performance indices do not merely consider the material properties, but the effective geometry of the structure and any other sources of damping are also included.

The problem of minimizing the vibration of a mechanical system is analyzed with respect to two load cases, which lead to two different types of performance index. In both the load cases, the input is a displacement excitation at the base of the structure. The first load case applies when the input is sinusoidal and its frequency is much smaller than the lowest natural frequency of the system. The second load case applies when the excitation spectrum contains the natural frequencies of the system.

The performance indices proposed by Cebon and Ashby (1994) are reported in the following for the two considered load cases.

Sinusoidal input

In *the first load case*, the first mode of vibration can be modeled as a single degree of freedom system, like the one shown in figure

5.1a. The transfer function between the relative displacement y and the displacement base input x is given by:

$$H(\omega) = \frac{Y}{X} = \frac{(\omega/\omega_1)^2}{1 + 2j\xi_1(\omega/\omega_1) - (\omega/\omega_1)^2} \tag{5.1}$$

where ω_1 and ξ_1 are the natural frequency and modal damping ratio of the lowest eigenmode, respectively. The magnitude of $H(\omega)$ is qualitatively shown in figure 5.1b. For a given excitation frequency $\omega \ll \omega_1$, *the relative vibration amplitude is minimized when the natural frequency is maximized*, since

$$|Y| = \left(\frac{\omega}{\omega_1}\right)^2 |X| \qquad \text{when } \frac{\omega}{\omega_1} \ll 1 \tag{5.2}$$

Even in the case of realistic structures, with many eigenfrequencies and complex mode shapes, the general conclusion of maximizing the first natural frequency holds. Furthermore, the same conclusion of maximizing the stiffness of the system is reached if it is assumed that the input to the system is an oscillating force, rather than a displacement base input. Thus, the performance index for the first load case coincides with the first natural frequency of the structure:

$$M_1 = \omega_1 \tag{5.3}$$

Broad band input

In the *second load case*, the excitation is 'broad-band' and most of the structural response occurs around resonant frequencies, where *damping plays a key role*. A random, broad-band input is assumed, whose power spectral density is

$$S_{xx}(\omega) = S_0 \left(\frac{\omega}{\omega_0}\right)^{-k} \tag{5.4}$$

where S_0, ω_0 and k are constants. If $k = 0$, the spectrum of the displacement input corresponds to a white noise input, that is generally unrealistic, because it implies an input with infinite power. If $k = 2$, the spectrum of the input velocity is constant, which gives finite power. For $k > 2$ the input becomes more concentrated at low frequency. The relationship between the

power spectral density of the deflection and the input is the square of the absolute value of the transfer function of the system $S_{yy}(\omega) = |H(\omega)|^2 S_{xx}(\omega)$.

The quantity to be minimized is the root mean square of the relative deflection σ_{yy}, whose squared (the variance) is the area defined by the power spectral density $S_{yy}(\omega)$:

$$\sigma_{yy}^2 = \int_0^\infty S_{yy}(\omega)d\omega = \int_0^\infty |H(\omega)|^2 S_{xx}(\omega)d\omega \tag{5.5}$$

The area under each resonant peak of the output spectrum $S_{yy}(\omega)$ is approximately

$$\left(\begin{array}{c}\text{Peak of}\\ H(\omega_n)\end{array}\right)^2 \left(\begin{array}{c}\text{Average}\\ \text{of } S_{xx}(\omega)\end{array}\right) \left(\begin{array}{c}\text{Mean square}\\ \text{bandwith}\end{array}\right) \tag{5.6}$$

where the 'mean square bandwidth' is $\pi\xi_n\omega_n$ (Newland, 1984). Thus, the integral of equation 5.5 can be approximated by a summation over the natural modes:

$$\sigma_{yy}^2 \approx \sum_{n=1}^{\infty} |H(\omega_n)|^2 S_{xx}(\omega_n)\pi\xi_n\omega_n \tag{5.7}$$

Considering that the value of the transfer function in correspondence of the n-th resonance is $H(\omega_n) = 1/2\xi_n = 1/\eta_n$,[1] the variance can be approximated by

$$\sigma_{yy}^2 \approx \frac{\pi S_0 \omega_0^k}{2} \sum_{n=1}^{\infty} \frac{1}{\eta_n \omega_n^{k-1}} \tag{5.8}$$

It is then possible to conclude that, in the case of a broad band input, minimizing the root mean square of the relative vibration σ_{yy} requires maximizing the performance index

$$M_2 = \eta_n \omega_n^{k-1} \tag{5.9}$$

1 When the damping is small and the system is excited near the resonance, the loss factor and the damping ratio are related by $\eta = 2\xi$.

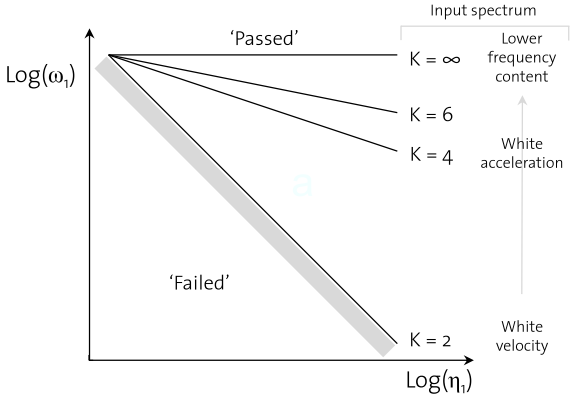

Figure 5.2: Schematic diagram for minimizing the root mean square deflection σ_{yy} of a structure subjected to an input with spectral density $S_0\,(\omega/\omega_0)^{-k}$ (Cebon and Ashby, 1994).

for all the eigenmodes excited by the input. The first eigenmodes contribute to the deflection of the structure to a greater extent than the higher frequency modes. Additionally, the importance of the low frequency modes increases when the power spectral density of the input is characterized by a larger k.

If we focus on the first vibration mode, we can notice a relationship between the performance indices in the two load cases, since the first natural frequency coincides with the first performance index:

$$M_2 = \eta_1 M_1^{k-1}$$

If different design solutions are plotted in a diagram with $\log \eta_1$ on the x-axis and $\log \omega_1$ on the y-axis, all the solutions laying on the line of slope $1/(1-k)$ have the same performance index M_2. The concept is schematically shown in figure 5.2. For $k = 2$, the slope of the selection line is -1. This means that, for a random input with a constant velocity spectrum, all the solutions below this line lead to larger deflections than the ones above the same line. For $k \to \infty$ (input concentrated at low frequencies) the selection line becomes horizontal, and the selection task

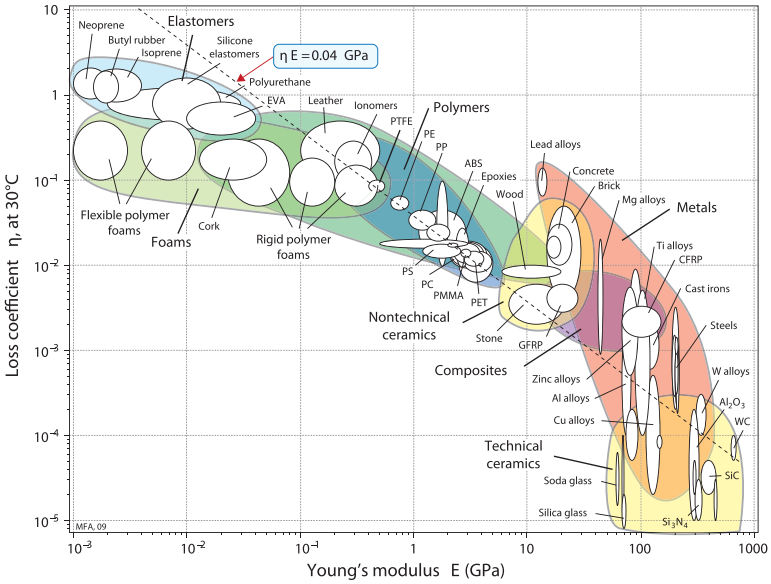

Figure 5.3: Loss factor plotted against Young's modulus for different classes of materials (Ashby, 2004).

corresponds to maximizing the first natural frequency, as for the first sinusoidal load case. The diagram reported in figure 5.2 clearly shows how the broader the input, the lower the efficacy of stiff structures. Indeed, when k is small (broad band input), a solution characterized by a lower natural frequency but higher damping may outperform a stiff one.

In figure 5.3, the loss factor is plotted against the Young's modulus for different classes of materials: these are conflicting properties, since materials with large values of loss factor have low modulus, and vice versa. Even though piezo-augmented structures allow to add large values of loss factor to the purely passive ones, they are also characterized by the same conflicting behavior, since stiff solutions lead to smaller electromechanical coupling for the same amount of piezoelectric material. From this simple example, it is possible to appreciate how the maximization of the index M_2 is not trivial, neither in a purely passive

design nor in an adaptive one. As anticipated in chapter 3, the design of piezo-augmented structures requires a compromise between the stiffness of the structure and the damping obtained with the piezoelectric element. At the end of this chapter, the diagram of figure 5.2 will be filled with actual design solutions of a realistic case study. This will allow a comparison of (i) a purely passive design with (ii) an adaptive structures designed with a sequential approach and (iii) an adaptive structures designed while considering the presence of piezoelectric elements since the early design phases.

5.2 CASE STUDY: CFRP PROPELLER BLADE

The selected case study is a scaled model of a CFRP propeller blade for wind tunnel testing, which has been investigated in the framework of a master thesis (Meier, 2012) carried out as collaboration between ETH Zurich and RUAG Aviation.

The investigated blade is meant for aerodynamic tests of counter-rotating open rotors, whose propellers are generally characterized by complex three-dimensional geometries with small cross sections, high stresses due to the centrifugal loads and are typically made out of carbon fiber reinforced plastic (CFRP). Counter-rotating open rotors are widely recognized as highly energy efficient propulsion systems. It is also well-known that their blades are subjected to large vibrations, mainly because of the rich spectrum of the aerodynamic forces. Since the purpose of the scaled model of the blade is to verify the aerodynamic performance of the propeller in a wind tunnel test, the structural vibrations have to be minimized in order to limit the spurious aerodynamic effect caused by its vibrations. The blade has to satisfy another important strength requirement: it has to carry the centrifugal load resulting from the nominal rotational speed of 10′000 RPM. The weight of the blade has a major impact on this second requirement, since the resulting centrifugal stresses are proportional to the mass of the blade. However, a lightweight solution, which reduces the centrifugal stresses at the root of the blade, typically has the tendency to be subjected to large amplitude vibrations and may be not acceptable if not properly

Design requirements

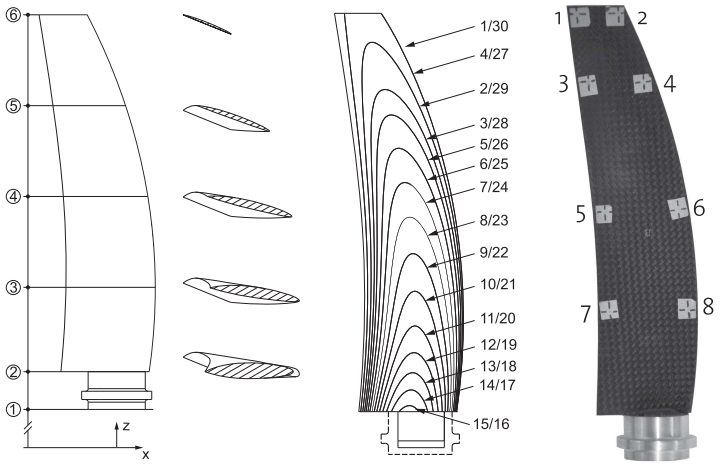

Figure 5.4: Geometry of the investigated blade. (a) Aerodynamic profiles at different sections along the span. (b) Lay-up of the carbon fiber layers. (c) Picture of the manufactured blade. A reflecting tape is glued on the blade in eight positions in order for the laser vibrometer to measure its velocity (Meier, 2012).

damped. The conflicting requirements, which constrain the design space of the blade, make this problem an appropriate example to show how the consideration of adaptive elements in the early design phases may lead to significant advantages in terms of performance of the whole structure.

Geometry

The external geometry of the blade is given by aerodynamic considerations and it is defined by five NACA airfoil profiles, as shown in figure 5.4a and reported in table 5.1. The inner structure of the blade is composed of 30 carbon fiber layers, arranged in a symmetric lay-up as depicted in figure 5.4b. The geometry of each layer has been defined in order to obtain an uniform fiber volume content among the whole volume of the blade (Meier, 2012).

Design parameters

The orientations of the carbon fiber layers are the 'passive'

Table 5.1: Airfoil profiles and dimensions of the blade.

Section #	Radial position [mm]	Chord [mm]	Thickness [mm]	NACA profile
1	57.96	-	-	-
2	72.5	34.0	0.18	NACA 16-218
3	105.0	34.7	0.12	NACA 16-412
4	140.0	33.5	0.09	NACA 16-409
5	175.0	29.7	0.06	NACA 16-406
6	210.0	20.0	0.04	NACA 16-304

design parameters and have a strong effect on the stiffness and the eigenfrequency of the structure. The adaptive design parameters are the possibility to introduce a piezoelectric patch and its position. The main goal of this chapter is to propose a design strategy that maximizes the advantages obtainable with an adaptive solution.

5.3 FINITE ELEMENT MODEL

A finite element model of the blade is developed in order to evaluate its natural frequencies and the electromechanical coupling (and therefore the attainable damping) of the piezoelectric patch. The software used for realizing the FE model, solving it and evaluating the results is ANSYS Mechanical APDL. The blade is modeled with solid elements, as detailed in table 5.2, so that each carbon fiber layer contains one element in the thickness direction. The mesh has therefore to comply with the lay-up and it is created with the help of the program ANSYS Composite PrePost (ACP).

Figure 5.5 shows a detailed view of the FE model of the root of the blade: five layers extend beyond the blade structure and are wrapped around a wedge in order to fix the blade to the foot (see figure 5.5a). Contacts between the carbon fiber layers, the wedge and the foot are modeled using *'Targe170'* and *'Conta174'*

Table 5.2: Element types used in the FE model

Description	Element type	# elements
CFRP layers	SOLID186: 3-D 20-Node Structural Solid	57590
Foot and wedge	SOLID187: 3-D 10-Node Tetrahedral Structural Solid	18504
Piezoelectric	SOLID226: 3-D 20-Node Coupled-Field Solid	717
Contact	TARGE170: 3-D Target Segment	10809
Contact	CONTA174: 3-D 8-Node Surface-to-Surface Contact	10809

elements. Displacement boundary conditions are then applied to the external surfaces of the foot.

The lay-up of the blade includes two types of carbon fiber layers: a fabric[2] is used for the external layer in order to improve the robustness and the surface quality of the external surface of the blade; all the other layers are uni-directional (UD). The orientation angles of the five UD layers wrapped around the wedge are fixed by the geometry of the blade. The orientation of all the other layers can be changed in order to tune the mechanical properties of the structure. The wedge and the foot are made out of aluminum 7075-T6. The piezoelectric patch is a QP16n transducer produced by MIDÉ with a high performance PZT ceramic (CTS - 3195HD). The properties of the materials are reported in tables 5.3 - 5.5.

2 The fabric is modeled as a laminate with a symmetric $\pm 45^{\circ}$ lay-up sequence of UD layers. The corresponding material properties are calculated according to the classical lamination theory.

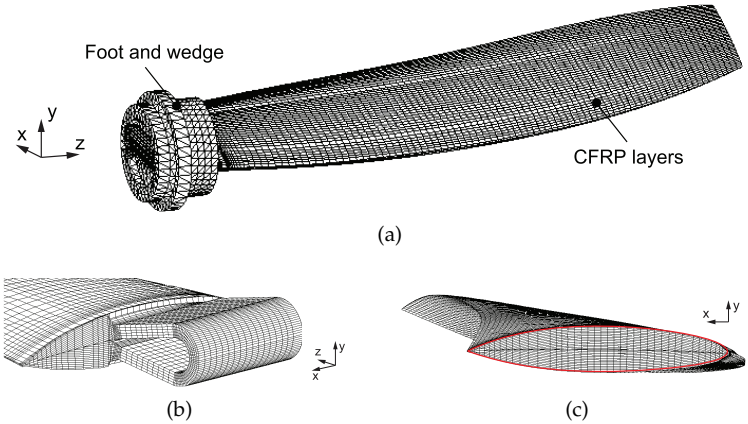

Figure 5.5: Finite Element model of the blade. Mesh (a) and detailed view of the root of the blade (b, c) (Meier, 2012).

Table 5.3: Material properties: UD carbon fiber layers

T700SC + Araldit 5052		
E_x	[MPa]	98177
E_y	[MPa]	6214
E_z	[MPa]	6214
G_{xy}	[MPa]	2418
G_{yz}	[MPa]	2805
G_{xz}	[MPa]	2418
ν_{xy}	-	0.231
ν_{yz}	-	0.3
ν_{xz}	-	0.231
ρ	[kg/m^3]	1550

Table 5.4: Material properties: aluminum

Aluminum 7075-T6		
E	[MPa]	71700
ν	[–]	0.33
ρ	[kg/m^3]	2810

Table 5.5: Material properties: piezoelectric ceramic

CTS - 3195HD					
S^E_{11}	[10^{-6} mm^2/N]	16.4	ε^S_{11}	-	916
S^E_{12}	[10^{-6} mm^2/N]	−5.74	ε^S_{33}	-	830
S^E_{13}	[10^{-6} mm^2/N]	−7.55	d_{31}	[10^{-12} C/N]	−190
S^E_{33}	[10^{-6} mm^2/N]	18.8	d_{33}	[10^{-12} C/N]	390
S^E_{44}	[10^{-6} mm^2/N]	44.3	d_{15}	[10^{-12} C/N]	584.5
S^E_{66}	[10^{-6} mm^2/N]	47.5	ρ	[kg/m^3]	7800

- S^E is the compliance matrix in short circuit state
- ε^S is the relative permittivity at constant strain
- d is the piezoelectric constants matrix

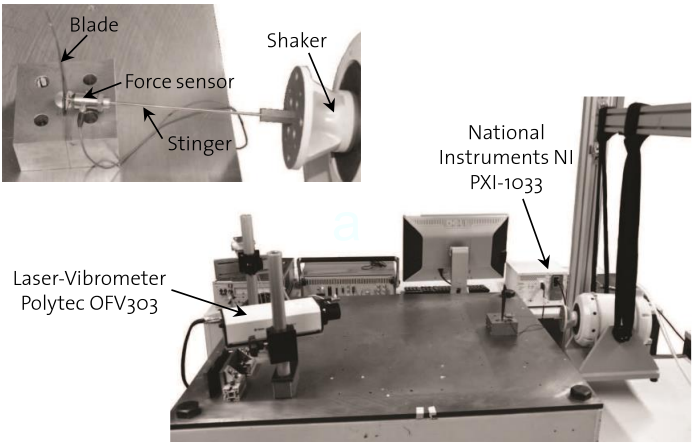

Figure 5.6: Picture of the test set-up.

5.4 EXPERIMENTAL VALIDATION

The FE model has been experimentally validated with respect to its natural frequencies, the mode shapes and the electromechanical coupling of the piezoelectric patch. All the necessary measurements have been carried out with the experimental set-up shown in figure 5.6. The set-up is the one presented in chapter 3, except for the fact that a laser vibrometer is used instead of the laser displacement meter, which would not be able to accurately measure the small displacements that characterize the response of the blade at the high frequencies.

Two CFRP blades are tested. In both the structures, all the carbon fiber layers are oriented in the span direction (except for the ones wrapped around the wedge, as explained in section 5.2). One structure (blade #1) is used to validate the purely mechanical response of the FE model with respect to the natural frequencies and the shapes of the vibration modes. In the second structure (blade #2), a piezoelectric patch is embedded between the third and the fourth layer (see figure 5.7) in a non-optimized position, with the only goal of validating the capability of the FE model to correctly represent the electromechanical coupling.

Figure 5.7: Picture of the piezoelectric patch embedded in the blade during the lamination process.

Table 5.6: Natural frequencies of blade #1. Comparison between the FE results and the experimental measurements.

	Eigenfrequencies [Hz]				
	1^{st}	2^{nd}	3^{rd}	4^{th}	5^{th}
FE results	338	917	1424	1757	2074
Experiment	322	879	1494	1768	1970
Difference [%]	5.0	4.3	−4.7	−0.6	5.3

Modal Analysis

The velocity is measured in the eight positions shown in figure 5.4c. The amplitude and the phase of the corresponding Frequency Response Functions (FRF) are reported in figure 5.8 for blade #1. The natural frequencies are compared with the ones obtained with the FE model in table 5.6, showing a good agreement, with an error of approximately 5%. The amplitude and phase information contained in the FRFs of the eight positions can be used to reconstruct the shape of the vibration modes, as shown in figure 5.9 for the first four modes. The first two modes are clearly dominated by the bending of the blade, while the third and fourth ones exhibit also a torsional contribution.

Electromechanical coupling

The capability of the FE model to correctly represent the electromechanical coupling is assessed in terms of the Generalized Electromechanical Coupling Coefficient K_{ij}, as introduced in chapter 2. Numerically, it can be simply obtained from the natural frequencies of the blade when the piezoelectric patch is in open and short circuit (see equation 2.12). The FE model of blade

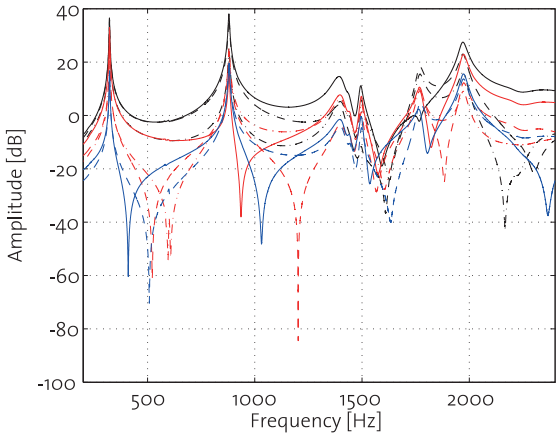

(a)

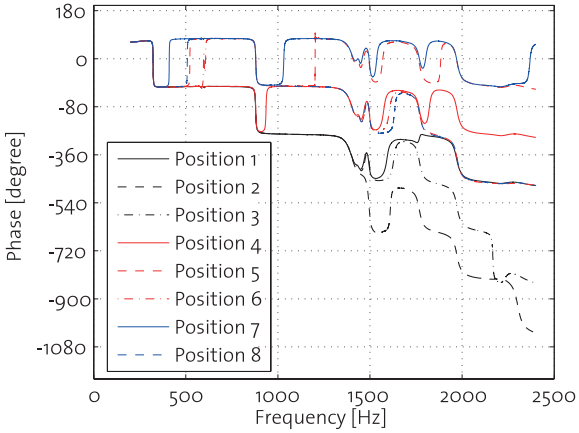

(b)

Figure 5.8: Amplitude and phase of the FRF functions measured for blade #1 in the eight positions shown in figure 5.4c (Meier, 2012).

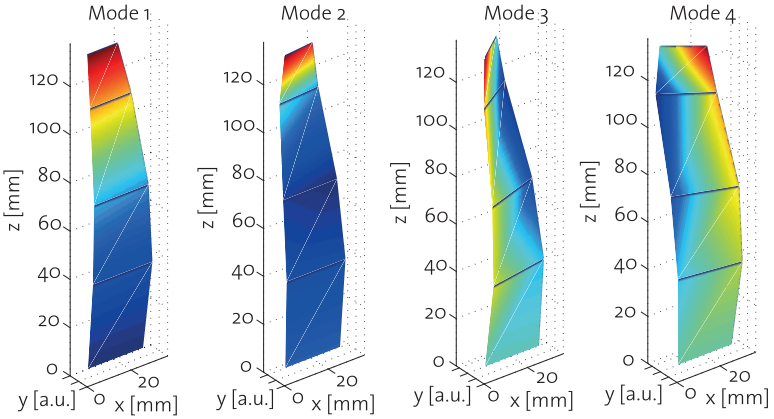

(a) Experimental measurements

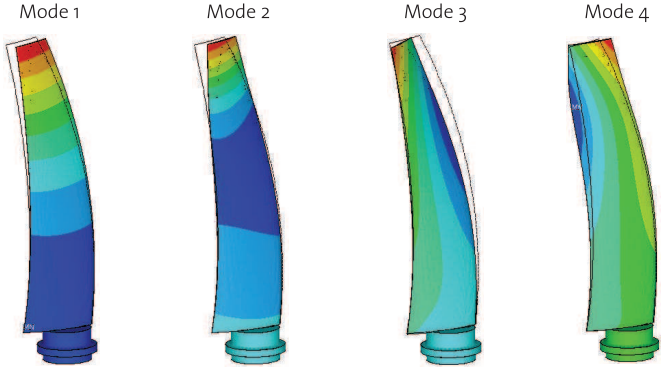

(b) FE results

Figure 5.9: Shapes of the vibration modes of blade #1. Comparison FE results and experimental measurements (Meier, 2012).

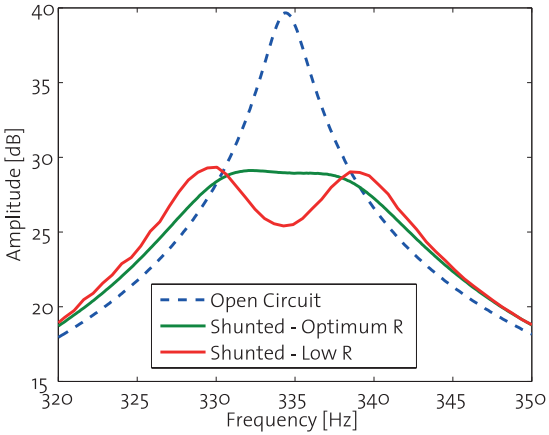

Figure 5.10: FRFs of blade #2 with different electrical boundary conditions for the piezoelectric patch (Meier, 2012).

#2 predicts a Generalized Electromechanical Coupling Coefficient for the first vibration mode of 4.3%.

Experimentally, the difference between the natural frequencies is too small to lead to an accurate measure, and the method proposed in chapter 3 is therefore applied. The FRFs obtained with three different electrical boundary conditions are reported in figure 5.10. The dashed blue line corresponds to the piezo in an open circuit state. The solid green line has been measured with the piezo connected to an optimally-tuned resonant shunt: a significant reduction in the vibration amplitude (10dB) can be observed respect to the open circuit state, even if the position of the piezo has not been optimized. The solid red line is the FRF obtained when the piezo is shunted through a resonant shunt with a small value of resistance. The red line clearly shows the two peaks typical of a RL-shunt response and is used to evaluate the electromechanical coupling. The experimental value of the Generalized Electromechanical Coupling Coefficient for the first vibration mode is 3.8%, which is in good agreement with the one predicted by the numerical model.

5.5 SEQUENTIAL DESIGN

Considering the nominal rotational speed of 10'000 RPM, the fundamental frequency of the excitation spectrum (166.7 Hz) is smaller than the lowest natural frequency of the system. If a sinusoidal input is assumed, the deflection of the blade is minimized when the first eigenfrequency is maximized, as explained in section 5.1.

In a sequential design approach, only the purely mechanical design parameters (in this case study, they corresponds to the orientation of the carbon fiber layers) are initially considered, while the adaptive degree of freedom (the position of the piezoelectric patch) is taken into account in a second phase.

First design phase

In the first design phase no source of damping is considered, and the stiffness of the structure is maximized. A parameter study is conducted on the natural frequencies of the blade with respect to the orientation angles of the second and the third carbon fiber layers. Because the first modes are dominated by a bending behavior, this first design phase intuitively leads to a blade with all the layers oriented in the span direction.

Second design phase

Due to the complex aerodynamic interferences that characterize the dynamic of a rotating blade, additional damping may be considered in a second design phase in order to reduce the vibrations induced by higher-order harmonics. In this design phase, the lay-up is frozen with all the layers in the span direction, and the position of the piezoelectric patch is optimized in order to maximize the electromechanical coupling, and consequently the attainable damping. The design variables are the piezoelectric positions in the chord and in the span directions. The results of this parametric study are presented in figure 5.11 for the first eigenmode. The optimal position lies close to the root of the blade. It results in a electromechanical coupling of $K_{ij} = 6.4\%$ that, assuming to connect the piezo to a tuned resonant shunt, would add a $\eta = 4.5\%$ of damping to the first vibration mode. On the other hand, the presence of the piezoelectric patch results in a small reduction of the first natural frequency (about 1%), due to higher density of the piezoelectric material respect to the carbon fiber layers.

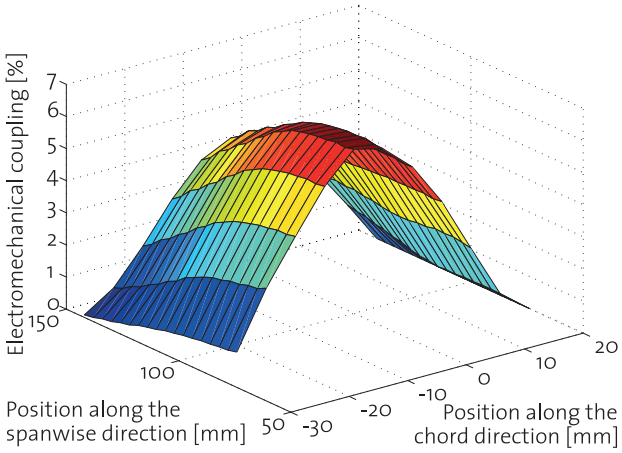

Figure 5.11: Parametric study: effect of the position of the piezoelectric patch on the generalized electromechanical coupling coefficient for the first eigenmode.

Similar results are obtained for the second vibration mode. The optimal position lies about half the span of the blade, it results in electromechanical coupling of $K_{ij} = 8.2\%$ (that corresponds to an additional damping of $\eta = 5.8\%$, if the piezo is connected to a resonant shunt) and a 4% reduction of the second natural frequency.

5.6 CONCURRENT DESIGN

While a stiff solution minimizes the vibrations of a structure subjected to a low-frequency sinusoidal input, it may not be the optimal one when the excitation spectrum is broad-band and contains the natural frequencies of the structure. In this case study, the concurrent design consists of a simultaneous design of the position of the piezoelectric patch and the orientation of the carbon fiber layers. The ultimate goal is to find a compromise between the stiffness of the structure and the attainable piezoelectric damping.

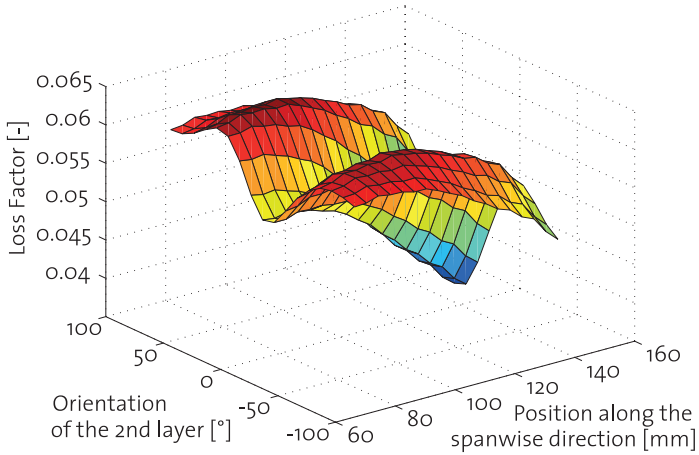

(a)

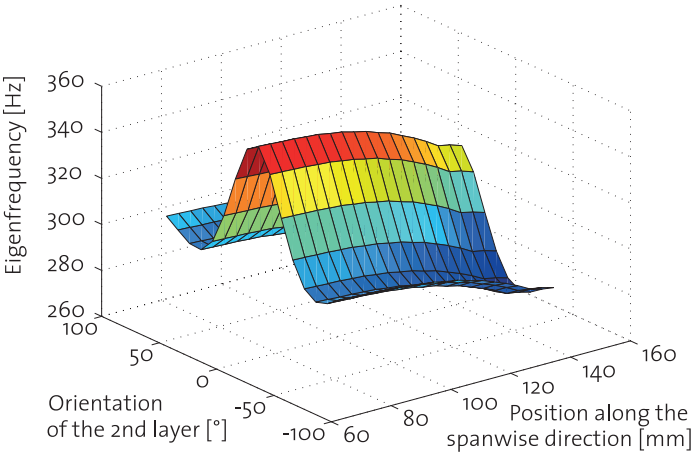

(b)

Figure 5.12: Results of the concurrent design of the blade in terms of loss factor (a) and eigenfrequency (b) for the first vibration mode. Solutions with low values of eigenfrequency lead to large values of loss factor.

The design variables selected for this example are the orientations of the second layer and the position of the piezo along the span direction. The results of the numerical simulations are depicted in figure 5.12, where the first natural frequency and the attainable loss factor[3] are reported for each solution. The results clearly show the inverse relationship between the stiffness and the attainable damping: by simply accepting less stiff solutions (i.e. when the layers are not oriented in the span direction), the loss factor can be significantly increased.

Compromise between stiffness and damping

Among the all possible solutions, the identification of the optimal one is not trivial, since it is neither the stiffest nor the most damped. As explained in the first section of this chapter, the root mean squared of the deflection is inversely proportional to the product $\eta\omega^{k-1}$ of the vibration modes excited by the input. The design solutions are thus compared in figure 5.13 on a single diagram, in terms of their first natural frequencies and loss factor.

The design solutions represented in figure 5.13 can be assessed with respect to the performance index M_2, introduced in section 5.1. The selection line corresponds to solutions that have the same performance index $M_2 = \eta\omega$, i.e. the same vibration amplitude when the input has constant velocity spectrum ($k = 2$). The red circle is the purely passive stiff blade resulting from the first design phase of the sequential approach. It has the highest eigenfrequency, and it is therefore the optimal solution only when the input is sinusoidal and its frequency is much smaller than the eigenfrequency (the selecting line in this case would be an horizontal line). The solution marked with the green circle is the result of the second phase of the sequential design. It has a slightly lower frequency than the purely passive one, but it has a much larger damping. However, this solution is not the optimal one when the input has a constant velocity

3 As shown in chapter 3, the loss factor depends on the electromechanical coupling and the shunt type. In this example, it is calculated using equation 3.3, assuming that the piezoelectric patch is connected to a resonant shunt. If the piezoelectric patch is connected to a different type of electrical shunt, the diagram reported in figure 3.6 can be used to find the relationship between the electromechanical coupling and the resulting damping. The total damping of the structure can be calculated as the sum of the purely passive damping (measured during the tests for blade #1 and #2) and the piezoelectric shunt damping.

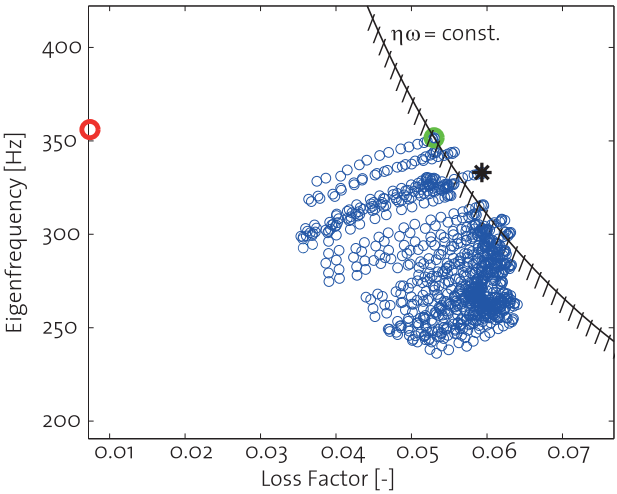

Figure 5.13: Results of the concurrent design of the blade. The loss factors and eigenfrequencies are reported on the same diagram in order to compare the solutions with respect to the performance index M_2.

spectrum. Among the solutions obtained with the concurrent approach (blue circles), the solution marked with the black star features the largest performance index $M_2 = \eta\omega$ and lead to the smallest amplitude deflections. It is interesting to observe that neither the solution with the largest damping is the optimal one, but a compromise has therefore been found.

Input spectrum

The choice of the best solution depends therefore on the spectrum of the input. When the excitation is concentrated at low frequencies (large values of k), the contribution of the eigenfrequency to the performance index $M_2 = \eta\omega^{k-1}$ is more important. On the other hand, when the excitation is broad band (small values of k) or contains the eigenmodes of the structures, the loss factor gains relatively higher importance, and less-stiff but highly damped solutions may be the best choice.

Extension of the design space

Additionally, if we now admit that the optimal solution, from a vibration point of view, is not the stiffest one, the stiffness reduction can be obtained by substituting carbon layers with a light core material, rather than changing their orientations. All the solutions lying on the selection line reported in figure 5.13 are equivalent to the one obtained with a conventional approach in terms of vibration amplitude, but may be obtained with a lighter lay-up. The main advantage of the concurrent approach is therefore the possibility to extend the design space to lighter solutions that would otherwise be rejected because characterized by lower natural frequencies. The weight reduction will subsequently lead to a reduction of the centrifugal loads and enhancement of the strength of the whole blade.

5.7 CONCLUSIONS

The main contribution of this chapter is the suggestion of a common performance index and a method to compare passive and adaptive design solutions in terms of vibration amplitudes, independently from the nature of the damping source. The proposed method focuses on finding a compromise between the stiffness of the structure and the attainable damping.

The method has been applied to the realistic case study of the design of a rotating blade. This example shows how

the adaptive solution outperforms the passive one when the excitation spectrum is broad band or contains the eigenmodes of the structure. An accurate knowledge of the excitation spectrum is required for a quantitative comparison of the solutions in terms of vibration amplitudes. On the other hand, when this knowledge is not available or uncertain, the adaptive design is in any case the most robust.

Additionally, the consideration of adaptive solutions since the early design phases allows to find a better compromise between stiffness and damping than a conventional sequential approach. This result has important implications that may look counterintuitive when designing a structure based on reducing its deformation. If the design space is open to less stiff solutions, which may be better or equally performing in terms of vibration amplitudes thanks to the adaptive elements, a new set of lighter solutions becomes available with positive impacts on the outcome of the design process.

Part III

ELECTROMECHANICAL METAMATERIALS

6

ADAPTIVE STRUCTURES: FROM DISCRETE TO PERIODIC SYSTEMS

While the first part of the thesis has shown that a deeper integration of the adaptive elements in the design of the host structure extends the design space to lighter or more efficient solutions, the second part is devoted to the integration of the adaptive elements even at a lower level, i.e. the metamaterial level. This chapter introduces the peculiarities of a design based on the metamaterial approach, where the final properties emerge from the organization of the 'artificial' atoms, and the introduction of adaptive materials in the building blocks can further extend their potentiality.

6.1 DEFINITION OF METAMATERIALS

Artificial 'atoms'

The creation of novel materials with advantageous properties and superior performance has been a crucial engineering challenge since the early days of mankind. The technological progress has always been intimately related to advancements in material development, and this has generally been obtained by affecting matter on a deeper structural level. The conventional approach to the development of new materials is that the lower the scale is at which we manipulate the material, the greater the extent is to which we can change its properties. The concept of metamaterials is an alternative way to this traditional structural hierarchy: instead of reducing the scale at which the materials are manipulated down to the atomic level, the concept of 'atom' is up-scaled to macroscopic and easy-to-manipulate building blocks, which can be arranged in a periodic configuration in order to obtained the desired 'metamaterial' response.

A definition of metamaterial has been given in the introductory chapter, and it is here divided into its phenomenological and organizational aspects.

- *Phenomenological aspect*: metamaterials are made of specific geometric arrangements of building blocks designed to achieve advantageous and unusual properties that differ substantially from the ones of the single components. In other words, certain properties of a metamaterial need to be qualitatively different from the ones of its components, so that new phenomena and novel properties should emerge when 'ordinary' pieces are brought together (Sihvola, 2002).
- *Organizational aspect*: metamaterials are composed of their building blocks in the same sense as matter consists of atoms (Lapine and Tretyakov, 2007). The main difference respect to 'ordinary' materials is that the building blocks are not limited to the elements of the periodic table of elements, but are designed, synthesized and assembled (on a much larger scale than the atomic one, with clear advantages) in order to obtain the desired properties on the macroscopic level.

Effective properties

The concept of 'material' implies that metamaterials are structured sufficiently finely compared with the characteristic scale of the phenomenon, so that their properties may be explained in terms of effective properties. The same assumption is made for ordinary materials when referring to their material parameters. For instance, although the elastic mechanical response of a crystalline solid subjected to external forces results from interactions at the atomic level and its behavior is generally complicated, the main effect can usually be reduced to a linear relationship between the applied stimulus and the materials response, and it can be described with the corresponding material parameter (Young's modulus).

6.2 FROM (META)MATERIAL PROPERTIES TO STRUCTURAL RESPONSE

Most of the peculiar properties of metamaterials arise from the way electromagnetic or mechanical waves propagate through them. When a propagating wave reaches a boundary, a wave reflection occurs with the nature of the reflected wave being

determined by the nature of the boundary. For instance, in the case of a mechanical wave traveling along a rod, the boundary conditions may be a fixed edge on one side (displacement is null) and a stress-free edge on the other (derivative of the displacement is null). The reflected waves from the boundaries will be such that, when they are added to the incident waves, the boundary conditions are respected. When the combination between incident and reflected waves leads to the formation of a *standing wave*, the structure encounters a *resonance*, whose normal modes and natural frequencies are related both to the dispersion properties of the medium and the boundary conditions of the structure.

In an analogous way, the presence of stiffness (or density) discontinuities in a medium scatters the propagating waves in order to guarantee the continuity of displacements and the equilibrium of forces. This case is particularly interesting for periodic systems like metamaterials. Indeed, the building block of the periodic system can be designed in order that the resulting interference between the propagating waves leads to a desired dispersion relation for the periodic system. This is a crucial concept, since the dispersion relations reflect how waves and energy propagate through the metamaterial and, therefore, are fundamental in determining its effective properties.

An example

An example of a periodic system is here presented in order to highlight the relations between the definition of its building block and the response of the finite structure. The analyzed system consists of simple masses connected by linear springs (Jensen, 2003), as shown in figure 6.1. Periodic systems that are characterized by a periodic variation of the acoustic properties of the material (i.e., elasticity and mass) are usually referred as *phononic crystals*.[1] One of the main properties of phononic crystals is the possibility of featuring phononic bandgaps, i.e. selected ranges

1 Strictly speaking, phononic crystals may not be categorized as metamaterials, since the phononic bandgaps arise from the interaction of waves with a wavelength of the same order of magnitude of the periodicity and, therefore, the subwavelength requirement is missing. However, the importance of this example is to show how the characteristics of the building block of a structured material affect its dispersion property and, finally, the global response of the system.

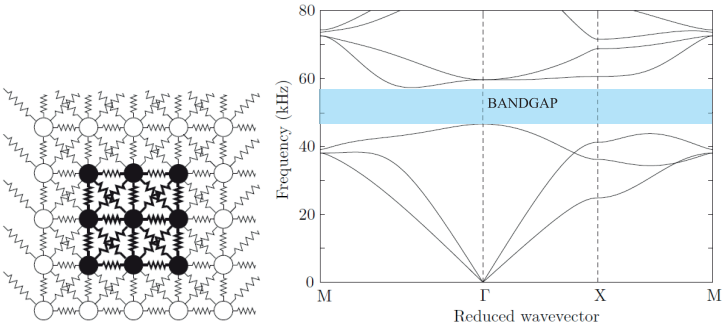

Figure 6.1: Building block (a) and dispersion relation (b) of a periodic system consisting of simple masses and springs (Jensen, 2003).

of frequencies were acoustic waves are prevented from being transmitted through the material.

Bandgap in the dispersion relation of the infinitely periodic structure

The building block shown in figure 6.1a consists of a 2D unit cell with a heavy and stiff inclusion of 3×3 masses and connecting springs (in bold) surrounded by a softer matrix material with additional masses and springs. The corresponding dispersion relation is reported in figure 6.1b and shows the frequency of propagating modes versus the reduced wavevector (indicating wavenumber and direction of propagation). The propagating modes (the solid lines) do not exist in the frequency range $46.6 - 57.3$ kHz. This implies that no waves in this range can propagate through the material regardless of the direction of propagation. The bandgap is the result of destructive interference between the waves scattered by the periodic distribution of masses and springs (*Bragg scattering*). In order for this interference to occur and a bandgap to be created, the spacing between the inclusions must satisfy certain conditions. These conditions are governed by the main frequency (and the corresponding wavelength) of the wave, and also by the contrast between the material properties of the inclusions and the background material.

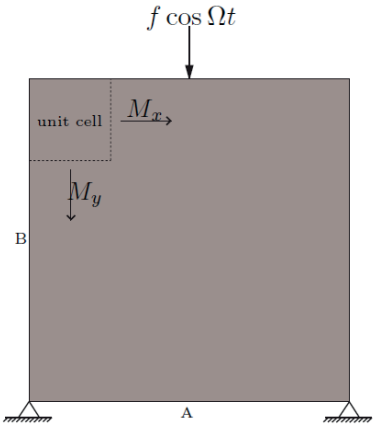

(a)

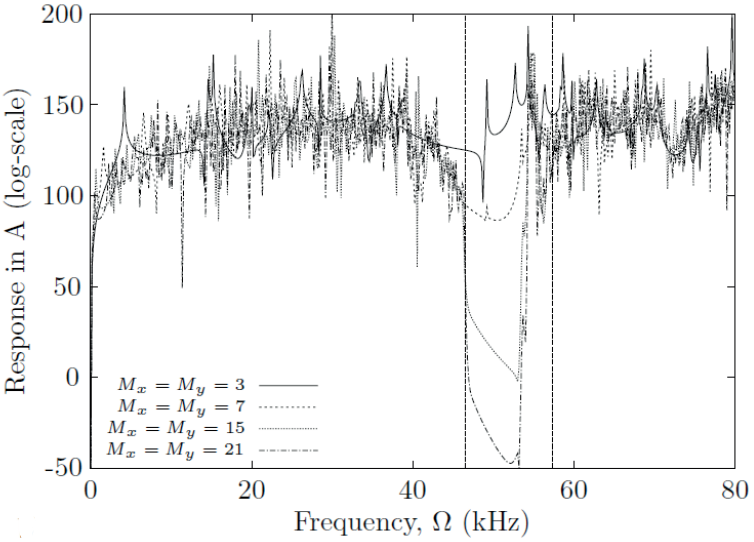

(b)

Figure 6.2: a) A simply supported structure with Mx × My unit cells subjected to a periodic load. b) Acceleration response calculated in point A with different numbers of unit cells in the structure (Jensen, 2003).

Low-amplitude vibrations in the response of the structure with finite-dimensions

The dispersion relation provides useful information about propagation of waves in an infinite material. Now, let us focus on the forced vibration response of a finite structure made from such a material. The finite structure presented in figure 6.2 is composed of a number of identical building blocks like the one shown in figure 6.1a. There is a correlation between the bandgap frequency range (indicated by vertical dashed lines) and a low-amplitude vibration response. If the structure is composed of many unit cells (such as 15×15 or more), the response amplitude dips exactly when the forcing frequency exceeds the lower bandgap frequency limit. This response dip is significant and more pronounced with more unit cells. When waves cannot propagate in the material, a high steady-state vibration level cannot build (and no standing waves, or resonances, appear) which explains this correlation.

Since the bandgap is a property of the 'material', the final structure made of this material will always feature a low vibration level range of frequencies, no matter the kind of boundary conditions, nor the size or geometry of the final structure.

6.3 TOP-DOWN AND BOTTOM-UP APPROACHES

A comparison between the metamaterial and the conventional approach to the design of a structure subjected to vibrational inputs is here proposed as an example to highlight the main differences and peculiarities of the two approaches. In a conventional top-down approach, like the one used in the first part of the thesis, the design variables that contribute in defining the dynamic response of the structure are mainly related to its geometry and the selected materials. Depending on the specific case study, the geometrical and material parameters are then designed in order to avoid resonances of the natural frequencies of the system with the excitation spectrum and/or to reduce the vibration amplitude. On the other hand, in a bottom-up approach the microstructure of the metamaterial can be designed, for instance, so that it exhibits bandgaps in the excitation frequency range. As shown in the example of the previous section, a structure made out of this metamaterial will always respond with low-amplitude

vibrations in the bandgaps frequency ranges, no matter neither the kind of boundary conditions nor the geometry of the final structure. A main difference in terms of performance of the final structures is, therefore, the independence from the geometry and boundary conditions of the metamaterial design approach, which can be associated to a *bottom-up* concept since the macroscopic properties of the final structure arise from the microstructure of the material.

The macroscopic properties of the final structure arise from the microstructure of the material

From a manufacturing point of view, the metamaterial approach takes instead advantage of a *top-down* approach. Indeed, one of the elements of fascination with metamaterials, at least from a conceptual level, is the freedom given by modern additive manufacturing technologies to 'synthesize' new building blocks, whereas the synthesis of conventional materials is governed and limited by kinetic or thermodynamic constraints. Metamaterials combine, therefore, the advantages related to a top-down manufacturing while exploiting the potentiality and robustness of a bottom-up design of its properties.

6.4 ADAPTIVE METAMATERIALS

Since the 'artificial' atoms of the metamaterial can be anything, it is not only possible to initially build up a metamaterial with required properties, but also to adjust and control them during the operation using convenient mechanism, or extend their potentiality with adaptive materials. From another point of view, the application of a metamaterial approach to the design of adaptive structures may lead to deeper exploitation of the adaptive materials. No matter the point of view, the combination of the concepts 'adaptive' and 'metamaterial' brings a remarkable number of research possibilities.

For instance, chapter 2 has highlighted how shunted piezoelectric transducers behave as time-dependent stiffness elements that may reach extreme values. If arranged in a periodic fashion, the resulting stiffness discontinuities can be exploited to adaptively modify the wave propagation properties of the metamaterial. The metamaterial approach completely differs from the conventional piezoelectric shunt damping, where specific eigenmodes of the

host structure are targeted by a discrete number of transducers that are basically used to dissipate the vibration energy. In a metamaterial approach, the piezoelectric elements may be used as variable stiffness elements to alter the band structure in such a way that the propagation of energy is inhibited for certain frequency ranges and the combination of wave propagation and boundary conditions cannot lead to the creation of structural vibrations.

Control of the wave dispersion in periodic media

In this thesis, the idea is to exploit the effective stiffness of shunted piezoelectric elements to control the wave dispersion in periodic media, with focus on adaptive bandgaps. Bandgaps are particularly significant because they represent forbidden energy states that, for instance, in a mechanical structure would lead to frequency ranges free from vibrations. The next two chapters present how the additional degrees of freedom offered by shunted piezoelectric transducers can be used to create, cancel or shift the frequency of the bandgaps in mechanical metamaterials.

7

TUNABLE WAVEGUIDE

One of the outstanding challenges in mechanical metamaterials development is the ability to tune their performance without requiring structural modifications. This chapter reports on the experimental demonstration of a tunable acoustic waveguide implemented within a two-dimensional phononic plate. The waveguide is equipped with a periodic array of shunted piezoelectric transducers. The resonance characteristics of the shunts lead to strong attenuation at tunable frequencies and are responsible for the creation of tunable acoustic bandgaps. The work presented in this chapter is the result of collaboration with Prof. M. Ruzzene and Dr. F. Casadei from the School of Aerospace Engineering at Georgia Institute of Technology. The results presented in this chapter have been published in the following journal paper:

> F. Casadei, T. Delpero, A. Bergamini, P. Ermanni, and M. Ruzzene, "Piezoelectric resonator arrays for tunable acoustic weaveguides and metamaterials," *J. Appl. Phys.* **2012**, 112 (6), 064902

7.1 CONCEPTUAL APPROACH

The interesting properties of phononic crystals and acoustic metamaterials rely on the ability to tailor the propagation of acoustic waves, for instance through the generation of acoustic bandgaps (Hsiao et al., 2007; Khelif et al., 2006; Mohammadi et al., 2008; Martinez-Sala et al., 1995).

The mechanical impedance mismatch between the periodic elements is a key factor for obtaining frequency bandgaps. They may originate from wave scattering occurring at wavelengths of the same order of the unit cell size (Bragg scattering) (Cheng et al., 2006), as shown in the example of the previous chapter, or may be induced by a local resonance within the unit cell of

the system (Lai et al., 2011; Huang and Sun, 2009; Liu et al., 2000). Considering that, for a given material, the dispersion properties define an inverse relation between the frequency and the length of the waves traveling through it, low frequencies Bragg-type bandgaps are associated with large wavelengths and require large structure. The local resonance mechanism is of particular interest for the possibility of generating low frequency bandgaps without increasing the lattice constant, and for the possibility of providing the medium with unusual mechanical properties at long wavelengths. The latter is the main objective in the study and development of acoustic metamaterials (Fang et al., 2006; Liu et al., 2000), while Bragg scattering is often exploited in phononic crystals designed to filter, localize and guide acoustic waves (Bonello et al., 2007; Wu et al., 2009).

Locally resonating acoustic metamaterials

Locally resonating acoustic metamaterials have been implemented by considering single (Yao et al., 2008) and multiple degrees of freedom resonating units such as soft inclusions periodically dispersed in a hard material matrix (Still et al., 2011; Hsu and Wu, 2007; Oudich et al., 2011; Wang et al., 2004; Cui et al., 2009; Hirsekorn et al., 2006; Xiao et al., 2008; Liu et al., 2000), or periodic arrays of tuned Helmoltz resonators in an acoustic waveguide (Fang et al., 2006; Cheng et al., 2008). While most of the proposed metamaterial configurations operate at fixed frequency ranges, recent investigations have considered the use of large deformations (Bertoldi and Boyce, 2008), or electromagneto mechanical couplings (Vasseur et al., 2011) as viable solutions to achieve tunable bandgaps and equivalent mechanical properties. Airoldi and Ruzzene (2011) recently showed that a periodic arrangement of piezoelectric patches bonded to a one-dimensional waveguide can be interpreted as a 1D metamaterial with local resonating units. The underlying idea, based on the pioneering work by Thorp et al. (2001, 2005), exploits the resonating behavior of shunted piezoelectric elements to generate a frequency bandgap centered at the resonance frequency of the electrical circuits. The tunable characteristics of shunted piezo patches allow the equivalent mechanical impedance to be tuned so that bandgaps are generated over desired frequency ranges, without any modifications to the structure.

Tunable waveguide

This chapter reports on a new tunable waveguide configuration, whereby Bragg scattering bandgaps are combined with piezoelectric resonators to confine and control the propagation of elastic waves in a phononic crystal plate (Wu et al., 2008). The waveguide consists of a periodic array of cylindrical stubs bonded to the plate surface. The stubs produce a large frequency bandgap that confines the propagation to the waveguide. A second array of piezoelectric resonators is added to the vertical portion of the waveguide for wave transmission control. The resonating characteristics of the shunted piezos lead to strong wave attenuation at the tuning frequency, and provide the waveguide with resonating mechanical properties which lead to negative group velocities. The tunable characteristics of shunted piezo patches allow the equivalent mechanical impedance to be tuned so that bandgaps are generated over desired frequency ranges, without any modifications to the structure. From this perspective, the waveguide can be considered as an example of a tunable acoustic metamaterial, with equivalent properties defined by the electromechanical resonators.

7.2 EXPERIMENTAL METHODS

Setup and materials

The considered phononic crystal consists of a thin aluminum plate (1 mm thick) with a periodic arrangement of surface-bonded cylindrical stubs of diameter $d = 7$ mm and height $h = 10$ mm. The stubs are made of aluminum and are arranged in a square lattice of constant $a = 10$ mm. Standard epoxy glue is used to bond the stubs to the plate surface.

An L-shaped waveguide is realized within a 17×17 lattice by removing parts of one row and one column of stubs as shown in figure 7.1a. The stubbed plate is characterized by a Bragg-type bandgap (Wu et al., 2009) between 100 and 130 kHz so that, in this frequency range, elastic waves are forced to propagate only in the region where the stubs have been removed (i.e. the waveguide). The vertical portion of the channel is equipped with a periodic array of 8×1 piezo-ceramic (PZT) disks (Steminc SMD10T04F: diameter $d_p = 10$ mm, capacity $C_p = 1.8$ nF). Each transducer is independently shunted through an inductive

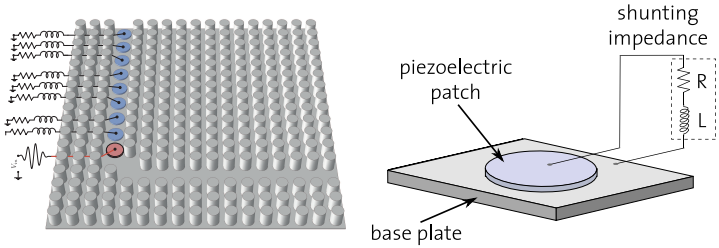

Figure 7.1: Tunable waveguide with electrical resonating units. a) Illustration of the phononic crystal plate with the cylindrical stubs and the L-shaped waveguide. The vertical portion of the waveguide is equipped with a periodic arrangement of piezoelectric discs. Eight transducers are independently shunted with an inductive circuit, while the one located near the bend (in red) is used for exciting the structure. b) Schematic model of the building block of the vertical channel. The combination between the capacity of the piezo and the electrical circuit creates the resonating unit that generates the tunable bandgap.

circuit realized by means of passive axial inductors mounted on a conventional breadboard configuration. The considered resonating unit is schematically shown in figure 7.1b where the resistive element accounts for any electrical loss introduced by wiring and connections.

Data processing

The wave propagation properties of the structure are characterized through two-dimensional wavefield measurements, recorded by a scanning laser vibrometer (Politec PSV-400). Measurements are conducted over a grid of 140×140 scan points with a spatial resolution of 1 mm in the horizontal and vertical directions. At each grid point, the laser measures the time history of the component of velocity $w(x_i, y_j, t)$ $i, j = 1 \dots 140$ normal to the plate surface. Each time history includes 512 samples and is recorded at a sampling frequency of 1.28 MHz.

The waves are excited by a piezoelectric transducer located near the bend in the L-shaped waveguide (depicted in red in

figure 7.1a). The transducer is driven by an input signal consisting of a four-cycle tone burst centered at 100 kHz, generated by a waveform generator (Agilent 33220A - 20MHz), and amplified by a piezo driver amplifier (Trek PZD 350).

The measured data are analyzed through spatial and temporal Fourier transforms to eliminate disturbances from boundary reflections and to obtain direct estimates of real and imaginary parts of the wavenumber. This data processing starts with a frequency-wavenumber filtering (Ruzzene, 2007) to remove boundary reflections. Next, the response recorded in the waveguide is spatially averaged through the width

$$\hat{w}(\ell, \omega) = \frac{1}{N_\ell} \sum_{i,j \in \ell} \hat{w}(x_i, y_j, \omega) \tag{7.1}$$

where ℓ denotes a line across the width of the channel comprised of N_ℓ scan points. A spatial Fourier Transform along the length of the channel leads to the frequency-wavenumber representation of the averaged response ($\hat{W}(k, \omega) = \mathcal{F}[\hat{w}(\ell, \omega)]$), whose amplitude is represented by the contours in figures 7.3 and 7.4, which are discussed in the next section.

Whereas the 2D Fourier transform of results facilitates the identification of a tunable bandgap, the experimental estimation of the wavenumber in terms of attenuation and propagation constants, shows its internal resonance nature. The wavenumber is generally a complex vector with a component for each propagating direction. The real part of the wavenumber describes the propagative characteristic, while the imaginary part defines the attenuation properties of the system. Both real and imaginary part of the wavenumber are quantitatively estimated as a function of frequency: at each frequency of interest, the real part of the wavenumber can be evaluated from the spatial phase change of the Fourier transform of the response along the vertical channel $\hat{w}(\ell, \omega)$, while the imaginary part can be evaluated from the spatial amplitude decay of the same Fourier transform (Airoldi and Ruzzene, 2011).

7.3 DISPERSION RELATIONS

Characterization of the phononic waveguide

The transmission characteristics and the tunable properties of the waveguide are evaluated through the analysis of two-dimensional wavefield measurements recorded on the back surface of the stubbed plate. The considered phonic plate, originally proposed by Wu et al. (2008), is characterized by a Bragg-type bandgap between 100 and 130 kHz (Wu et al., 2009). This frequency range is defined by the material and geometry of plate and stubs and cannot be changed after the system is assembled. Figure 7.2 shows that the system behaves as an effective waveguide only at frequencies inside the bandgap (figure 7.2b) of the considered phononic crystal plate, while elastic waves are free to propagate in every direction at frequencies below (figure 7.2a) and above (figure 7.2c) the bandgap region. The bandgap frequency range is shown in figure 7.2d that represents the frequency spectrum averaged along the red dashed line in sub-figures 7.2a-7.2c.

Effect of the open circuit piezos

The resonant shunted piezos located in the vertical channel feature an effective frequency-dependent stiffness, whose real and imaginary part show strong variation close to the resonance frequency, as explained in section 2.2. Of note is the fact that away from the resonance conditions, or for the case of open circuit, the contribution of the piezo disks to the overall stiffness of the waveguide appears as negligible. Therefore, the added stiffness corresponding to the array of disks is not sufficient to generate Bragg-scattering within the frequency range of interest, so that waves propagate almost undisturbed within the channel.

The two-dimensional map of the wavefield recorded with open circuits shown in figures 7.2a-7.2c clearly illustrates how the wave transmission within the channel is not altered by the presence of the piezo disks. Also, figure 7.3 shows the contour of the frequency/wavenumber domain representation of the wavefield recorded along the vertical waveguide. The contours are overlapped to the theoretical dispersion branch of the first antisymmetric (A_0) Lamb wave mode for the considered plate. The close match between the contours and the theoretical dispersion, and the continuous frequency/wavenumber distribution defined by the contours, suggest how the behavior of the

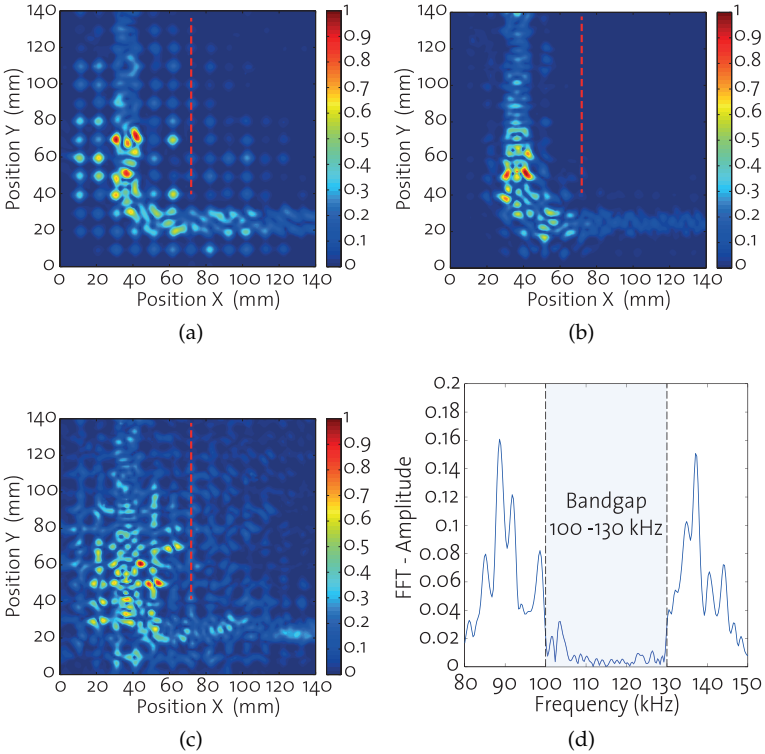

Figure 7.2: Full wavefield measurements demonstrating the waveguiding capability of the phononic crystal plate. Fourier transform of the measured wavefield below (a - 92 kHz), within (b - 117 kHz) and above the bandgap (c - 152 kHz). Sub-figure (d) reports the frequency spectrum averaged along the red dashed line in sub-figures (a-c).

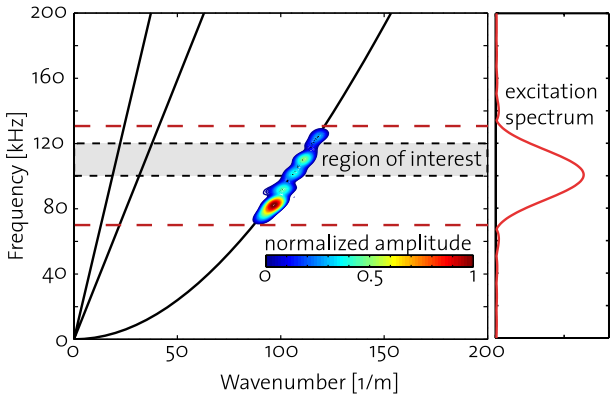

Figure 7.3: Measured and calculated dispersion properties of the vertical channel with open circuits. The structure is excited in a frequency range between 70 kHz and 130 kHz. The measured response along the vertical channel is processed and represented with contour lines in the frequency-wavenumber domain. The black solid lines represent the theoretical dispersion curves computed for a uniform 1 mm thick aluminum plate.

waveguide closely resembles that of a plane plate of the thickness considered in the experiments and that the presence of the open-circuit piezos has little effect on wave transmission.

Effect of the resonating piezos

Shunting of the piezos through the electrical networks produces a resonant, complex modulus, which in turn generates an additional tunable bandgap centered at the resonance frequency of the electrical networks. The tunable properties of the waveguide are illustrated by wavefield measurements with circuits designed to resonate at different frequencies. Specifically, two sets of inductors ($L_1 = 1890\,\mu H$, $L_2 = 1560\,\mu H$) are used to tune the resonating units within the bandgap of the stubbed plate. In each case, contours of the frequency/wavenumber representation of the response, shown in figure 7.4, indicate that the resulting medium features a bandgap centered at the tuning frequencies.

The measured data also allow the experimental evaluation of real and imaginary part of the wavenumber, also known as

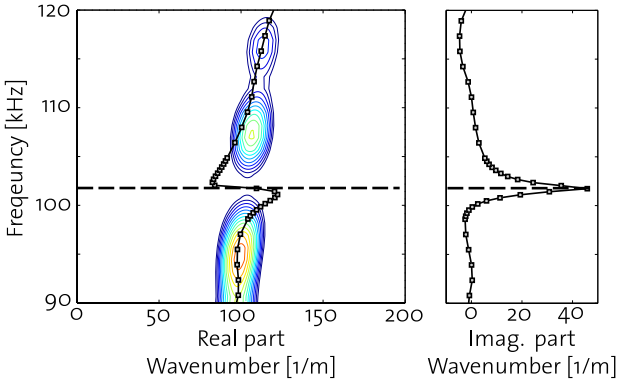

(a)

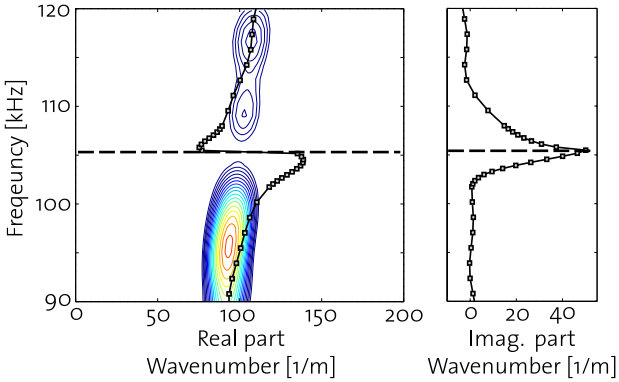

(b)

Figure 7.4: Experimental evidence of the resonant-type bandgap obtained by shunting the piezos with $L = 1890\,\mu H$ (a) and $L = 1560\,\mu H$ (b). The contour lines are the frequency/wavenumber representation of the response measured in the vertical channel. The black lines display the estimated real and imaginary parts of the wavenumber.

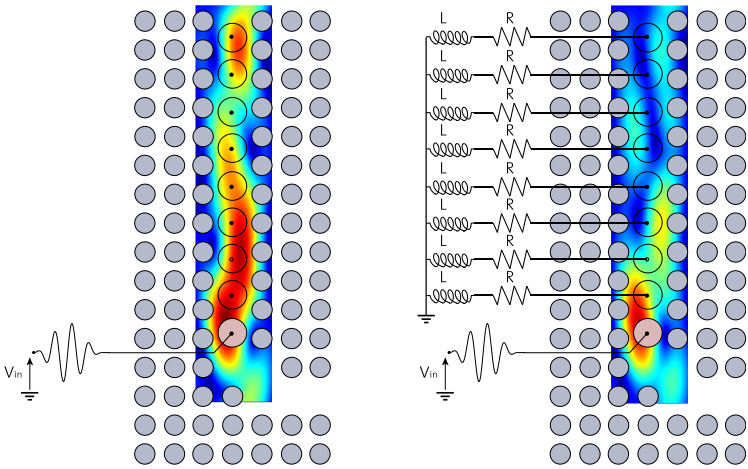

Figure 7.5: Maps of the Fourier transform of the measured response in the channel at 110 kHz, for both the open circuit configuration (a) and the shunted case (b).

Attenuation and propagation constants

attenuation and propagation constant. The real component of the wavenumber, overlapped as a solid line with square markers to the contour plots in figure 7.4, reveals the back-bending of the dispersion curve typical of internally resonating metamaterials. In this range of frequencies, elastic waves travel with a negative group velocity, antiparallel to the phase velocity. Also, the imaginary part exhibits a sharp peak of attenuation in a small range of frequencies centered at the resonance of the electrical circuit.

The resulting attenuation properties of the waveguide are responsible for the onset of the tunable bandgap, and can be correlated to the frequency variation of the effective modulus of the resonating units as shown in figure 2.6. Furthermore, the back-bending characteristics of the dispersion curves and the associated negative group velocity confirm the interpretation of the proposed waveguide as a tunable, internally resonating metamaterial.

Metamaterial with tunable dispersion relations

The investigated structure can be described like a metamaterial with tunable dispersion relations. The peculiarity lies in the waveguiding capability of the phonic structure whose dispersion relations can be tuned without changing any neither mechanical nor geometrical property of the structure. An evident proof of this tunability is reported in figure 7.5, where the amplitudes of the Fourier transform coefficients corresponding to 110 kHz are reported for the vertical channel in both the open circuit state and shunted conditions (with $L_3 = 1330\,\mu H$). The periodic arrangement of shunted piezoelectric discs allows to switch between a condition (open circuit) in which the mechanical waves are free to travel through the channel and a condition (shunted) where the waves with a frequency of 110 kHz are stopped. Moreover, the frequency at which the waves are evanescent can be tuned simply by changing the electrical components, without modifying the physical structure of the phononic crystal plate.

7.4 CONCLUSIONS

The experiments presented herein demonstrate the possibility of implementing an elastic waveguide with tunable dispersion properties. In conventional phononic crystals, acoustic waves are diffracted only at wavelengths of the order of the lattice constant. In contrast, the proposed concept allows controlling the dispersion relations of the system so that bandgaps are generated at selected frequency ranges without modifying the lattice constants of the crystal. This phenomenon is also independent of the spatial periodicity of the resonating units and is controlled by the effective frequency-dependent modulus of the shunted piezoelectric transducers. The resulting metamaterial therefore behaves as a homogenized medium with tunable attenuation and resonant properties.

The proposed concept suggests novel opportunities in several fields of engineering and material science for the design of tunable acoustic metamaterials, acoustic switches and logic ports which can be actively controlled through external stimuli, and for applications which include vibration isolation, noise attenuation, as well as wave guiding, localization, and filtering.

The multi-field coupling is here identified as the enabling mechanism for the generation of tunable internal resonances, and the achievement of unusual wave mechanics. Although in the present study the mechanism has been demonstrated through a simple experimental apparatus, these results open a new frontier for the development of a novel class of materials that exploit different forms of energy and multi-field coupling for the achievement of tunable mechanical properties.

8

PHONONIC CRYSTALS WITH ADAPTIVE CONNECTIVITY

In this chapter, the time-dependent effective stiffness of shunted piezoelectric discs is used to tune the connectivity between the constituting elements of a phononic crystal. The band structure of a phononic crystal depends on the interaction between neighboring elements and can be therefore controlled by tuning the mechanical stiffness of the links connecting its constituting elements. The metamaterial proposed in this chapter is the first implementation of a phononic crystal with adaptive connectivity. The results presented in this chapter have been published in the following journal paper:

> A. Bergamini, T. Delpero, L. De Simoni, L. Di Lillo, M. Ruzzene and P. Ermanni, "Phononic crystal with adaptive connectivity," *Adv. Mater.* **2014**, 26 (9), 1343-1347

8.1 CONNECTIVITY AND MATERIAL PROPERTIES

Connectivity in phononic crystals

The properties of metamaterials result from the chosen geometric arrangement of the unit cells as well as from the bulk behavior of the materials they are composed (Lapine and Tretyakov, 2007; Zheludev and Kivshar, 2012). While in a mathematical sense, the *connectivity* between elements of a lattice is plainly defined by its topology (Listing, 1848; Euler, 1741), in a physical context it implies the ability of neighbors to interact with one another. In this chapter, the first implementation of a metamaterial with variable mechanical connectivity, whose effective properties can be tuned by exploiting a transducive material, is presented. In the phononic crystal described by Wu et al. (2008) the periodic distribution of masses connected to the continuous substrate is responsible for the generation of Bragg-type bandgaps. Here it is shown that by interposing variable stiffness links between the

substrate and the masses, the connectivity between the elements of the phononic crystal and therefore its band structure can be adaptively controlled.

Geometrical pattern and structural hierarchy of metamaterials

In the last decade, several examples of metamaterials whose peculiar properties can directly be ascribed to the specific geometrical connectivity patterns between their constituting elements have been presented. With respect to the dynamic properties, atypical dispersion relations, such as negative group velocity (Fang et al., 2006), stop bands (Jensen, 2003) and acoustic cloaking (Zhang et al., 2011; Chen and Chan, 2007; Cummer and Schurig, 2007) have been obtained by tailoring the propagation of acoustic waves scattered by mechanical impedance discontinuities coupled, in some instances, with internally resonating units (Liu et al., 2000; Lai et al., 2011). With respect to the quasi-static mechanical properties, negative Poisson's ratio (Bueckmann et al., 2012; Xu et al., 1999), stiffer than diamond materials (Jaglinski et al., 2007), extreme damping in composite materials with negative stiffness inclusions (Lakes et al., 2001), as well as materials with out-of-the-ordinary ratios of bulk to shear modulus have been reported (Kadic et al., 2012), whose macroscale physical properties result from the structural hierarchy and topology across micro- and meso-scales.

Allotropes of conventional and metamaterials

In an analogous way to how the dispersion properties of crystalline materials define their properties, the macroscale properties of the metamaterials presented in the previous examples are defined by their periodicity and connectivity patterns. It is then clear that allotropes of the same element (both in conventional materials and metamaterials) are characterized by differing physical properties originating from the different connectivity of the crystal lattices (for instance, diamond and graphite crystal structures are responsible for the emergence of different physical properties). However, the ability to steer the mechanical properties of conventional materials made of proper atoms is limited by the processes that lead to formation of their crystal lattices, specifically by their thermodynamics and kinetics. On the other hand, the freedom that nano-, micro- or meso-structures provide for the design of the unit cell represents one of the elements of fascination with them. Especially at the meso- and micro-scale,

the top down approach to the fabrication of metamaterials allows forgoing the practical issues that material scientists face. As a result of this approach, the map of connectivity between each unit cell and its neighbors, the mass of the constituting elements and elastic properties of the binding elements could be chosen independently of each other. Additionally, since the 'artificial' atoms of the metamaterial can be anything, it is not only possible to initially build up a metamaterial with required properties, but also to adjust and control them during the operation using, for instance, adaptive materials.

8.2 ADAPTIVE CONNECTIVITY

Adaptive periodicity

This chapter presents a phononic crystal that includes tunable stiffness elements, to obtain a variable mechanical coupling between the substrate and the stubs responsible for the scattering (see figure 8.1). The central idea is to control the connectivity of the stubs-substrate pattern. The variable connectivity elements are realized by piezoelectric discs shunted through an inductive circuit such that they behave as frequency dependent stiffness links (as explained in section 2.2) between the substrate and the stubs. In this context, the concept of mechanical connectivity is defined as the ability of the physical bonds between elements to transfer mechanical stress. Under conditions of electrical resonance, the stiffness of the physical connection can be drastically reduced: elements that would otherwise be mechanically connected to one another will be disconnected allowing for a change in the periodicity patterns. Hence, the periodicity of the phononic crystal, which is responsible for the presence of the band gap, can be altered in a prescribed frequency range, and a neat pass band can be obtained. This modification of the interaction of a phononic crystal with a mechanical wave travelling through it, can thus be ascribed to a change of the mechanical connectivity of the system.

The concept of phononic crystal with adaptive connectivity is qualitatively represented in figure 8.2. The diagram on the left reports the dispersion relation of the phononic crystal: the Bragg-type bandgap occurs at a wavenumber related to the lattice

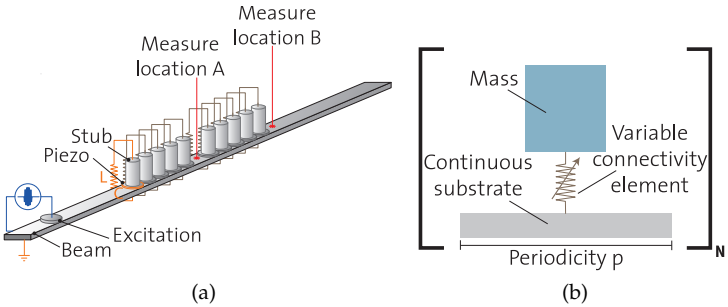

Figure 8.1: Phononic crystal with tunable (frequency-dependent) connectivity. a) Schematic view of the considered phononic crystal with the cylindrical stubs and the piezoelectric discs. b) Detailed view of the adaptive unit cell: the variable stiffness element changes the mechanical connectivity of the unit cell from a periodic structure to a simple continuous substrate.

periodicity p, as defined in figure 8.1b. The diagram on the right reports the real (solid line) and the imaginary (dashed line) parts of the effective stiffness of a resonant shunted piezoelectric disc. Just below the resonance frequency, the real part is strongly reduced and isolates the stubs responsible for the bandgap, creating therefore a neat pass band in the dispersion relation.

Tunable dispersion properties

Tunability of dispersion properties has been already demonstrated in photonic crystals (Feng et al., 2005) and theoretically investigated in phononic (Robillard et al., 2009) crystals. In these systems, however, external fields, such as temperature or magnetic field, are used to modify the properties of the bulk materials and therefore their dispersion properties. Tunable phononic bandgaps have also been investigated by altering the geometry of the system (Goffaux and Vigneron, 2001) and obtained in arrays of cylindrical elements by changing the orientation and precompression of the constituting elements (Li et al., 2012). The approach presented in this chapter is different, since the modification of the phononic crystal is obtained neither by changing the bulk material properties nor the geometry of the constituting elements, but the connectivity of the crystal structure.

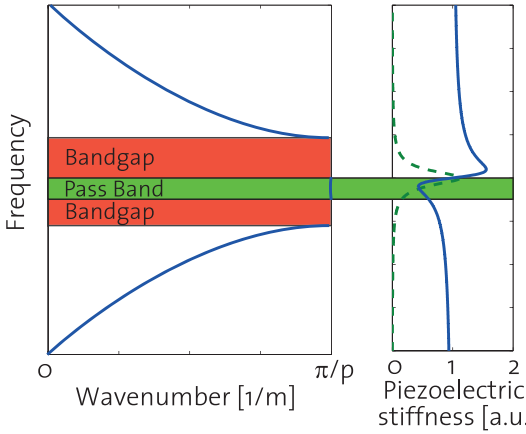

Figure 8.2: Qualitative representation of the effect of frequency dependent stiffness elements on the band structure of the phononic crystal.

8.3 EXPERIMENTAL METHODS

Description of the phononic crystal

The unit cell of the phononic crystal consists of an aluminum substrate ($10 \times 10 \times 1$ mm) with a cylindrical stub of diameter $d = 7$ mm and height $h = 10$ mm, also made of aluminum. This configuration was chosen considering the work presented by Wu et al. (2008) in order to have, in the open circuit state, a broad bandgap around 100 kHz. The frequency-dependent connectivity of the unit cell is introduced by a piezoelectric disc (Steminc SMD10T04F: diameter $d = 10$ mm, nominal capacity $Cp = 1.8$ nF) that is glued with conductive epoxy between the stub and the substrate, and it is connected to the shunting inductor. The investigated phononic crystal consists of ten of these unit cells arranged in a 1D array configuration as two subsequent series of five elements, as depicted in figure 8.3. Despite the small nominal value required for the inductors, they are implemented with the Antoniou inductance-simulation circuit (Antoniou, 1969). This semi-active implementation allows their fine tuning in order

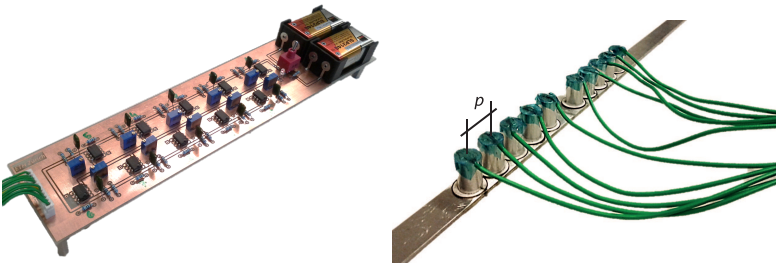

(a) (b)

Figure 8.3: Picture of the Printed Circuit Board with the synthetic inductors (a) and picture of the investigated array of stubs and piezoelectric discs (b).

to have the same resonance frequency for all the piezoelectric resonators.[1]

Experimental setup and data processing

The wave propagation properties of the structure are investigated through wavefield measurements, recorded by a scanning laser vibrometer (Politec PSV-400). Measurements are conducted over a grid of 9×250 scan points with a spatial resolution of 0.6 mm. At each grid point, the laser measures the time history of the out-of-plane component of velocity. Each time history includes 512 samples and is recorded at a sampling frequency of 1.28 MHz. The structure is excited with an additional piezoelectric actuator providing a burst chirp signal between 70 and 130 kHz. The measured data are analyzed by temporal Fourier transform to obtain the frequency spectrum reported in figure 8.4. Additionally, a spatial Fourier Transform along a line located after the phononic crystal leads to the frequency-wavenumber representation of the response whose amplitude is represented by the contours in figure 8.5.

1 The tuning process of the electrical resonators is performed by exciting the piezoelectric capacitance in series with tunable inductor circuits. The voltage over the inductor is measured by connecting it to an oscilloscope by means of BNC cable. The parasitic capacitance of the cable (0.7 nF) adds to the capacitance of the piezoelectric thus reducing the value of the measured resonating frequency. Under operational conditions, the value of is roughly 15% higher for all circuits.

8.4 BAND STRUCTURE AND DISPERSION RELATION

Figures 8.4a and 8.4b report the frequency spectra of the wavefield measured respectively after five (measure location A in figure 8.1a) and ten (measure location B) stubs when the piezoelectric discs are in an open circuit state. In this configuration, the system behaves as a standard phononic crystal, allowing waves propagation only in a certain frequency range determined by the structural arrangement of the atom-like elements. After five stubs the destructive wave interference starts to cause an amplitude reduction around 100 kHz, which becomes a clear and broad bandgap between 80 and 110 kHz after ten stubs. This frequency range is set by the material and geometrical properties of the system, and—in a standard phononic crystal—it cannot be changed after the system is assembled. Yet, when the piezoelectric discs are shunted through the tuned inductors, the stubs are decoupled from the vibration of the substrate at a prescribed frequency, which is essentially determined by the electromechanical coupling behavior of the circuitry-stubs-substrate system. The spectrum of the wavefield in the shunted operating mode is shown in figure 8.4c. Clearly, a permitted frequency range for the energy associated to the traveling wave is appearing between 90 and 100 kHz, right in the middle of the forbidden energies' range.

This result corroborates the assumption that the energy flowing through the substrate is not dissipated in the electrical circuits: the shunted piezoelectric discs effectively behave as "zero-stiffness" elements at a prescribed frequency and cloak the stubs from the waves in the substrate. The physical reason at the basis of the change in the effective stiffness of piezoelectric resonators has to be found in the strong electromechanical coupling capabilities offered by piezoelectric materials. The exchange processes which take place between the electrical and mechanical domains imply that the response of these materials depends on both the mechanical and electrical boundary conditions defining the system. For instance, their mechanical stiffness cannot be defined without specifying the electrical boundary conditions, such as open or short circuit operating modes. More in general, the

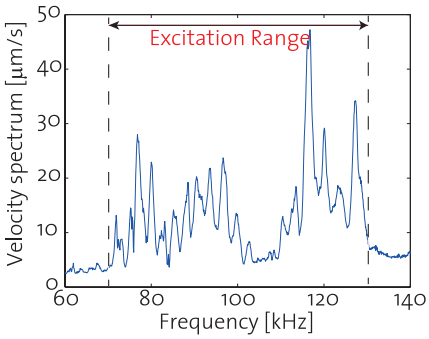

(a)

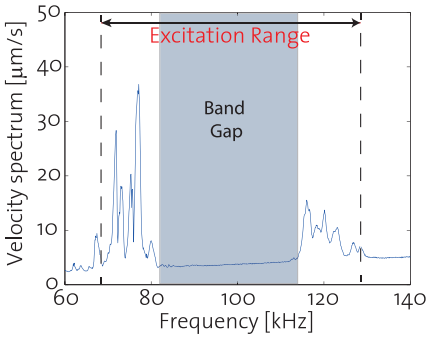

(b)

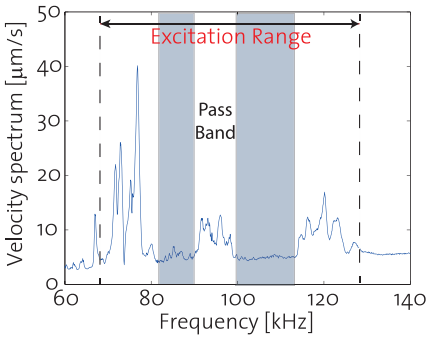

(c)

Figure 8.4: Experimental characterization of the tunable band structure of the phononic crystal in the open circuit (a-b) and in the shunted (b) states.

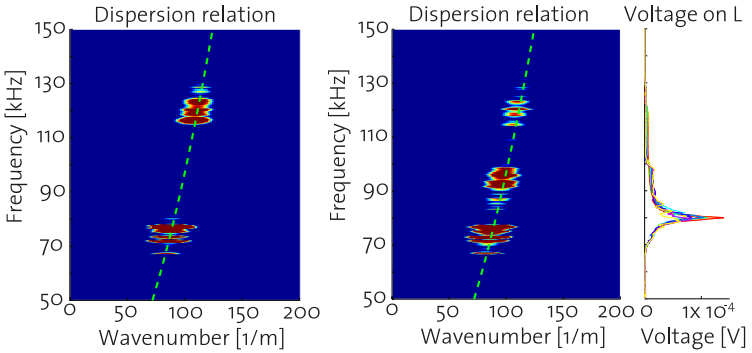

Figure 8.5: Measured and calculated dispersion properties of the phononic crystal in the open circuit (a) and in the shunted (b) states. The green dashed lines represent the theoretical dispersion curves of the first antisymmetric Lamb wave mode computed for a uniform 1 mm thick aluminum plate. For the shunted state, also the spectra of the voltage measured on the inductors are reported.

electrical boundary conditions in a piezoelectric resonator define the amount of electric energy storable in the form of electric field over a certain frequency range. Particularly, an enhancement in the energy storing capabilities is obtained at frequencies near the resonance. The stored electric energy is transferred to the mechanical domain by the converse piezoelectric effect affecting the mechanical response of the system. This energy exchange mechanism leads to a reduction or increase of the mechanical stiffness depending on the phase difference between the voltage across the piezo and its displacement.

To gain insights into the band structure of the phononic crystal under study, the wavefield is also represented in the frequency/wavenumber domain, in figure 8.5. The contour of the velocity response is displayed for both the open circuit and shunted configuration, and they are overlapped to the theoretical dispersion curve of the first antisymmetric Lamb wave mode (dashed green curve) for the sole substrate. The analysis of

the frequency response of the system is limited to the excitation range, $70 - 130$ kHz. The bandgap in the open circuit state and the pass band in the shunted configuration are clearly visible. The spectra of the voltage measured on the inductors are also reported on the left side of figure 8.5b. These spectra have been obtained by individually exciting the electric resonator circuits that were tuned to have the same resonance frequency. The shift between the tuning frequency and the pass band is attributed to the effect of the additional capacitance of the cable used for measuring the resonating voltage during the tuning phase, as explained in the footnote in the previous section.

8.5 CONCLUSIONS

The behavior of the piezo-augmented phononic crystal demonstrates the ability to manipulate the mechanical connectivity of a system. This task is fulfilled in this work by means of the frequency-dependent stiffness of the piezoelectric elements. The substantial reduction of the stiffness around the resonance frequency of a shunted piezoelectric element is tantamount to the break of an atomic bond (i.e. connectivity between the stubs in this work) that, for that frequency, makes the structure of the phononic crystal disappear. The presented results demonstrate the first implementation of a variable connectivity metamaterial (in the definition of Lee et al. (2012)) and of some of its properties.

The most immediate demonstration of the application of such a system will be, for example, a tunable logic port based on elastic waves, where channels composed of tunable phononic crystals in a two-dimensional structure will be used to separate different frequency components from a mixed frequency signal. The possibility to open a neat pass band in the middle of a bandgap could theoretically lead to extreme ratios between the signal in the pass band and the noise in band gap. Yet, the importance of our findings lies in the proposed approach even more than in the immediate results: a fairly small amount of adaptive material can be used to produce remarkable effects thanks to the exploitation of the system periodicity. This example of periodic structure comprised of active material components

shows the potential of the type of semi-active augmentation of metamaterials, where the properties (in this case mechanical) of part of the unit cell are modified exploiting a transductive material (in this case piezoelectric material). The same concept is expected to be applicable also to other physical domains.

The remarkable effect of the energy exchange between the mechanical and the electrical domain and the possibility to control it by means of simple analog circuits point to a new opportunity that the presented system offers: the development of a new class of 'programmable' materials, whose mechanical properties can be controlled via the modification of the parameters of arrays of simple analog or mixed electrical circuits. For this purpose, the development and integration of the necessary electrical circuits will be as important for achieving useful and out of the ordinary material properties as the geometrical design and material selection. As expected, a slight modification of the properties of the unit cell results in a dramatic change in the overall properties of the periodic structure.

While the functionality of the proposed concept has been demonstrated by simultaneously altering the connectivity of all the unit cells, shunting only a subset of the piezoelectric discs would also be possible in a following study. This approach would make the phononic crystal able to reach a whole set of effective periodicities, which would all be multiples of the fundamental one and would depend on the number of active piezo discs.

Part IV

CONCLUSIONS

9 CONCLUSIONS AND OUTLOOK

9.1 SUMMARY AND IMPLICATIONS OF RESEARCH FINDINGS

The work presented in this thesis has investigated the implications of including shunted piezoelectric elements in the design of adaptive structures. The focus was set on how the additional degrees of freedom introduced in the design space can lead to a qualitative step in the dynamic performance of the systems, compared to the plain mechanical one.

In the first part of the thesis the integration of shunted piezoelectric elements in the design of adaptive structures has been investigated with respect to their effect on vibration reduction. In particular, shunted piezoelectric elements are considered beyond their immediate intended purpose of adding damping and are employed as additional degrees of freedom that extend the design space to solutions able to fulfill more stringent requirements than the simply passive structure, or fulfill all the requirements with a minor weight.

Achieving this goal required a high degree of robustness of the shunt damping techniques and of the modeling of their damping performance. An approach for comparing the damping performance of different shunting strategies has been therefore initially presented and experimentally verified. It is based on non-dimensional parameters and allows for predicting the damping performance of piezo-augmented structures independently from the size and the geometry of the structure. A novel autonomous shunt has also been proposed, whose peculiarity lies in the introduction of an energy harvesting module to provide the energy required by the electronic components of the shunt. The performance of the proposed shunt is of particular interest due to its robustness with respect to the amplitude and frequency of the vibrations that may vary with the operating conditions of the host structure.

A concurrent design strategy has then been applied to the realistic case study of a rotating blade, where purely passive design solutions have been compared to adaptive ones in terms of vibration amplitude. The main contribution of the first part of this thesis has been in demonstrating how the concurrent consideration of adaptive and passive design variables in the early design phases allows finding a better compromise between stiffness and damping than a conventional sequential approach. A concurrent approach that relies on a robust source of damping can extend the design space to a new set of lighter, less stiff and more easily damped solutions, with a cascade of beneficial impacts on the result of the design process. The idea of relaxing the stiffness requirements of the structure may look counter-intuitive when designing a structure with the ultimate goal of reducing its deformation under dynamic excitation. The method presented in this thesis allows quantifying when this approach is valuable. Even though an accurate knowledge of the excitation spectrum is required for a quantitative comparison of the solutions in terms of vibration amplitudes, the adaptive design is in any case the most robust when this knowledge is not available or uncertain.

The second part of the thesis has focused on exploiting the adaptive materials at a lower level, i.e. the metamaterial level. Two examples have been presented to show how a fairly small amount of adaptive material can be used to produce remarkable effects on the dynamic response of the system thanks to the exploitation of the periodicity of metamaterials. In these examples, the effective stiffness of shunted piezoelectric elements is used to control the wave dispersion in periodic media, with focus on tunable bandgaps.

The first example is a tunable acoustic waveguide implemented with a periodic array of shunted piezoelectric transducers within a two-dimensional phononic plate. The resonance characteristics of the shunts lead to strong attenuation at tunable frequencies and are responsible for the creation of tunable acoustic bandgaps. The approach presented in the second example is different, since the time-dependent effective stiffness of shunted piezoelectric discs is used to control the connectivity between the constituting

elements of a phononic crystal. The substantial reduction of the stiffness around the resonance frequency of a shunted piezoelectric element breaks the connectivity between the substrate, where the waves propagate, and the periodically arranged masses, which are responsible for the Bragg-type bandgap. The periodicity of the phononic crystal is therefore canceled only at the resonance frequency. Both the proposed concepts suggest novel opportunities in several fields of engineering and material science for the design of tunable acoustic metamaterials, acoustic switches and logic ports which can be actively controlled through external stimuli and where channels composed of tunable metamaterials can be used to separate different frequency components from a mixed frequency signal.

The importance of the results presented in the second part lies more in their implications than in the immediate applications. The strong electromechanical coupling of piezoelectric materials allows obtaining remarkable effects in the mechanical response of the system by manipulating energy in the electrical domain, which can be easily done with simple analog circuits. The results presented in the second part of this thesis are examples of how the multi-field coupling of adaptive materials can further extend the already large freedom offered by the metamaterial approach for tailoring the dispersion properties of periodic structures.

9.2 OUTLOOK

Even though the potential of adaptive augmentation of structures is considerably high and piezoelectric materials represent a mature technology by their own, shunted piezoelectric materials have not yet been applied outside the research environment, besides few examples in sport equipment. The work presented in this thesis has the ambition of proposing new design approaches to better handle and exploit the freedom offered by the integration of shunted piezoelectric elements in adaptive structures. The goal of the proposed design approaches is to make use of the adaptive materials in order to obtain a significant improvement in the dynamic response of structures that could justify the increased complexity and cost of an adaptive solution. The

following is a presentation of topics that could be investigated to promote the further development and applications of shunted piezoelectric elements.

The approach presented in this work for the prediction of the performance of piezoelectric shunt damping could be extended to other shunting techniques (besides resonant and switching shunts) or active piezoelectric damping strategies, leading to a common diagram where the comparison of different piezo-based damping techniques is possible. This would represent a useful tool in the design of adaptive structures.

Among the large variety of shunt circuits available, switching shunts represent an attractive solution because of their robustness and self-powered implementation. While the improved performance of the switching shunt implemented in this work arises from an efficient switch, the application of more complex global maxima and minima detection techniques could further improve the broadband characteristic of this shunt. Additionally, its inherent non-linearity leads to the excitation of other vibration modes, besides reducing the amplitude of the targeted one, which could worsen the acoustic emission of the structure. If this side effect could be limited, for instance by reducing the sharpness of the switch using a larger inductor in the circuit, the switching shunt could represent an interesting solution both for vibration and acoustic emission reduction purposes.

While the research on piezoelectric shunt damping has reached a high level of maturity, the research possibilities in the field of adaptive metamaterials are remarkable. One of the main challenges is the creation of low frequency bandgaps while reducing the size and mass of the unit cell. The introduction of piezoelectric materials in the unit cell allows to transfer the realization of local resonators into the electrical domain and to loosen the strict relationship between the mass/stiffness ratio and eigenfrequency of the local resonator. The miniaturization and the integration of the electrical circuits in the metamaterial represent also an important technological aspect that should be investigated.

Additionally, the multi-field interaction offered by piezoelectric materials increases the possibilities of manipulating the prop-

agating energy. In this work, independent electrical resonators have only been considered. Among all the possible configurations of electrical circuits, the introduction of non-linearities and the series or parallel connections of the resonators may represent interesting configurations worth to be studied in the next future.

In the two examples of metamaterials presented in this thesis, the multi-field coupling is identified as the enabling mechanism for the generation of tunable internal resonances, and the achievement of unusual wave mechanics. Although in the present work the mechanism has been demonstrated in the mechanical domain, the concept of adaptive augmentation of the unit cell of a metamaterial is expected to be applicable also to other physical domains. The presented results open a new frontier for the development of a novel class of 'programmable' materials, which exploit different forms of energy and whose properties can be controlled via the modification, for instance, of simple analog electrical circuits.

BIBLIOGRAPHY

Airoldi, L. and Ruzzene, M. 2011. "Design of tunable acoustic metamaterials through periodic arrays of resonant shunted piezos," New Journal of Physics, 13(11):113010. (Cited on pages 102 and 105.)

Andreaus, U. and Porfiri, M. 2007. "Effect of electrical uncertainties on resonant piezoelectric shunting," Journal of Intelligent Material Systems and Structures, 18(5):477–485. (Cited on page 22.)

ANSI/IEEE 1988. IEEE Standard on Piezoelectricity, ANSI/IEEE Std 176-1987, New York, USA, the Institute of Electrical and Electronics Engineers, Inc. (Cited on pages 18 and 19.)

Antoniou, A. 1969. "Realisation of gyrators using operational amplifiers, and their use in rc-active-network synthesis," Electrical Engineers, Proceedings of the Institution of, 116(11):1838 –1850. (Cited on pages 58 and 117.)

Ashby, M. 2004. Materials Selection in Mechanical Design, Elsevier Science. (Cited on pages 67 and 72.)

Bachmann, F. and Ermanni, P. 2010. "Integration of encapsulated piezoelectric actuators in highly loaded cfrp structures," volume 7643, 76432H, SPIE. (Cited on page 41.)

Badel, A. et al. 2006. "Piezoelectric vibration control by synchronized switching on adaptive voltage sources: Towards wideband semi-active damping," The Journal of the Acoustical Society of America, 119(5):2815–2825. (Cited on page 34.)

Baravelli, E. and Ruzzene, M. 2013. "Internally resonating lattices for bandgap generation and low-frequency vibration control," Journal of Sound and Vibration, 332(25):6562 – 6579. (Cited on page 6.)

Becker, J. et al. 2006. "Finite element-based analysis of shunted piezoelectric structures for vibration damping," Computers and Structures, 84(31-32):2340 – 2350. (Cited on page 5.)

Behrens, S. et al. 2003. "A broadband controller for shunt piezoelectric damping of structural vibration," Smart Materials and Structures, 12(1):18. (Cited on page 5.)

Belloli, A. and Ermanni, P. 2007. "Optimum placement of piezoelectric ceramic modules for vibration suppression of highly constrained structures," Smart Materials and Structures, 16(5):1662. (Cited on page 5.)

Bertoldi, K. and Boyce, M. 2008. "Mechanically triggered transformations of phononic band gaps in periodic elastomeric structures," Physical Review B, 77(5):052105. (Cited on page 102.)

Bonello, B. et al. 2007. "Lamb waves in plates covered by a two-dimensional phononic film," Applied physics letters, 90:021909. (Cited on page 102.)

Bueckmann, T. et al. 2012. "Tailored 3d mechanical metamaterials made by dip-in direct-laser-writing optical lithography," Advanced Materials, 24(20):2710–2714. (Cited on pages 7 and 114.)

Casadei, F. et al. 2010. "Broadband vibration control through periodic arrays of resonant shunts: experimental investigation on plates," Smart Materials and Structures, 19(1):015002. (Cited on page 8.)

Cebon, D. and Ashby, N.F. 1994. "Materials selection for precision instruments," Measurement Science and Technology, 5(3):296. (Cited on pages 67, 68, and 71.)

Chen, H. and Chan, C.T. 2007. "Acoustic cloaking in three dimensions using acoustic metamaterials," Applied Physics Letters, 91(18):183518. (Cited on page 114.)

Cheng, W. et al. 2006. "Observation and tuning of hypersonic bandgaps in colloidal crystals," Nature materials, 5(10):830–836. (Cited on page 101.)

Cheng, Y. et al. 2008. "One-dimensional structured ultrasonic metamaterials with simultaneously negative dynamic density and modulus," Physical Review B, 77(4):045134. (Cited on page 102.)

Clark, W.W. 2000. "Vibration control with state-switched piezoelectric materials," Journal of Intelligent Material Systems and Structures, 11(4):263–271. (Cited on pages 31 and 32.)

Corr, L.R. and Clark, W.W. 2002. "Comparison of low-frequency piezoelectric switching shunt techniques for structural damping," Smart Materials and Structures, 11(3):370. (Cited on pages 5, 32, and 54.)

Corr, L.R. and Clark, W.W. 2003. "A novel semi-active multimodal vibration control law for a piezoceramic actuator," Journal of Vibration and Acoustics, 125(2):214–222. (Cited on page 5.)

Côté, F. et al. 2004. "Dynamic and static modelling of piezoelectric composite structures using a thermal analogy with msc/nastran," Composite Structures, 65(3-4):471 – 484. (Cited on page 5.)

Cui, Z. et al. 2009. "Experimental and calculated research on a large band gap constituting of tubes with periodic narrow slits," Applied Acoustics, 70(8):1087–1093. (Cited on page 102.)

Cummer, S.A. and Schurig, D. 2007. "One path to acoustic cloaking," New Journal of Physics, 9(3):45. (Cited on page 114.)

Davis, C. and Lesieutre, G. 1995. "A modal strain energy approach to the prediction of resistively shunted piezoceramic damping," Journal of Sound and Vibration, 184(1):129 – 139. (Cited on pages 6 and 32.)

Den Hartog, J. 1956. Mechanical Vibrations, McGraw-Hill Book Company, Fourth edition. (Cited on page 43.)

Ducarne, J. et al. 2010. "Structural vibration reduction by switch shunting of piezoelectric elements: Modeling and optimization," Journal of Intelligent Material Systems and Structures, 21(8):797–816. (Cited on pages 32 and 35.)

Euler, L. 1741. "Solutio problematis ad geometriam situs pertinentis," Commentarii academiae scientiarum Petropolitanae. (Cited on page 113.)

Fang, N. et al. 2006. "Ultrasonic metamaterials with negative modulus," Nature materials, 5(6):452–456. (Cited on pages 102 and 114.)

Feng, L. et al. 2005. "Tunable negative refractions in two-dimensional photonic crystals with superconductor constituents," Journal of Applied Physics, 97(7):073104. (Cited on page 116.)

Forward, R.L. 1979. "Electronic damping of vibrations in optical structures," Appl. Opt., 18(5):690–697. (Cited on pages 5 and 21.)

Frecker, M.I. 2003. "Recent advances in optimization of smart structures and actuators," Journal of Intelligent Material Systems and Structures, 14(4-5):207–216. (Cited on page 6.)

Goffaux, C. and Vigneron, J.P. 2001. "Theoretical study of a tunable phononic band gap system," Phys. Rev. B, 64:075118. (Cited on page 116.)

Guyomar, D. and Badel, A. 2006. "Nonlinear semi-passive multimodal vibration damping: An efficient probabilistic approach," Journal of Sound and Vibration, 294(1-2):249 – 268. (Cited on page 62.)

Hagood, N.W. and von Flotow, A. 1991. "Damping of structural vibrations with piezoelectric materials and passive electrical networks," Journal of Sound and Vibration, 146(2):243 – 268. (Cited on pages 5, 22, 36, and 39.)

Hansen, J.P. and Vizzini, A.J. 2000. "Fatigue response of a host structure with interlaced embedded devices," Journal

of Intelligent Material Systems and Structures, 11(11):902–909. (Cited on page 5.)

Herold, S. et al. 2004. "Transient simulation of adaptive structures," Journal of Intelligent Material Systems and Structures, 15(3):215–224. (Cited on page 5.)

Hirsekorn, M. et al. 2006. "Elastic wave propagation in locally resonant sonic material: Comparison between local interaction simulation approach and modal analysis," Journal of applied physics, 99:124912. (Cited on page 102.)

Hollkamp, J.J. 1994. "Multimodal passive vibration suppression with piezoelectric materials and resonant shunts," Journal of Intelligent Material Systems and Structures, 5(1):49–57. (Cited on pages 38 and 44.)

Hsiao, F. et al. 2007. "Waveguiding inside the complete band gap of a phononic crystal slab," Physical Review E, 76(5):056601. (Cited on page 101.)

Hsu, J. and Wu, T. 2007. "Lamb waves in binary locally resonant phononic plates with two-dimensional lattices," Applied physics letters, 90:201904. (Cited on page 102.)

Huang, H. and Sun, C. 2009. "Wave attenuation mechanism in an acoustic metamaterial with negative effective mass density," New Journal of Physics, 11:013003. (Cited on page 102.)

Jaglinski, T. et al. 2007. "Composite materials with viscoelastic stiffness greater than diamond," Science, 315(5812):620–622. (Cited on page 114.)

Jensen, J.S. 2003. "Phononic band gaps and vibrations in one-and two-dimensional mass–spring structures," Journal of Sound and Vibration, 266(5):1053–1078. (Cited on pages 95, 96, 97, and 114.)

Kadic, M. et al. 2012. "On the practicability of pentamode mechanical metamaterials," Applied Physics Letters, 100(19):191901. (Cited on page 114.)

Khelif, A. et al. 2006. "Complete band gaps in two-dimensional phononic crystal slabs," Physical Review E, 74(4):046610. (Cited on page 101.)

Lai, Y. et al. 2011. "Hybrid elastic solids," Nature Materials, 10(8):620–624. (Cited on pages 102 and 114.)

Lakes, R. et al. 2001. "Extreme damping in composite materials with negative-stiffness inclusions." Nature, 410(6828):565–7. (Cited on page 114.)

Lallart, M. et al. 2008. "Self-powered circuit for broadband, multimodal piezoelectric vibration control," Sensors and Actuators A: Physical, 143(2):377 – 382. (Cited on pages 36 and 56.)

Lapine, M. and Tretyakov, S. 2007. "Contemporary notes on metamaterials," Microwaves, Antennas Propagation, IET, 1(1):3 –11. (Cited on pages 94 and 113.)

Larbi, W. et al. 2010. "Structural-acoustic vibration reduction using switched shunt piezoelectric patches: A finite element analysis," Journal of Vibration and Acoustics, 132(5):051006. (Cited on page 5.)

Laughlin, R.B. 2006. A different universe: Reinventing physics from the bottom down, Basic Books. (Cited on page vii.)

Lee, J.H. et al. 2012. "Micro-/nanostructured mechanical metamaterials," Advanced Materials, 24(36):4782–4810. (Cited on pages 7 and 122.)

Lefeuvre, E. et al. 2006. "Semi-passive piezoelectric structural damping by synchronized switching on voltage sources," Journal of Intelligent Material Systems and Structures, 17(8-9):653–660. (Cited on page 32.)

Leo, D.J. 2007. Engineering Analysis of Smart Material Systems, John Wiley & Sons, Inc. (Cited on page 17.)

Lesieutre, G. et al. 2004. "Damping as a result of piezoelectric energy harvesting," Journal of Sound and Vibration, 269(3-5):991 – 1001. (Cited on pages 6 and 57.)

Li, F. et al. 2012. "Tunable phononic crystals based on cylindrical hertzian contact," Applied Physics Letters, 101(17):171903. (Cited on page 116.)

Li, J. and Chan, C.T. 2004. "Double-negative acoustic metamaterial," Phys. Rev. E, 70:055602. (Cited on page 7.)

Listing, J. 1848. Vorstudien zur topologie. (Cited on page 113.)

Liu, Z. et al. 2000. "Locally resonant sonic materials," Science, 289(5485):1734–1736. (Cited on pages 7, 102, and 114.)

Martinez-Sala, R. et al. 1995. "Sound attenuation by sculpture," Nature, 378(6554). (Cited on page 101.)

Meier, M. 2012. "Optimierung von flugzeugpropellerblättern für aerodynamische untersuchungen im windkanal," Master's thesis, ETH Zürich. (Cited on pages 73, 74, 77, 81, 82, and 83.)

Melnykowycz, M.M. 2008. "Long term reliabilty of active fiber composites (afc)," Ph.D. thesis, ETH Zurich. (Cited on page 5.)

Mohammadi, S. et al. 2008. "Evidence of large high frequency complete phononic band gaps in silicon phononic crystal plates," Applied Physics Letters, 92(22):221905–221905. (Cited on page 101.)

Newland, D.E. 1984. An introduction to random vibrations and spectral analysis, Longman New York. (Cited on page 70.)

Niederberger, D. 2005. "Smart damping materials using shunt control," Ph.D. thesis, ETH, Zürich. (Cited on pages 21 and 22.)

Niederberger, D. and Morari, M. 2006. "An autonomous shunt circuit for vibration damping," Smart Materials and Structures, 15(2):359. (Cited on pages 36, 53, 55, 56, 59, and 60.)

Niederberger, D. et al. 2004. "Adaptive multi-mode resonant piezoelectric shunt damping," Smart Materials and Structures, 13(5):1025. (Cited on page 23.)

Oudich, M. et al. 2011. "Experimental evidence of locally resonant sonic band gap in two-dimensional phononic stubbed plates," Phys. Rev. B, 84:165136. (Cited on page 102.)

Pendry, J.B. et al. 2006. "Controlling electromagnetic fields," Science, 312(5781):1780–1782. (Cited on page 7.)

Plagianakos, T.S. and Saravanos, D.A. 2003. "Hybrid multidamped composite plates with viscoelastic composite plies and shunted piezoelectric layers," Journal of Intelligent Material Systems and Structures, 14(1):57–66. (Cited on page 6.)

Porfiri, M. et al. 2007. "Identification of electromechanical modal parameters of linear piezoelectric structures," Smart Materials and Structures, 16(2):323. (Cited on page 43.)

Richard, C. et al. 2000. "Enhanced semi-passive damping using continuous switching of a piezoelectric device on an inductor," volume 3989, 288–299, SPIE. (Cited on page 32.)

Robillard, J.F. et al. 2009. "Tunable magnetoelastic phononic crystals," Applied Physics Letters, 95(12):124104. (Cited on page 116.)

Ruzzene, M. 2007. "Frequency-wavenumber domain filtering for improved damage visualization," Smart Materials and Structures, 16(6):2116. (Cited on page 105.)

Saravanos, D. 1999. "Damped vibration of composite plates with passive piezoelectric-resistor elements," Journal of Sound and Vibration, 221(5):867 – 885. (Cited on page 6.)

Shen, H. et al. 2010. "A low-power circuit for piezoelectric vibration control by synchronized switching on voltage sources," Sensors and Actuators A: Physical, 161(1-2):245 – 255. (Cited on page 54.)

Sihvola, A. 2002. Electromagnetic emergence in metamaterials, Springer. (Cited on page 94.)

Singh, D.A. and Vizzini, A.J. 1994. "Structural integrity of composite laminates with interlaced actuators," Smart Materials and Structures, 3(1):71. (Cited on page 5.)

Smith, D.R. et al. 2000. "Composite medium with simultaneously negative permeability and permittivity," Phys. Rev. Lett., 84:4184–4187. (Cited on page 7.)

Still, T. et al. 2011. "Collective hypersonic excitations in strongly multiple scattering colloids," Physical review letters, 106(17):175505. (Cited on page 102.)

Thomas, O. et al. 2009. "Vibrations of an elastic structure with shunted piezoelectric patches: efficient finite element formulation and electromechanical coupling coefficients," International Journal for Numerical Methods in Engineering, 80(2):235–268. (Cited on pages 5 and 25.)

Thomas, O. et al. 2012. "Performance of piezoelectric shunts for vibration reduction," Smart Materials and Structures, 21(1):015008. (Cited on pages 6 and 32.)

Thorp, O. et al. 2001. "Attenuation and localization of wave propagation in rods with periodic shunted piezoelectric patches," Smart Materials and Structures, 10(5):979. (Cited on pages 8 and 102.)

Thorp, O. et al. 2005. "Attenuation of wave propagation in fluid-loaded shells with periodic shunted piezoelectric rings," Smart materials and structures, 14:594. (Cited on page 102.)

Ungar, E.E. and Edward M. Kerwin, J. 1962. "Loss factors of viscoelastic systems in terms of energy concepts," The Journal of the Acoustical Society of America, 34(7):954–957. (Cited on page 38.)

Vasseur, J. et al. 2011. "Band structures tunability of bulk 2d phononic crystals made of magneto-elastic materials," AIP Advances, 1(4):041904–041904. (Cited on page 102.)

Wang, G. et al. 2004. "Two-dimensional locally resonant phononic crystals with binary structures," Physical review letters, 93(15):154302. (Cited on page 102.)

Wu, T. et al. 2008. "Evidence of complete band gap and resonances in a plate with periodic stubbed surface," Applied

Physics Letters, 93:111902. (Cited on pages 103, 106, 113, and 117.)

Wu, T.C. et al. 2009. "Waveguiding and frequency selection of lamb waves in a plate with a periodic stubbed surface," Phys. Rev. B, 79:104306. (Cited on pages 102, 103, and 106.)

Xiao, W. et al. 2008. "Flexural vibration band gaps in a thin plate containing a periodic array of hemmed discs," Applied Acoustics, 69(3):255–261. (Cited on page 102.)

Xu, B. et al. 1999. "Making negative poisson's ratio microstructures by soft lithography," Advanced Materials, 11(14):1186–1189. (Cited on page 114.)

Yao, S. et al. 2008. "Experimental study on negative effective mass in a 1d mass–spring system," New Journal of Physics, 10:043020. (Cited on page 102.)

Yilmaz, C. and Hulbert, G. 2010. "Theory of phononic gaps induced by inertial amplification in finite structures," Physics Letters A, 374(34):3576 – 3584. (Cited on page 6.)

Zhang, S. et al. 2011. "Broadband acoustic cloak for ultrasound waves," Phys. Rev. Lett., 106:024301. (Cited on page 114.)

Zheludev, N.I. and Kivshar, Y.S. 2012. "From metamaterials to metadevices." Nature materials, 11(11):917–24. (Cited on page 113.)

OWN PUBLICATIONS

The contents of this dissertation have led to the following journal publications and conference contributions:

JOURNAL PUBLICATIONS

A. A. Bergamini, T. Delpero, L. De Simoni, L. Di Lillo, M. Ruzzene and P. Ermanni, "Phononic crystal with adaptive connectivity," *Adv. Mater.* **2014**, 26 (9), 1343-1347

B. S. Krödel, T. Delpero, A. Bergamini, P. Ermanni, and D.M. Kochmann, "3D auxetic microlattices with independently controllable acoustic band gaps and quasi-static elastic moduli," *Adv. Eng. Mater.* **2014**, 16 (4), 357-363

C. T. Delpero, A. Bergamini, and P. Ermanni, "Identification of electromechanical parameters in piezoelectric shunt damping and loss factor prediction," *J. Intell. Mater. Syst. Struct.* **2013**, 24 (3), 287-298

D. T. Delpero, L. Di Lillo, A. Bergamini, and P. Ermanni, "Energy harvesting module for the improvement of the damping performance of autonomous synchronized switching on inductance," *J. Intell. Mater. Syst. Struct.* **2013**, 24 (7), 837-845

E. A.F. Arrieta, T. Delpero, A. Bergamini, and P. Ermanni, "Broadband vibration energy harvesting based on cantilevered piezoelectric bi-stable composites," *Appl. Phys. Lett.* **2013**, 102 (17), 173904

F. F. Casadei, T. Delpero, A. Bergamini, P. Ermanni, and M. Ruzzene, "Piezoelectric resonator arrays for tunable acoustic weaveguides and metamaterials," *J. Appl. Phys.* **2012**, 112 (6), 064902

G. F. Bachmann, R. de Oliveira, A. Sigg, V. Schnyder, T. Delpero, R. Jaehne, A. Bergamini, V. Michaud, and P. Ermanni, "Passive damping of composite blades using embedded piezoelectric modules or shape memory alloy wires - A comparative study," *Smart Mater. Struct.* **2012**, 21 (7), 075027

CONFERENCE CONTRIBUTIONS

A. Andres F. Arrieta, T. Delpero, A. Bergamini, and P. Ermanni, "A cantilevered piezoelectric bi-stable composite concept for broadband energy harvesting," *SPIE 2013 Active and Passive Smart Structures and Integrated Systems*, San Diego, CA, USA, March 10, **2013**, 8688, 86880G

B. T. Delpero, L. De Simoni, L. Di Lillo, A. Bergamini, and P. Ermanni, "Piezoelectric resonators for tunable phononic crystals," *Piezo 2103 Electroceramics for End-users VII conference*, Les Arcs 1800, France, March 17-20, **2013**

C. T. Delpero, F. Casadei, A. Bergamini, P. Ermanni, and M. Ruzzene, "Experimental characterization of two-dimensional tunable metamaterials," *ASME 2012 Conference on Smart Materials, Adaptive Structures and Intelligent Systems*, Stone Mountain, GA, USA, September 19-21, **2012**, 187-193

D. T. Delpero, A. Bergamini, and P. Ermanni, "Piezoelectric vibration damping using autonomous switching shunt," *Smart Systems Integration 2012,* Zurich, Switzerland, March 21-22, **2012**

E. T. Delpero, L. Di Lillo, A. Bergamini, and P. Ermanni, "Piezoelectric vibration damping using autonomous synchronized switching on inductance," *ASME 2011 Conference on Smart Materials, Adaptive Structures and Intelligent Systems*, Scottsdale, AZ, USA, September 18-21, **2011**, 427-433

F. T. Delpero, A. Bergamini, and P. Ermanni, "Shunted Piezoelectric Damping - Identification of the Electromechanical Parameters and Prediction of the Dissipated Energy," *22nd*

International Conference on Adaptive Structures Technologies (ICAST2011), Corfu, Greece, October 10-12, **2011**